Experimental and Numerical Investigations on Cylindrical Shell Panels

MTech. Thesis

By

LAKAVATH ANIL

(Roll Number: 2402104009)



DEPARTMENT OF CIVIL ENGINEERING

INDIAN INSTITUTE OF TECHNOLOGY INDORE

MAY 18 (2026)

Experimental and Numerical Investigations on Cylindrical Shell Panels

A THESIS

Submitted in partial fulfillment of the

requirements for the award of the degree

of

Master of Technology

by

LAKAVATH ANIL



DEPARTMENT OF CIVIL ENGINEERING

INDIAN INSTITUTE OF TECHNOLOGY INDORE

MAY 2026

INDIAN INSTITUTE OF TECHNOLOGY INDORE

CANDIDATE'S DECLARATION

I hereby certify that the work which is being presented in the thesis entitled "**Experimental and Numerical Investigations on Cylindrical Shell Panels"** in the partial fulfillment of the requirements for the award of the degree of **MASTER OF TECHNOLOGY** and submitted in the **DEPARTMENT OF CIVIL ENGINEERING, Indian Institute of Technology Indore**, is an authentic record of my own work carried out during the time period from July 2025 to May 2026 under the supervision of Dr. Kaustav Bakshi, Assistant Professor, Department of Civil engineering, IIT Indore.

The matter presented in this thesis has not been submitted by me for the award of any other degree of this or any other institute.



Signature of the student
LAKAVATH ANIL

This is to certify that the above statement made by the candidate is correct to the best of my/our knowledge.



Signature of the Supervisor of
MTech. thesis

Dr. KAUSTAV BAKSHI

LAKAVATH ANIL has successfully given his/her MTech. Oral Examination held on 11th May 2026.



Signature of Supervisor of MTech. thesis
Date:18/05/2026



Convener, DPGC
Date: 18/05/2026

ACKNOWLEDGEMENTS

The author wishes to express his deepest appreciation and heartfelt gratitude to his supervisor, Dr. Kaustav Bakshi, Assistant Professor, Department of Civil Engineering, Indian Institute of Technology Indore, whose unwavering guidance, constructive feedback, and continuous encouragement proved invaluable at every stage of this research. His intellectual input and mentorship have been a constant source of motivation throughout the entire course of this work.

The author also extends sincere thanks to the library of IIT Indore for providing access to essential academic resources that greatly supported the progress of this study. A special acknowledgement is due to the author's parents, whose selfless sacrifices, persistent encouragement, and unconditional support since the very beginning of his academic journey have been the foundation upon which this work stands.

Finally, the author gratefully acknowledges all individuals who contributed, directly or indirectly, to the successful completion of this thesis. Their collective efforts and goodwill are deeply appreciated.

Date: 18 MAY 2026

Place: IIT Indore

Signature of the Candidate: **LAKAVATH ANIL**

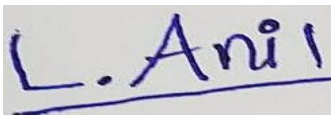

DEDICATION

First and foremost, I owe my deepest gratitude to my parents, whose unconditional love, selfless sacrifices, and unwavering belief in my abilities have been my greatest strength throughout this journey. This work is as much theirs as it is mine.

I am sincerely grateful to Dr. Kaustav Bakshi for his exceptional mentorship, thoughtful guidance, and constant encouragement at every step of this research, which proved instrumental in shaping both this work and my growth as a scholar.

I also extend my heartfelt thanks to my PhD seniors and friends for their timely support, motivation, and companionship, which made this journey far more enriching and rewarding.

ABSTRACT

The nonlinear flexural behavior of skew-angled stiffened cylindrical shell panels under mixed boundary conditions and varied transverse loads remains poorly documented in the literature. This study develops a C^0-continuous iso-parametric finite element model using eight-node shell elements and three-node stiffener elements, incorporating geometric nonlinearity via FSDT-based strain-displacement relations solved through Newton-Raphson iteration, validated against published analytical and experimental benchmarks. Parametric studies covering uniform, sinusoidal (sin–sin), and cosinusoidal (cos–cos) pressure loads across five boundary conditions (CCCC, SSSS, SCSC, CSCS,) examine the effects of skew angle, lamination sequence, material grade (graphite/epoxy and glass/epoxy), curvature ratio (R_{yy}/b), thickness ratio (a/h), and stiffener configuration. Sinusoidal loading yields minimum deflections while uniform pressure proves most structurally demanding; cosinusoidal loading governs bending moments M_x and M_y in several configurations, confirming that deflection alone is an inadequate performance measure. Graphite/epoxy panels consistently outperform glass/epoxy equivalents; angle-ply [(45°/−45°) s] laminates are optimal under SSSS conditions while cross-ply [(0°/90°) s] laminates perform best under CCCC, with the twisting moment M_{xy} dominating angle-ply panels at large skew angles. Although increasing stiffener count generally enhance panel stiffness, the optimal arrangement remains boundary-condition-dependent, establishing that both deflections and stress resultants must be evaluated jointly for reliable panel selection in engineering applications.

TABLE OF CONTENTS

Chapter	Title of the Chapter	Page No.
	List of Figures	*xi*
	List of Tables	*xv*
	Nomenclature	*xvii*
Chapter 1	**INTRODUCTION**	**19-28**
	1.1 Background and motivation	19
	1.2 Classification of Shell Structures	21
	1.3 Shell Structures through the Last Century	22
	1.4 Introduction to laminated composite	24
	1.5 Methods of analysis	26
Chapter 2	**LITERATURE REVIEW**	**29-47**
	2.1 General	29
	2.2 Development of Shell Theories	30
	2.3 Unstiffened Shell Analysis	36
	2.4 Stiffened Shell Analysis.	40
	2.5 Skewed Shell Analysis.	44
	2.6 Critical Discussion and Research Gaps	47

Chapter 3 SCOPE AND SIGNIFICANCE OF THE PRESENT STUDY 50-52

3.1 General 50

3.2 Present study 50

Chapter 4 MATHEMATICAL FORMULATION 53-78

4.1 General 53

4.2 Finite element method 54

4.3 Selection of element 54

4.4 Discretization of Shell Surface 55

4.5 Selection of Shape Functions 56

4.6 Selection of Generalized Degrees of Freedom 57

4.7 Strain- Displacement Relationship 59

4.8 Force-Displacement Relationship 67

4.9 Generalized Inertia Matrix 77

Chapter 5 NUMERICAL RESULTS 79-87

5.1 General 79

5.2 Geometric and Material Properties 80

5.3 Boundary Conditions 81

5.4 Non-dimensional Deflections under Uniform Pressure 81

5.5 Non-dimensional Deflections under Sinusoidal (Sin-Sin) Pressure 84

5.6 Non-dimensional Deflections under Cosinusoidal (Cos-Cos) Pressure 84

5.7 Stress Resultants 85

5.8 Selection of Optimal Configurations 86

5.9 Summary 86

Chapter 6 RESULTS AND DISCUSSIONS 88-112

6.1 General 88

6.2 Results and Discussions 88

Chapter 7 CONCLUSIONS 113-116

7.1 General 113

7.2 Conclusions 113

Chapter 8 SCOPE FOR FUTURE WORK 117

Chapter 9 REFERENCES 118-126

LIST OF FIGURES

Fig. No.	Figure Name	Page No.
4.1	Stiffened cylindrical shell panel	53
4.2	Eight noded element and shape functions.	55
4.3	Elements for (a) x – stiffener and (b) y - stiffener.	58
4.4	Degrees of freedom of skewed stiffened panel.	59
4.5	Skewed cylindrical panel with biaxial stiffeners	63
4.6	Stress components in three-dimensional continuum	67
4.7	Axis Systems in a unidirectional Lamina	71
4.8	Force and Moment Resultants on A Shell Structure	75
6.9	Load-deflection curve of cylindrical panel under uniform pressure.	90
6.10	Load-deflection curve of cylindrical panel under sin-sin pressure	93
6.11	Load-deflection curve of cylindrical panel under cos-cos pressure	97
6.12	Cylindrical panel ($\phi=0^0$) with CCCC boundary condition	105
6.13	Cylindrical panel ($\phi=0^0$) with SSSS boundary condition	107
6.14	Cylindrical panel ($\phi=0^0$) with SCSC boundary condition	109
6.15	Cylindrical panel ($\phi=0^0$) with CCSS boundary condition	111

LIST OF TABLES

Table No.	Table content	Page No.
5.1	Non-dimensional central deflections of simply supported composite spherical shell under uniformly distributed load	79
5.2	Material properties of laminated composites (graphite/epoxy and glass/epoxy)	80
5.3	Non-dimensional deflections ($\delta \times 10^4$) of biaxially stiffened cross-ply cylindrical panels under uniform pressure	81
5.4	Non-dimensional deflections ($\delta \times 10^4$) of biaxially stiffened angle-ply cylindrical panels under uniform pressure	83
6.5	Non-dimensional deflections (δ) of biaxially stiffened cross-ply cylindrical panels under sin-sin pressure.	91
6.6	Non-dimensional deflections (δ) of biaxially stiffened angle-ply cylindrical panels under sin-sin pressure.	92
6.7	Non-dimensional deflections (δ) of biaxially stiffened cross-ply cylindrical panels under cos-cos pressure.	94
6.8	Non-dimensional deflections (δ) of biaxially stiffened angle-ply cylindrical panels under cos-cos pressure.	95
6.9	Non-dimensional stress resultants of biaxially stiffened cylindrical panels under uniform pressure	99
6.10	Non-dimensional stress resultants of biaxially stiffened cylindrical panels under sin-sin pressure.	101

6.11 Non-dimensional stress resultants of biaxially stiffened cylindrical panels under cos-cos pressure. 103

NOMENCLATURE

Variables	Representations
X, Y, Z	Global coordinates of the laminate.
x, y, z	Local coordinate of the laminate.
ϕ	Skew angle
a, b	Length and width of shell in plan
h	Shell thickness
R_{xx}, R_{yy}, R_{xy}	Radii of curvatures along respective directions
r_{xx}, r_{yy}	Equivalent radii of curvature for skewed configuration
{d}, {δ}	Deformation vectors in global and local axes
$\{u, v, w, \alpha, \beta\}$	Nodal degrees of freedom in x-y axes
$\{U, V, W, \theta_x, \theta_y\}$	Nodal degrees of freedom in X-Y axes
ε	Total strain vector (linear + nonlinear)
$\{\varepsilon\}^L$	Linear strain component
$\{\varepsilon\}^{NL}$	Nonlinear strain component
κ	shear correction factor
$\{F\}$	Stress resultants vector
q_z	Transverse (downward) load intensity

Π	Total potential energy
w	Transverse displacement in cm.
δ	Non-dimensional transverse displacement of shell [$wE_{22}h^3/qa^4$]
z_k, z_{k-1}	Top and bottom distance of the κth ply from mid-plane of a laminate.
θ	Angle of lamination with respect to X axis of the shell.
n_p	Number of lamine
$[B_L]$ and $[B_{NL}]$	linear and nonlinear strain – displacement matrices
ξ, η	Natural co-ordinates of iso-parametric elements

Chapter 1

INTRODUCTION

1.1 Background and Motivation

Structural engineers have long drawn inspiration from the natural world, where evolution has refined load-bearing forms over millions of years. Objects as commonplace as a bird's egg, a human cranium, or the outer casing of a nut are, in structural terms, shell elements thin curved surfaces whose capacity to resist applied forces far exceeds what would be achievable with a flat plate of the same mass. The fundamental reason for this superiority lies in geometry: when a surface is curved, externally applied forces tend to resolve into stresses acting within the plane of the surface a state referred to as membrane action rather than being resisted primarily through bending. Because membrane stresses are distributed efficiently throughout the material thickness, the structure can carry substantial loads with very little material, making shells inherently weight-efficient.

This principle, though not formally codified until the nineteenth century, was empirically understood by builders much earlier. The Pantheon in Rome, whose unreinforced concrete dome spans more than 43 meters and has endured for nearly nineteen centuries with minimal intervention, represents perhaps the most celebrated demonstration of shell action in antiquity. Equally impressive is the Hagia Sophia in Constantinople (modern Istanbul), completed in AD 537, in which a central dome flanked by a series of half-domes was used to roof an enormous congregational space a structural achievement that continued to astonish both engineers and architects. Medieval cathedral builders in Western Europe, working without formal analytical tools, arrived at pointed arches, ribbed vaults, and compound dome systems whose structural logic exploiting curvature to minimize bending and carry loads efficiently to supports is recognizable to any modern structural engineer.

The Industrial Revolution introduced both new structural demands and new construction materials, accelerating the scientific study of shell behavior. Steam boilers subjected to internal pressure, submarine pressure hulls subjected to intense external hydrostatic loading, and the thin metal outer skins of early flying machines all constituted, in engineering terms, shell structures. The need to design these reliably stimulated the development of a formal mathematical theory of shells, drawing on classical differential

geometry and the mechanics of elastic continua. By the mid-twentieth century, improvements in reinforced concrete technology had enabled architects and structural engineers to realise extraordinarily slender shell roofs that combined structural economy with architectural expressiveness. Pioneering figures such as Félix Candela in Mexico, Pier Luigi Nervi in Italy, and Heinz Isler in Switzerland produced works celebrated as much for their formal beauty as for their structural ingenuity.

In parallel, the aerospace and defense sectors were pursuing a quite different trajectory in shell technology, driven by the imperative to minimize structural weight. In aircraft, missiles, and spacecraft, every reduction in structural mass translates directly into improved range, payload, or fuel economy. This pressure led to the systematic development of fibre-reinforced composite materials laminates in which high-strength, high-stiffness fibres are embedded within a polymer matrix whose specific stiffness and specific strength substantially exceed those of conventional metallic alloys. The integration of composite materials with shell geometry has opened up an expansive research domain that continues to attract sustained attention, and it is precisely this intersection that provides the context for the present study.

Contemporary engineering practice across the civil, aerospace, marine, and mechanical sectors increasingly calls for lightweight, high-performance structures, and this demand has brought laminated composite shells to the forefront of structural research. Among the various shell geometries that have been investigated, the elliptic paraboloid has emerged as a particularly attractive candidate. Its doubly curved surface confers a high degree of geometric stiffness, enabling the shell to sustain considerable external loads with minimal material volume, while its singly-ruled character means that it can be constructed using straight-line formwork, a practical advantage that distinguishes it from many other doubly curved forms. When the shell surface is additionally reinforced with attached ribs or frames commonly termed stiffeners its resistance to bending and buckling is further enhanced. The angular orientation of these stiffeners with respect to the shell's principal geometric axes has a pronounced influence on structural behaviour; in particular, skewed stiffening configurations introduce coupled bending-twisting responses that complicate both analysis and design.

A further layer of complexity arises from the boundary conditions that prevail in practical construction. In theoretical treatments of shell behavior, edge supports are typically idealized as either perfectly clamped or perfectly simply supported, and these idealizations are applied uniformly around the entire perimeter. In practice, however, such uniformity is rarely achieved. A shell roof may be rigidly connected to stiff columns along two edges while bearing on a relatively flexible beam along the remaining edges; internal point supports may be present;

or variations in construction quality may produce non-uniform stiffness around the boundary. These departures from ideality modify the internal force distribution, generate localized stress concentrations, and alter the overall load-displacement response in ways that uniform-boundary analyses are unable to predict. The manner in which non-uniform support conditions interact with composite material anisotropy, shell curvature, and stiffener skewness to govern the nonlinear bending response is therefore a question of direct practical significance, and it forms the central focus of the present investigation.

A systematic review of the existing literature reveals that, although substantial research has been conducted on composite shells under uniform boundary conditions, and while individual studies have examined the separate effects of stiffening or geometric nonlinearity, the combined problem of a skewed-stiffened laminated composite elliptic paraboloidal shell subject to non-uniform boundary conditions has not previously been addressed in a comprehensive and systematic manner. This gap is consequential because the governing factors composite material anisotropy, geometric nonlinearity, stiffener skewness, and boundary non-uniformity are not independent; they interact in complex, coupled ways that cannot be adequately understood by examining each in isolation. The present study is therefore motivated by the need to close this gap, to develop and validate a finite element formulation capable of capturing all relevant coupling effects, and to deploy that formulation to generate systematic results of direct relevance to structural design.

1.2 Classification of Shell Structures

To appreciate the significance of the specific shell geometry investigated in this thesis, it is helpful to situate it within the broader taxonomy of shell structures. The most fundamental classification distinguishes between singly curved and doubly curved shells, and this distinction has consequences for both structural performance and constructional practicality.

A singly curved shell possesses curvature in one principal direction only. Cylindrical shells are the most prevalent representative of this category, curving in the circumferential direction while remaining straight along the generator. Conical shells and barrel vaults are further examples. Because such surfaces can be generated by translating a straight line along a curved directrix, they belong to the family of ruled surfaces, and this property carries an important practical implication: the formwork required to cast a concrete singly curved shell, or the tooling needed to fabricate a composite one, can be assembled from straight elements.

This substantially reduces construction cost and complexity. Accordingly, singly curved shells find widespread application in industrial structures, storage vessels, culverts, and tunnels.

Doubly curved shells carry curvature in two independent directions simultaneously. This additional geometric dimension generally renders them stiffer and more efficient in distributing loads, since internal forces can propagate along two load paths rather than one. The analytical description of doubly curved surfaces is, however, more involved, and their construction typically demands more sophisticated formwork. Within the doubly curved family, shells are further classified according to the sign relationship between the two principal curvatures. Where both curvatures share the same sign meaning the surface bends in the same sense in every direction the surface is termed synclastic; spherical domes and elliptic paraboloids belong to this class. Where the two principal curvatures are of opposite sign, so that the surface curves upward in one direction and downward in the orthogonal direction, the surface is described as anticlastic; the hyperbolic paraboloid is the most familiar example. Conoidal shells represent an intermediate case, being doubly curved yet possessing one straight edge, which affords certain practical advantages in roofing applications.

The elliptic paraboloid merits particular attention in the present context, as it is the geometry investigated throughout this thesis. Its mid-surface is described by an equation of the form $z = x^2/a^2 + y^2/b^2$, where a and b are parameters governing the curvature in the two principal coordinate directions. When a and b are equal, the surface reduces to a circular paraboloid; when they differ, the curvature is unequal in the two directions, producing the characteristic elliptic form. Although the elliptic paraboloid is a doubly curved, synclastic surface, it is also singly ruled that is, it can be generated by a continuously moving straight line in three-dimensional space. This property means that straight-line construction methods remain applicable, retaining the practical advantages of ruled surfaces while simultaneously benefiting from the structural efficiency of double curvature. It is this combination geometric stiffness, weight efficiency, aesthetic versatility, and constructional tractability that has made the elliptic paraboloid an increasingly popular subject of structural research over recent decades.

1.3 Shell Structures through the Last Century

The twentieth century witnessed the maturation of shell structures from a specialized curiosity into a mainstream engineering tool deployed across virtually every sector of the built environment. This evolution was driven by the convergence of new materials, improved

analytical understanding, and an expanding appetite for large-span, lightweight, and architecturally expressive structures.

In civil and architectural engineering, the early decades of the century saw reinforced concrete establish itself as the dominant medium for ambitious shell construction. The material's capacity to be formed into virtually any curved shape at relatively modest cost made it ideally suited to shell applications, and a community of engineers steadily developed both the theoretical tools and the practical techniques required to build thin concrete shells economically. The field reached its creative peak in the 1950s and 1960s. Félix Candela exploited the ruled-surface geometry of the hyperbolic paraboloid to construct a series of shell roofs in Mexico including the widely reproduced Los Manantiales Restaurant of 1958 in which elegant saddle-shaped surfaces were realised with concrete shells of remarkable slenderness. Pier Luigi Nervi demonstrated in Italy that prefabricated ferrocement ribs, combined with thin cast-in-place infill panels, could span large areas with both structural efficiency and visual refinement. The CNIT building in Paris, completed in 1958, covered a triangular plan of approximately 200 metres per side with a double-layer concrete shell only a few centimetres in thickness, standing at the time as the world's largest reinforced concrete shell structure.

Shell construction simultaneously found widespread application in more utilitarian contexts. Water reservoirs, sewage treatment covers, industrial domes, and the hyperbolic cooling towers that became characteristic features of the mid-century landscape all exploited shell action to enclose large volumes or resist substantial pressure loads with minimum material. Aircraft hangar roofs, bus terminals, and sports facilities adopted barrel and cylindrical shell forms to achieve wide, obstruction-free floor areas. Nuclear power stations required containment domes designed to resist both accidental internal overpressure and external impact loads, representing some of the most demanding shell design challenges of the postwar period.

The marine sector had long relied on shell principles in the design of ship hulls, and the twentieth century saw naval architecture develop into a rigorous discipline capable of analysing the interactions between hull plating, transverse frames, and longitudinal stiffeners with considerable precision. The development of submarine technology imposed especially demanding requirements: pressure hulls must sustain high external hydrostatic loads without buckling, a failure mode acutely sensitive to geometric imperfections and residual fabrication stresses. The consequent advances in shell buckling theory had broad implications well beyond the naval context.

The most transformative developments in shell technology during this period, however, occurred in the aerospace sector. Aircraft fuselages are inherently thin-walled shell structures, and the relentless drive to reduce structural weight while maintaining adequate stiffness and strength sustained a continuous programme of research and development throughout the century. The advent of jet propulsion and, subsequently, space launch vehicles pushed structural demands to unprecedented levels. Rocket fairings, satellite bus structures, re-entry vehicle heat shields, and pressurised spacecraft modules all required shell-form components of extraordinary specific performance. It was these requirements that catalysed the development of fibre-reinforced composite materials and established the technical foundations from which the laminated composite shells studied in this thesis are directly derived.

By the close of the twentieth century, the cumulative effect of these developments had transformed the field. Shell theory had been rigorously formulated; the finite element method had matured into a reliable and general computational tool for shell analysis; and advanced composite materials had been refined to the point where their structural application could proceed with confidence. The conditions were thus established for the research agenda of the present era, which focuses increasingly on the complex interactions among composite material behaviour, geometric nonlinearity, non-ideal boundary conditions, and structural details such as stiffeners interactions that collectively determine the response of real shell structures in engineering practice.

1.4 Introduction to Laminated Composites

The term composite material encompasses an exceptionally broad class of engineered substances, ranging from the mud bricks reinforced with organic fibres employed in ancient construction to the highly engineered carbon-fibre-reinforced polymer systems used in contemporary aerospace structures. Despite this diversity, all composite materials share a defining characteristic: they are formed by combining two or more chemically distinct constituents at the macroscopic scale, with the deliberate objective of producing a material whose collective properties surpass those of any individual constituent acting alone. In the structural composites relevant to this thesis, the constituent roles are fulfilled by a reinforcing fibre phase which provides stiffness and tensile strength and a continuous polymer matrix phase, which binds the fibres together, facilitates load redistribution among them, provides resistance to compressive fibre buckling, and shields the reinforcement from environmental degradation.

The origins of modern structural composites in engineering applications can be traced to the pressures of the Second World War. The rapid expansion of military aviation created an acute demand for aluminium alloys, and concerns about the potential disruption of bauxite supply chains prompted researchers at Aero Research Limited in Britain to develop a fibre-reinforced alternative. Their product a material subsequently known as Gordon Aerolite, fabricated by impregnating untwisted flax fibres with a phenolic resin was employed in the manufacture of aircraft structural components including fuselage frames and skin panels, marking the first systematic use of a fibre-reinforced composite in a modern load-bearing application. The manufacturing, testing, and design knowledge accumulated during this wartime programme provided the conceptual foundation upon which subsequent developments were built.

The structural rationale for combining fibres and matrix becomes clear when the individual contributions of each constituent are considered. Fibres whether fabricated from glass, carbon, boron, aramid, or other high-performance materials exhibit exceptional tensile stiffness and strength along their axis, but they are geometrically unstable under compression mechanically fragile in isolation, and effectively impossible to handle or form into structural shapes without a surrounding medium. The polymer matrix, by contrast, is relatively compliant and of modest strength, but it can be moulded into complex geometries, provides continuous lateral support to the fibres that prevents compressive buckling, transfers load between individual fibres and between fibre bundles, and affords protection against moisture ingress and chemical attack. The combination of these two constituents yields a structural material whose specific stiffness and specific strength properties normalised by density substantially exceed those of conventional engineering metals such as steel and aluminium alloys.

The fundamental building block of a laminated composite is the individual ply, or lamina. A lamina is produced by impregnating an array of fibres which may be continuous and unidirectional, woven into a bidirectional fabric, or discontinuous with liquid resin and consolidating the assembly under heat and pressure to produce a thin, solid sheet. In a unidirectional lamina, all fibres are aligned in a single direction, conferring strongly directional mechanical properties: stiffness and strength are high parallel to the fibre axis and considerably lower in the transverse direction. Rather than being a limitation, this directional character is an exploitable feature. By stacking multiple laminae with their fibres oriented at selected angles for example 0°, ±45°, and 90° and bonding the assembly into a single laminate, the designer can tailor the overall stiffness and strength distribution to suit the anticipated loading. The choice of ply angles, ply thicknesses, and stacking sequence collectively determines the

laminate's in-plane and bending stiffnesses, the degree of coupling between extension and bending, and the effective thermal expansion behaviour a degree of design flexibility that is simply unavailable in conventional isotropic materials.

This tailor ability is among the most significant structural advantages that laminated composites offer relative to homogeneous materials such as steel. In an isotropic plate or shell, the designer can alter structural performance only by varying thickness or adding separate stiffening elements. In a laminated composite counterpart, fibre orientation and stacking sequence provide additional design variables through which performance can be optimised a much larger design space. These attributes have made laminated composites particularly attractive in weight-sensitive applications: in aerospace structures, where mass reduction translates directly into fuel savings or payload capacity; in marine structures, where reduced structural weight improves vessel speed and carrying capacity; and increasingly in civil infrastructure, where long spans, chemically aggressive environments, or the need to minimise foundation loads make the high specific stiffness and inherent corrosion resistance of composite materials especially valuable.

Laminated composite shells, which combine the geometric efficiency of shell forms with the material efficiency of composite laminates, have accordingly attracted sustained and growing research attention since the 1960s. Their structural performance potential is extraordinary, but so too is the complexity of their behavior. Laminate anisotropy gives rise to coupling phenomena that have no counterpart in isotropic shells: in-plane loading may induce out-of-plane bending, applied moments may produce twisting deformations, and thermal loading may cause warping. The failure mechanisms of composite laminates are substantially more involved than those of metals, encompassing fibre fracture, matrix cracking, fibre-matrix interfacial debonding, and delamination between plies. Developing analytical and numerical frameworks capable of capturing these coupled and potentially nonlinear behaviors has been the central challenge of composite shell research over the past several decades, and it remains an active area of investigation, one to which the present study seeks to contribute.

1.5 Methods of Analysis

The mathematical analysis of shell structures presents inherent difficulties of a high order. Even for geometrically simple shell forms under idealised loading conditions, the governing equations of classical shell theory are high-order partial differential equations for which closed-form solutions exist only in a narrow and special set of circumstances. For shells

of engineering relevance with complex geometries, position-dependent material properties, non-uniform boundary conditions, and realistic loading recourse to approximate numerical methods is essentially always necessary. Several such methods have been developed and applied in the context of composite shell analysis, each possessing characteristic strengths and limitations.

The finite difference method represents one of the earliest systematic numerical approaches applied to shell problems. It replaces the continuous differential operators in the governing equations with discrete difference approximations evaluated over a regular grid of points covering the shell surface. For problems with simple, regular geometries and straightforward boundary conditions, the method is computationally efficient and conceptually transparent. However, it becomes progressively less convenient as the shell geometry becomes irregular, as boundary conditions vary around the perimeter, or as material properties vary spatially. Its application in composite shell research has largely been superseded by more versatile alternatives.

Energy-based methods including the Rayleigh method, the Rayleigh-Ritz method, and the Galerkin method adopt a fundamentally different strategy. Rather than discretising the governing differential equations, these approaches approximate the displacement field as a linear combination of assumed basis functions, typically polynomial or trigonometric series, and determine the expansion coefficients by invoking either a stationarity condition on the total potential energy or an orthogonality condition on the residual. When appropriate basis functions are available, these methods can yield highly accurate results with relatively few unknowns, and they have been widely used for shells of simple geometry under standard boundary conditions. Their principal limitation is that suitable basis functions are difficult to construct for irregular geometries, non-uniform boundary conditions, or problems involving material or geometric nonlinearity, and they do not lend themselves naturally to general-purpose implementation.

The dynamic relaxation method is an iterative pseudo-transient procedure in which the static equilibrium equations are solved by integrating artificial equations of motion including damping terms forward in time until the kinetic energy of the system dissipates to a negligible level, at which point the configuration approximates the static equilibrium solution. The method does not require the assembly or inversion of a global stiffness matrix, which is advantageous for certain nonlinear problems and for form-finding applications. However, convergence rates can be slow, and the method has not achieved the widespread adoption in composite shell research that the finite element method has attained.

The finite element method has become, by an overwhelming margin, the dominant analytical tool for composite shell structures, and a survey of the literature leaves no room for doubt on this point. The method partitions the shell surface into a mesh of discrete elements, represents the displacement field within each element through polynomial shape functions associated with nodal degrees of freedom, and assembles the element contributions into a global system of algebraic equations that is solved for the nodal displacements. The outstanding attribute of the method is its generality: it is applicable to virtually any shell geometry, material distribution, boundary condition configuration, and loading pattern, and it extends naturally to geometrically and materially nonlinear problems through iterative solution strategies such as the Newton-Raphson method. In the present study, where the shell possesses a doubly curved elliptic paraboloidal geometry reinforced with skewed stiffeners, the structural material is an anisotropic laminated composite, the boundary conditions are non-uniform, and the analysis must account for geometric nonlinearity, the finite element method is the clearly appropriate choice.

Chapter 2

LITERATURE REVIEW

2.1 General

Shell structures have occupied a central place in structural engineering for centuries. From the ancient masonry domes of Rome and Byzantium to the contemporary aerospace panels of commercial aircraft, from submarine pressure hulls to offshore platform jackets, from wind turbine towers to large-span architectural roofs, the recurring appeal of shell forms lies in their extraordinary structural efficiency. That efficiency is rooted in the geometric principle that a curved surface can redirect applied loads primarily into in-plane membrane stresses rather than bending actions, enabling wall thicknesses that are vanishingly small relative to the span. A well-designed shell can achieve a strength-to-weight ratio an order of magnitude higher than that of an equivalent flat plate or beam-column assembly, a fact that has motivated generations of researchers to investigate shell behavior under increasingly complex loading, material, and geometric conditions.

The breadth of the shell literature is formidable. Over the past century and a half, contributions have emerged from applied mathematicians developing elegant closed-form theories, from structural engineers solving practical design problems, and more recently from computational mechanics exploiting the power of finite element methods and high-performance computing. Early investigators such as Love (1888) and Novozhilov (1953) established the mathematical foundations, while mid-twentieth century researchers extended those foundations to composite materials and numerical computation. The last three decades have witnessed an explosion of work on functionally graded materials, carbon nanotube reinforced composites, smart piezoelectric shells, iso-geometric analysis, and data-driven computational methods.

The literature reviewed in this chapter has been organized to reflect this historical and thematic progression. The chapter opens with the evolution of shell theories, tracing the path from classical thin-shell assumptions through first-order and higher-order shear deformation theories to modern unified formulations capable of handling thick laminates, functionally graded materials, and fully nonlinear kinematics. It then examines the finite element treatment of cylindrical shells the dominant class in literature, first for linear and then for geometrically nonlinear conditions. Separate sections address unstiffened shells, stiffened shells, and skewed

shell panels, each covering both linear and nonlinear analyses. A final critical synthesis identifies the specific gaps that remain in the open literature and motivates the present research. The review spans publications from the foundational classical works of the nineteenth century through journal articles appearing in 2025 and early 2026. Throughout, special attention is given to studies involving laminated fiber-reinforced composite materials, since these now dominate weight-sensitive applications and introduce coupling phenomena absent in isotropic shells. Approximately half the coverage is devoted to cylindrical shells and shell theories owing to their dominance in the literature; the remaining half covers spherical, conoidal, hyperbolic paraboloidal, elliptic paraboloidal, and skewed shell forms, together with the stiffened variants of each class.

2.2 Development of Shell Theories

2.2.1 Classical Thin-Shell Theories

The systematic mathematical treatment of shell structures was initiated by Lamé and Clapeyron (1833), who derived governing equations for shells of revolution under axisymmetric loading using a purely membrane assumption that neglects all bending rigidity. Membrane theory yields useful results for thin shells far from boundaries and concentrated loads but is deficient wherever moment transfer is important. Aron (1874) provided the first general elasticity-based shell theory by applying the kinematic hypothesis independently introduced by Kirchhoff for plates and by Love for shells. The Kirchhoff-Love hypothesis states that material fibres originally normal to the mid-surface remain straight, inextensible, and normal to the deformed mid-surface. Combined with the assumptions of negligible transverse normal stress and linear displacement variation through the thickness, this yields a two-dimensional theory entirely characterized by mid-surface strains and changes of curvature. Love (1888) presented the first complete thin-shell theory in a form suitable for engineering computation, encompassing arbitrary shell geometry and serving as the departure point for most subsequent thin-shell investigations. Novozhilov (1953) gave a rigorous mathematical derivation of the same equations and carefully delineated their range of validity, clarifying assumptions that had previously been left implicit. Vlasov (1949) contributed an influential reformulation with particular emphasis on cylindrical and conical geometries. Reissner (1955) extended the scope by incorporating bending-membrane coupling for rotationally symmetric problems. A landmark survey by Naghdi (1956) compared the many competing formulations

of thin-shell theory that had proliferated by the mid-twentieth century, providing unified notation that facilitated later comparative studies.

Sanders (1959) and Koiter (1960a) independently proposed shell theories that are consistent to second order in the thickness-to-radius ratio and that satisfy the requirement of predicting rigid-body motions without spurious strains. These Sanders-Koiter equations became the standard reference for comparative studies of shell vibration and buckling. Leissa (1973) conducted the most comprehensive review of thin-shell vibration theories up to that date, tabulating natural frequency solutions for dozens of boundary condition and geometry combinations and demonstrating that significant numerical differences can arise between alternative formulations of nominally equivalent accuracy. Bert (1980) extended this comparative framework to composite material shells. Marguerre (1938) extended the Kirchhoff-Love framework to the geometric nonlinear range for shallow shells. Donnell (1934) proposed a simplified nonlinear theory specifically for thin shallow cylindrical shells, widely used for vibration and buckling studies because of the ease with which it permits semi-analytical solution.

2.2.2 First-Order Shear Deformation Theory

The Kirchhoff-Love theory proves unreliable when the ratio of shell thickness to the smallest characteristic wavelength of the deformation exceeds approximately one-tenth. For moderately thick shells and for laminated composites where the interlaminar shear stiffness is relatively low, transverse shear deformation makes a significant contribution to overall flexibility. Reissner (1945) and Mindlin (1951) addressed this limitation by developing what is now called the first-order shear deformation theory (FSDT), also known as the Reissner-Mindlin theory. FSDT relaxes the normality constraint of Kirchhoff-Love by introducing independent rotational degrees of freedom for the two in-plane directions, so that the cross-section is allowed to rotate independently of the mid-surface normal.

FSDT assumes that transverse shear strains are uniform through the shell thickness, which violates traction-free boundary conditions on the top and bottom surfaces. A shear correction factor is therefore introduced to scale shear stiffness terms so that the strain energy stored by shear deformation matches the value predicted by three-dimensional elasticity theory. Whitney (1973) carried out a systematic study of shear correction factors for laminated plates and showed that they depend on the stacking sequence, material properties, and loading type. Noor and Peters (1989) and Huang (1993) provided further analyses under thermal loading conditions. These stgive established that FSDT with appropriately calibrated correction factors

gives sufficiently accurate predictions of deflections, stress resultants, and natural frequencies for shells with thickness-to-span ratios up to about one-fifth.

The application of FSDT to laminated composite shells was carried out in a series of influential papers by Reddy (1984), who derived consistent variational equations and reported benchmark solutions for cylindrical, spherical, and doubly curved shells under various boundary conditions. Ghosh and Bandyopadhyay (1989, 1994) implemented FSDT in a finite element framework for composite conoidal shells and demonstrated good agreement with three-dimensional elasticity solutions. Chakravorty and Bandyopadhyay (1995) extended this to doubly curved panels, and Nayak and Bandyopadhyay (2005) applied FSDT to stiffened conoidal shells with complex boundary conditions. These studies collectively established FSDT as the workhorse theory for practical finite element analyses of laminated shell structures throughout the first decade of the twenty-first century. More recently, Tornabene et al. (2015, 2017) presented a generalized differential quadrature (GDQ) approach based on FSDT applied to functionally graded materials, carbon nanotube reinforced composites, and sandwich configurations, confirming that FSDT remains accurate and computationally efficient for problems where the primary concern is global structural response.

2.2.3 Higher-Order Shear Deformation Theories

For shells with thickness-to-span ratios greater than about one-tenth, and especially for thick laminated composites where the ratio of in-plane stiffness to transverse shear stiffness can be very large, FSDT does not provide a sufficiently accurate representation of the through-thickness stress field. Higher-order shear deformation theories (HSDT) were developed to eliminate the need for shear correction factors and to capture the parabolic variation of shear stresses that three-dimensional elasticity theory predicts. Levinson (1980), Murthy (1981), and Lo et al. (1977) proposed various forms of HSDT in which the in-plane displacements are expressed as cubic functions of the thickness coordinate, so that shear strains vary parabolically and vanish at the free surfaces automatically.

Reddy (1984) formulated the most widely used HSDT for laminated shells, now commonly referred to as the Reddy third-order shear deformation theory (TSDT). This theory assumes a parabolic variation of transverse shear strains across the thickness and satisfies zero shear stress conditions at the top and bottom surfaces without any correction factor. Reddy and Liu (1985) derived governing equations for a doubly curved shell using this theory and produced exact solutions for simply supported cross-ply cylindrical shells under static loads and free vibration, which have been widely used as benchmark data. Pan and Reddy (2002)

applied TSDT to composite spherical shells and reported detailed stress distributions showing significant improvements over FSDT near the interfaces of dissimilar laminae. Kant and Swaminathan (2002) presented analytical solutions for composite and sandwich shells using a higher-order theory that includes both thickness stretching and parabolic shear deformation. Amabili and Reddy (2010) proposed a new higher-order nonlinear shell theory incorporating both transverse shear deformation and thickness stretching within a fully nonlinear strain-displacement framework, demonstrating superior accuracy for large-amplitude vibrations compared with both FSDT and the Reddy TSDT. Amabili (2011, 2013, 2014) further extended and validated this formulation, eventually incorporating transverse normal strain terms to achieve a fully three-dimensional representation within a two-dimensional structural model. Mantari et al. (2012) introduced a generalized HSDT using a sinusoidal thickness function for laminated doubly curved shells. Thai and Kim (2015) surveyed higher-order plate and shell theories systematically and demonstrated that theories accounting for thickness stretching consistently outperform those that neglect it when shell thickness exceeds one-eighth of the span.

Carrera (1999, 2002, 2003) developed the Carrera Unified Formulation (CUF), which expresses through-thickness displacement variation using arbitrary expansion functions and generates any desired plate or shell theory by selecting appropriate orders. CUF has been implemented in finite element, iso-geometric, and spectral methods for composite, piezoelectric, and functionally graded shell structures. Demasi (2008, 2009) extended this to a generalized unified formulation (GUF) that further generalizes the expansion independently for each displacement component. Iso-geometric analysis (IGA), introduced by Hughes et al. (2005), has become increasingly prominent in shell analysis because NURBS basis functions naturally represent curved geometries exactly and have high inter-element continuity beneficial for thin shell formulations requiring C^1 continuity. Kiendl et al. (2009) developed the Kirchhoff-Love iso-geometric shell element; Echter et al. (2013) proposed an HSDT iso-geometric shell formulation with thickness locking treatment; Nguyen-Thanh et al. (2022) extended this to large deformation analysis of composite shells with cutouts.

2.2.4 Laminated Composite Shell Theories

The replacement of traditional metals by laminated fiber-reinforced polymer composites accelerated dramatically from the 1970s onward, driven by the aerospace, naval, and wind energy industries. Composites offer high specific stiffness and strength, excellent fatigue life, resistance to corrosion, and the ability to tailor mechanical properties by varying

fiber orientation and stacking sequence. These attributes are particularly valuable in shell structures where weight saving is paramount. The constitutive behavior of laminates is significantly more complex than that of isotropic materials: in-plane anisotropy, bending-stretching coupling in unsymmetric laminates, and low interlaminar shear stiffness all require careful theoretical treatment.

Hildebrand et al. (1949) made the first attempt to incorporate material anisotropy into shell equations. Ambartsumyan (1953) introduced the bending-stretching coupling matrix into laminated shell analysis and applied Love's theory to orthotropic shells, identifying that coupling between bending and membrane actions fundamentally alters static and dynamic response. The classical lamination theory for plates and shells, based on Kirchhoff-Love kinematics and the equivalent single-layer assumption, was fully developed by Ashton and Whitney (1970) and Jones (1975). Both noted that composites are significantly more sensitive to transverse shear than metals because in-plane moduli can be fifty to one hundred times larger than the interlaminar shear modulus. Whitney and Pagano (1970) extended FSDT to laminated anisotropic plates and derived closed-form solutions for bending under sinusoidal loading. Bert and Reddy (1982) and Bert and Kumar (1982) produced closed-form bending solutions for laminated cylindrical and spherical shells that became standard benchmarks.

The development of layer-wise theories represented a significant advancement for thick composites. Pagano (1969, 1970) produced three-dimensional elasticity solutions for laminated plates under sinusoidal loading that remain the gold standard for benchmarking approximate theories. Reddy (1987) developed a layer-wise plate theory extended to shells, in which each layer has its own through-thickness displacement variation and interlaminar continuity conditions are enforced exactly. This approach captures the zigzag pattern of in-plane displacements in heterogeneous laminates at higher computational cost than equivalent single-layer theories. Functionally graded materials (FGMs), in which properties vary continuously through the thickness, were introduced by Koizumi (1993). Loy et al. (1999) computed natural frequencies of FGM cylindrical shells using Love's thin-shell theory; Tornabene (2009) and Tornabene et al. (2011, 2013) used GDQ with FSDT and HSDT for comprehensive FGM doubly curved shell studies.

Nanocomposite shells reinforced with carbon nanotubes (CNTs) emerged as an important class in the 2010s. Shen (2011) studied nonlinear bending of CNT-reinforced composite cylindrical panels in thermal environments using HSDT; Zhang et al. (2014) examined vibration of CNT reinforced FGM doubly curved panels; Mehar et al. (2021) used HSDT-based FEM for nonlinear static responses of CNT/polymer conical shells. Piezoelectric

and smart composite shells integrating piezoelectric patches for active vibration control have also received considerable attention. Lam et al. (2002) studied active vibration suppression of composite cylindrical shells with embedded piezoelectric sensors and actuators. Vinyas (2020) presented a comprehensive finite element investigation of smart magneto-electro-elastic composite shells, covering static deflection, natural frequencies, and controlled response under combined electromagnetic and mechanical loading.

2.2.5 Recent Advances in Shell Theory (2015–2026)

The period from 2015 to 2026 has been marked by several important conceptual and computational advances. Carrera et al. (2016) further developed CUF-based models with zig-zag effects for multi-layered structures with soft cores. Vescovini and Dozio (2016) applied variable-order kinematic models within a Ritz framework to vibration of composite multilayered shells, showing that adaptively chosen expansion orders give higher accuracy than uniform-order models at the same computational cost. Machine learning approaches have begun to appear in shell analysis: Liu et al. (2021) employed deep learning to predict nonlinear vibration frequencies of functionally graded plates and shells, achieving accuracy comparable to conventional FEM at a fraction of the computational cost once trained. Flaschel et al. (2021) demonstrated unsupervised discovery of constitutive shell models from experimental displacement data using physics-informed neural networks.

Phase-field methods have been applied to fracture and delamination in composite shells. Reinoso et al. (2017) combined a phase-field fracture model with an HSDT shell formulation to model propagation of cracks through laminated composite panels under quasi-static and dynamic loading. Quintanas-Corominas et al. (2022) used a phase-field model to study intralaminar and interlaminar damage in composite cylindrical shells, providing detailed damage maps under complex loading histories previously difficult to obtain numerically. Topology optimization of composite shell structures has also developed significantly, with Groen et al. (2019) using concurrent thickness and fiber orientation optimization for aerospace panels, and Wu et al. (2022) applying iso-geometric shell analysis within a bi-directional evolutionary structural optimization framework. Recent 2024–2025 contributions include Benounas et al. (2024) on FGM spherical shell panels with cutouts, Draiche et al. (2024) on non-polynomial HSDT for doubly curved shells, Long et al. (2025) on C1-continuous layer-wise models for multi-layered spherical shells, and a comprehensive review by Sayyad and Ghugal (2024) cataloguing over three hundred works published from 2016 to 2024.

2.3 Unstiffened Shell Analysis

2.3.1 Linear Static Analysis

Linear static analysis forms the foundation of shell structural assessment and has been extensively studied for cylindrical geometries. The Donnell-Mushtari-Vlasov (DMV) equations represent the simplest linear theory for thin cylinders, while the more accurate Sanders-Koiter equations are preferred when in-plane displacements are significant. Closed-form solutions exist only for simply supported boundary conditions under sinusoidal loads; most practical problems require numerical methods. Chandrashekhara (1989) used iso-parametric eight-noded shell elements with FSDT to study static deflections and stress resultants in composite doubly curved shells cylindrical, spherical, and hyperbolic paraboloidal under uniformly distributed loading. The study demonstrated that lamination sequence significantly influences the magnitude and distribution of transverse shear stresses, particularly near the supported edges.

Ghosh and Bandyopadhyay (1990) studied deflections and stress resultants of laminated composite paraboloidal shells using eight, nine, and twelve-noded iso-parametric elements, confirming that nine-noded elements with reduced integration provide the best balance of accuracy and efficiency. Reddy (1984) reported exact bending solutions for moderately thick laminated composite cylindrical and spherical shells under sinusoidal loading using his HSDT formulation; these remain standard benchmarks for finite element validation. Ram and Babu (2001, 2002) used HSDT and iso-parametric elements to study deflections and stresses in laminated composite spherical shell caps with and without circular cutouts, showing that cutouts of moderate size cause significant stress concentration near the opening but have a relatively modest effect on global deflection of thin shells. Das and Chakravorty (2007) applied eight-noded elements with FSDT to static bending of composite conoidal shells, producing comprehensive parametric data covering aspect ratio, curvature, and lamination sequence.

In recent years, several new approaches to linear static shell analysis have emerged. Natarajan et al. (2014) implemented FSDT in an iso-geometric framework for laminated composite cylindrical shells with cutouts, demonstrating the advantage of exact geometric representation for curved shells. Thai et al. (2015) used iso-geometric HSDT to analyze static bending of functionally graded cylindrical and spherical shells and reported superior accuracy over conventional FSDT with fewer degrees of freedom. Nguyen et al. (2020) developed a smoothed finite element method for composite doubly curved shells that reduces sensitivity to

mesh distortion. Pham et al. (2024) combined iso-geometric analysis with a refined quasi-3D theory to study static deflection and stress distribution in composite doubly curved shells under non-uniform pressure distributions, reporting detailed through-thickness stress profiles not captured accurately by conventional equivalent single-layer theories.

2.3.2 Linear Free Vibration Analysis

The free vibration of cylindrical shells has received more research attention than perhaps any other shell problem, partly because of its practical importance for noise and vibration control in aircraft fuselages, pressure vessels, and piping systems, and partly because the large number of natural frequencies and mode shapes that cylindrical shells possess makes the problem mathematically rich. Early analytical solutions were obtained by Rayleigh (1894) using energy methods, and Flügge (1934) and Arnold and Warburton (1953) produced the first reliable frequency solutions for simply supported finite cylinders using full thin-shell theory. Leissa (1973) compiled a comprehensive tabulation of frequency parameters for cylindrical shells with various boundary conditions, identifying the significant numerical differences between frequencies predicted by different shell theories at high circumferential mode numbers. This work provided definitive benchmark data that has been used to validate FEM implementations ever since.

Bardell et al. (1997) reported free vibration results for thin laminated composite cylindrically curved panels using the h-p finite element method, covering a wide range of aspect ratios, thickness ratios, and lamination sequences. Chakravorty et al. (1995) studied fundamental frequencies of point-supported laminated composite cylindrical shells for varying curvature parameters and lamination configurations, demonstrating that the number and position of point supports strongly influence the lowest frequency a finding of direct practical relevance since industrial shells are often supported at discrete locations. Lee and Han (2006) used finite elements to report free and forced vibration of laminated cylindrical shells under central loading. Dogan and Arslan (2009) provided systematic parametric data on free vibration frequencies of shallow cylindrical shells for varying curvature ratios. Ganapathi et al. (2002, 2003, 2004) carried out a sequence of studies on laminated non-circular cylindrical shells with oval and elliptic cross-sections under combined thermal and mechanical loading using HSDT-based FEM.

Tornabene et al. (2013, 2014) produced extensive GDQ-based frequency solutions for FGM doubly curved shells and shell panels with various geometric shapes and boundary conditions, establishing GDQ as a powerful alternative to FEM for shells with regular

geometries. Sofiyev (2016, 2019) reported analytical solutions for free vibration of FGM truncated conical shells using Galerkin method combined with Donnell's shell theory, covering the effects of material grading law, semi-vertex angle, and aspect ratio. Qatu et al. (2012) reviewed vibration of laminated composite thick and thin shells from 1989 to 2012, noting that the effect of boundary conditions on natural frequencies is particularly pronounced for shells compared with flat plates because membrane and bending actions are strongly coupled through curvature. Sayyad and Ghugal (2015) reviewed vibration of composite plates and shells using various shear deformation theories. Recent contributions by Thai et al. (2023) and Van Do and Ong (2024) have applied quasi-3D theories and machine learning accelerated IGA to vibration of multilayered shells, further extending the capabilities available to researchers.

2.3.3 Nonlinear Static Analysis

Geometric nonlinearity in shells arises when deformations become comparable to the shell thickness, causing the stiffness to change with loading. For thin shells under lateral pressure or concentrated loads, the load-deflection relationship becomes nonlinear even before material yield is reached. The earliest nonlinear theoretical frameworks for cylindrical shells were provided by Donnell (1934) and Novozhilov (1953). The Sanders (1963) and Koiter (1960b, 1966) nonlinear theories represent the most reliable frameworks for large-amplitude analyses. Saigal et al. (1986) were the first to apply a total Lagrangian finite element formulation to nonlinear static analysis of laminated composite thin shells with initial geometric imperfections, using a nine-noded iso-parametric element, showing that imperfections of the order of the shell thickness cause significant deviation from the perfect-shell nonlinear load-deflection path.

Schimmels and Palazotto (1994) used the arc-length method to trace the complete load-deflection path for composite spherical shells under point loading, including snap-through instability at the limit point and snap-back behavior in the post-buckling range. Ferreira and Barbosa (2000) studied buckling of laminated cylindrical shells using nine-noded Lagrangian elements and von-Karman nonlinearity, comparing Newton-Raphson and arc-length solution strategies. Han et al. (2008) used a nine-noded Lagrangian element with modified FSDT for geometrically nonlinear analysis of laminated composite thin shells under combined in-plane and lateral loading. Zhao and Liew (2009) applied Sanders nonlinear strain theory with the arc-length method to composite cylindrical shells and reported detailed nonlinear load-deflection curves for various boundary conditions and lamination sequences. Van et al. (2014) combined

von-Karman theory with FSDT and total Lagrangian approach for clamped and hinged cylindrical shells.

The nonlinear static analysis of functionally graded shells has received growing attention. Shen (2009) studied nonlinear bending of FGM cylindrical panels in thermal environments using a perturbation technique and von-Karman nonlinearity, reporting that thermal pre-stress significantly reduces the load-deflection stiffness. Na and Kim (2010) studied the nonlinear bending response of FGM cylindrical shells under thermal and mechanical loading using FSDT finite elements. Arefi and Zenkour (2017) studied nonlinear static analysis of FGM plates and shells using modified couple stress theory, which incorporates microstructural length-scale effects. Gupta and Pradyumna (2021, 2023) conducted nonlinear bending analyses of composite shells with variable fiber angle tow using HSDT and continuation methods, showing that tow-steered designs can achieve significantly lower deflections than conventional straight-fiber laminates under the same loading. Pinho et al. (2022) combined non-orthogonal tensors with finite elements for nonlinear load-deflection paths of shallow and non-shallow shell panels, demonstrating the importance of exact strain measures oversimplified von-Karman-type approximations for deep shells.

2.3.4 Nonlinear Free Vibration Analysis

Nonlinear vibration of shells is considerably more complex than its linear counterpart because the amplitude of vibration affects the instantaneous stiffness, leading to frequency-amplitude dependence, internal resonances, and potentially chaotic response at sufficiently large amplitudes. The seminal work by Evensen (1967) established the hardening-softening duality in the nonlinear frequency response of cylindrical shells, showing that thin shells exhibit softening-type behavior at moderate amplitudes while thick shells may show hardening behavior. Amabili et al. (1998, 1999) made major contributions to understanding large-amplitude vibration of circular cylindrical shells, using a multi-mode Galerkin expansion and continuation methods to compute nonlinear frequency-response curves, including the influence of companion mode participation. Amabili and Paidoussis (2003) published a comprehensive review of geometrically nonlinear vibration of cylindrical shells that remains the most authoritative reference on this topic.

Nanda and Bandyopadhyay (2007, 2008, 2009) systematically studied free and forced nonlinear vibrations of laminated cylindrical and spherical shells using von-Karman nonlinearity, eight-noded iso-parametric elements, and a predictor-corrector time integration scheme, covering a wide range of boundary conditions, lamination sequences, and loading

frequencies. The same group studied transient responses of shells with cutouts and initial geometric imperfections, showing that imperfections generally soften the frequency response. Tsai and Palazotto (1991) had earlier studied nonlinear forced vibrations of composite cylindrical shells under harmonic excitation using HSDT and the total Lagrangian approach. Bich and Nguyen (2012) studied nonlinear vibration of FGM cylindrical shells using improved Donnell's theory with Galerkin method and Runge-Kutta time integration. Amabili and Reddy (2010) applied their new higher-order nonlinear theory to dynamic analysis of laminated composite circular cylindrical shells with geometric imperfections, showing that the theory predicts a significantly different frequency-amplitude relationship from the Donnell or Sanders-Koiter theories for shells with thickness-to-radius ratios above about one-thirtieth.

Recent nonlinear dynamic studies include those of Thai and Kim (2017), who used IGA with HSDT for large-amplitude vibration of FGM cylindrical and spherical shells, and Wang and Zu (2017), who studied nonlinear dynamics of a rotational FGM cylindrical shell subject to aerodynamic and temperature loading, revealing bifurcations and chaotic responses under certain combinations of rotation speed and temperature gradient. In 2024–2025, Li et al. (2024) used a data-driven reduced-order model to predict nonlinear frequency responses of composite cylindrical shells with geometric uncertainties, demonstrating that uncertainties in fiber angle and thickness can lead to substantial scatter in the nonlinear response even when the linear natural frequencies are only mildly affected. Karimiasl et al. (2024) studied nonlinear vibration of composite doubly curved panels with active piezoelectric control layers under hygrothermal loading, combining geometrically exact shell kinematics with fully coupled electromechanical constitutive equations. These emerging studies indicate a strong trend toward integrating multi-physics effects, uncertainty quantification, and data-driven methods in nonlinear shell dynamics.

2.4 Stiffened Shell Analysis

2.4.1 General Aspects of Shell Stiffening

In structural applications requiring large load-carrying capacity over extended spans, cylindrical, spherical, and doubly curved shells are routinely reinforced with ring frames, longitudinal stringers, or grillage-type stiffener layouts. Stiffeners increase the bending rigidity of the shell locally and redirect membrane forces more efficiently to the supports, substantially raising the buckling load and reducing peak deflections and stresses. In aircraft fuselage construction, stringer-frame systems are standard; in offshore and submarine structures, ring-

stiffened cylinders are the norm; in civil engineering roofing, longitudinal and transverse ribs are used to support composite shell panels over long spans. The design of stiffened shells thus requires understanding of the coupled stiffener-shell response under both linear and nonlinear conditions.

The numerical modeling of stiffeners within the shell finite element framework has followed two principal approaches. In the smeared stiffener approach, the stiffener properties are distributed uniformly over the panel area, converting the discrete orthotropic system into an equivalent uniform shell with modified stiffness coefficients. This is computationally convenient but loses information about local stress concentrations at stiffener-skin junctions. In the discrete stiffener approach, stiffeners are modeled explicitly as beam elements connected to the shell midsurface with appropriate offset transformations, preserving the local response at the cost of greater mesh complexity. Most modern finite element packages adopt the discrete approach. The eccentricity of the stiffener with respect to the shell mid-surface introduces additional bending-stretching coupling that must be accounted for through the offset transformation, and this coupling has a significant influence on the nonlinear response.

2.4.2 Linear Analysis

Early finite element work on stiffened shells was carried out by Almroth et al. (1969), who modeled ring-stiffened cylinders under external pressure using smeared stiffener properties and demonstrated good agreement with experimental buckling loads. Bushnell (1976) developed the BOSOR code for linear and nonlinear analysis of ring-stiffened shells of revolution, which became the standard tool for axisymmetric stiffened shell design and was widely used in the aerospace and offshore industries throughout the 1970s and 1980s. Mustafa and Ali (1989) used the smeared approach for a comprehensive parametric study of stiffened cylindrical shells, covering the full design space of stiffener spacing, cross-section size, and panel curvature.

Chattopadhyay et al. (1995) studied static deflections of stiffened laminated composite plates using von-Karman nonlinear strain-displacement relations with Newton-Raphson iterations, developing methods for eccentric stiffener placement directly applicable to cylindrical shell panels. Nayak and Bandyopadhyay (2002) studied free vibration of stiffened composite conoidal shells using eight-noded doubly curved elements, developing stiffener modeling techniques that underpin most subsequent analyses in this geometry. In their 2005 follow-up, nine-noded elements showed improved accuracy in frequency prediction, particularly for higher modes where the element aspect ratio has a stronger influence. Their

2006 work on forced vibration of stiffened isotropic conoids established benchmark data for time-history responses under harmonic loading. Das and Chakravorty (2010) studied stiffened laminated composite conoidal and cylindrical shell panels with varying stiffener orientations and showed that diagonal stiffeners provide better torsional rigidity than orthogonal arrangements for skew-loaded panels.

Samanta and Mukhopadhyay (1999) made an important methodological contribution by developing an FEM formulation that allows stiffeners to be placed at any location within a shell element without requiring mesh lines to coincide with the stiffener positions, greatly simplifying mesh generation for complex stiffener layouts. Jafari and Bagheri (2006) computed natural frequencies and mode shapes for orthogonally stiffened cylinders using an analytical smeared stiffener formulation. Thinh and Nguyen (2013) studied free vibration of stiffened composite cylindrical shells with different stiffener cross-sections using three-dimensional finite elements, demonstrating that the stiffener cross-sectional shape significantly affects the higher natural frequencies. Zhao et al. (2014) applied GDQ to vibration analysis of orthogonally stiffened FGM cylindrical shells, varying the material grading law and stiffener distribution. Wang et al. (2020) developed an analytical-numerical method for free vibration of ring and stringer stiffened cylindrical shells using transfer matrix approach, reporting results with computation times far shorter than equivalent FEM analyses. Recent contributions include Tran et al. (2023), who applied iso-geometric analysis to linear buckling and free vibration of stiffened laminated composite cylindrical shells demonstrating exact geometry representation and superior convergence, and Ansari et al. (2024), who studied the effect of oblique stiffeners on free vibration characteristics of composite cylindrical shells.

2.4.3 Nonlinear Analysis

Nonlinear analysis of stiffened shells is significantly more involved than the unstiffened case because stiffeners introduce geometric irregularities that trigger local buckling modes and create complex post-buckling paths. Singer et al. (1979) reported experimental buckling loads for stringer-stiffened cylinders under axial compression and compared them with theoretical predictions from both smeared and discrete stiffener models, finding that the discrete approach consistently gave better agreement. Gunay (1999) worked on geometrically nonlinear analysis of stiffened cylindrical shallow shells, using the von-Karman assumption and Newton-Raphson iterations, showing that geometric nonlinearity has a stronger influence on stiffened shells than on equivalent unstiffened panels because the stiffeners raise the fundamental linear frequency and reduce lateral compliance. Liao and Reddy (1990) were the first to apply a nonlinear

formulation to stiffened spherical panels, using a nine-noded iso-parametric element with von-Karman nonlinearity.

Goswami and Mukhopadhyay (1995) studied stiffened composite panels with eccentric stiffeners in the geometric nonlinear range, using a twelve-noded iso-parametric element and demonstrating that eccentricity of the stiffener with respect to the shell midsurface introduces bending-stretching coupling even in symmetric laminates. Bich et al. (2013) developed an analytical solution for eccentrically stiffened FGM cylindrical shells with initial geometric imperfections under combined thermal and mechanical loads using Donnell's nonlinear theory and Galerkin method. Bich et al. (2014) extended this to doubly curved FGM panels with imperfections, deriving explicit expressions for the nonlinear buckling loads and post-buckling equilibrium paths. Patel et al. (2005) used HSDT-based FEM to study post-buckling of stiffened composite cylindrical shells under combined axial compression and lateral pressure, tracing the equilibrium path through the limit point using arc-length method, highlighting the sensitivity of the post-buckling path to initial geometric imperfections in the stiffener profile. Lam and Sathiyamoorthy (1999) performed nonlinear transient analysis of ring-stiffened cylinders under explosion loading using finite elements, finding that stiffeners significantly reduce peak deflections but increase the rate of strain buildup in the skin near the stiffener attachment points. Foroutan et al. (2022) studied nonlinear static and dynamic response of stringer-stiffened FGM cylindrical shells under combined axial and lateral loading, employing a smeared stiffener model and Galerkin method with Runge-Kutta integration for the dynamic case. In 2023–2025, Duc et al. (2023) studied nonlinear dynamic response of eccentrically stiffened FGM doubly curved panels with piezoelectric actuators under combined thermal, aerodynamic, and mechanical loading, showing that active piezoelectric control can substantially reduce the amplitude of forced vibration in stiffened FGM panels. Kim et al. (2024) applied iso-geometric analysis to nonlinear buckling of stiffened composite cylindrical shells under axial compression; Nguyen et al. (2025) presented a comprehensive nonlinear dynamic analysis of ring-stiffened cylindrical shells made of FGM nanocomposites under combined mechanical and hygrothermal loading.

2.4.4 Stiffened Spherical, Conoidal, and Other Shell Forms

Research on stiffened non-cylindrical shell forms is considerably less extensive than that for cylindrical shells, but several important contributions exist. Goswami and Mukhopadhyay (1994) showed that bending performance of elliptic paraboloidal panels can be

significantly improved by adding stiffeners in a linear formulation. Samanta and Mukhopadhyay (1999) extended their mesh-independent stiffener technique to composite curved panels including cylindrical and spherical configurations. Das and Chakravorty (2010) provided comprehensive guidelines for stiffener placement in conoidal shell roofs based on parametric finite element studies covering a wide range of aspect ratios and curvature parameters, recommending specific configurations for different loading patterns and geometries.

Bich et al. (2013, 2014) studied eccentrically stiffened FGM cylindrical and doubly curved panels and produced analytical post-buckling solutions, showing that stiffeners with the same total material volume provide higher buckling resistance when arranged in the direction of the larger compressive stress, and that geometric imperfections are more pronounced in stiffened than in unstiffened panels. Trinh et al. (2021) used FSDT and Bubnov-Galerkin method to compute nonlinear buckling loads for FGM spherical panels with orthogonal stiffener systems. Tung and Thanh (2022) incorporated hygrothermal loading effects into the analysis of stiffened composite spherical shells. Kumari and Chakravorty (2010, 2011) showed that stiffeners can partially compensate for the frequency reduction caused by delamination in composite conoidal shells. Chaubey et al. (2020) presented a comprehensive parametric study of stiffened composite conoidal shells under static loading, covering eccentric stiffeners of varying cross-section and reporting in-plane stress resultants along with deflection predictions.

2.5 Skewed Shell Analysis

2.5.1 Background and Motivation

Skewed or parallelogram-shaped shell panels have received substantially less research attention than their rectangular counterparts, despite occurring naturally in several important engineering contexts. In industrial roofing, modular skewed shell units are used to cover trapezoidal plan areas efficiently. In aerospace structures, swept-back wing panels and oblique hull sections involve shells whose edges are non-orthogonal in plan. In naval architecture, stern and bow shell panels have skewed geometries arising from the three-dimensional curvature of the hull form. The structural response of skewed shells differs qualitatively from that of rectangular shells because the skew angle introduces shear-bending coupling even in laminates that would be symmetrically uncoupled in a rectangular configuration. The corners of skewed shells also experience stress concentrations that have no equivalent in rectangular panels.

Most published research on skewed panels has been confined to flat plate configurations. Wang (1997) used a B-spline Rayleigh-Ritz method for multi-modal frequencies of Mindlin skew plates and documented the strong influence of skew angle on frequency parameters, particularly for highly oblique geometries where some frequencies decrease sharply with increasing skew. Ashour (2009) used the finite strip method for frequencies of clamped angle-ply skew plates and demonstrated that the material coupling effects of the laminate interact in a complex manner with the geometric skew coupling. Noh and Lee (2014) studied instability of simply supported skewed plates with delamination. Kallannavar et al. (2020) used eight-noded elements to study frequencies of laminated composite, hybrid, and sandwiched skew plates, covering a wide range of skew angles and lamination sequences. Kiani and Zur (2022) reported frequency parameters for the first six vibration modes of skew plates with clamped, simply supported, and free boundaries.

Nonlinear studies on skewed flat plates include those of Liao and Lee (1993) on buckling of angle-ply plates, Malekzadeh and Karami (2006) on deflections and stresses using differential quadrature, and Singha and Ganapathi (2004) and Singha and Daripa (2007) on frequencies of clamped and simply supported composite plates. Daripa and Singha (2009) investigated corner stress concentration effects on nonlinear stability of skew plates, showing that yielding initiates at the acute corners under large lateral loads. Upadhyay and Shukla (2013) used von-Karman nonlinearity and HSDT for nonlinear bending of skew composite plates and reported detailed stress distributions for varying skew angle and lamination. These flat plate studies provide a foundation for understanding skewed curved panels, but the curvature introduces additional stiffness and coupling effects that cannot be captured by plate models.

2.5.2 Linear Analysis

Research on skewed curved shell panels is markedly limited compared with the extensive literature on rectangular shells. The transformation from rectangular to skewed geometry requires the use of oblique coordinate systems that complicate both the formulation of governing equations and the numerical implementation of boundary conditions. Early attempts to address skewed shell analysis used approximate methods based on the Ritz technique with oblique coordinate polynomial expansions. For flat skew plates, Durvasula (1969) derived exact Rayleigh-Ritz frequency solutions for simply supported skew plates in oblique coordinates. Kaul and Cadambe (1956) reported deflection results for skew plates under uniform pressure using a series solution. The extension of these approaches to doubly

curved geometries is non-trivial because the Lamé parameters governing the metric of the curved surface are modified by the skew angle in a way that depends on the specific shell form. Chaubey et al. (2018) made the first reported systematic investigation of skewed elliptic paraboloidal shell panels, studying their free vibration characteristics using a linear FSDT-based finite element formulation in oblique coordinates. They reported natural frequencies and mode shapes for varying skew angles (0° to 45°), curvature ratios, aspect ratios, thickness ratios, and boundary conditions. The study revealed that increasing skew angle generally reduces the fundamental frequency and alters the mode shapes substantially compared with rectangular panels of the same area and curvature. The influence of skew angle was found to be more pronounced for simply supported than for clamped boundaries, and the interaction between skew and curvature was shown to be complex and non-monotonic. For skewed cylindrical shells, Chao et al. (1988) studied bending of skewed laminated composite cylindrical panels using a C0 finite element formulation and oblique coordinate transformation, reporting deflections and in-plane stresses for various skew angles and lamination configurations. Haldar and Manna (2003) analyzed skewed cylindrical and conical shell panels using a high-precision triangular shell element. Leissa et al. (1993) studied vibration of cantilevered skewed flat plates and curved panels using the Ritz method.

For skewed conoidal shells, Das and Chakravorty (2009) reported static bending results for point-supported configurations, establishing that skew angle significantly modifies the deflection pattern and the location of peak stress resultants. In more recent work, Hosseini-Hashemi et al. (2018) studied free vibration of moderately thick skewed FGM plates using the Ritz method with oblique plate functions. Kumar et al. (2019) applied the extended finite element method (XFEM) to linear static analysis of skewed laminated composite plates with cracks, demonstrating that stress intensity factors at crack tips are sensitive to skew angle. Zhou and Wang (2023) used IGA to study linear bending and free vibration of skewed thick composite cylindrical panels, demonstrating that IGA provides more accurate results than conventional FEM for highly skewed geometries (skew angle greater than 40°) because the NURBS parametrization naturally handles the oblique domain without coordinate transformation errors. Dat et al. (2024) applied a cell-based smoothed FSDT to static analysis of skewed composite shell panels with cutouts under various loading conditions, showing good accuracy even for meshes with highly distorted elements.

2.5.3 Nonlinear Analysis

Nonlinear analysis of skewed shell panels is even less developed than the linear counterpart, reflecting the combined challenges of handling non-orthogonal coordinates, curved geometry, and large deformation kinematics simultaneously. The few available nonlinear studies of skewed panels are predominantly for flat plates. The extension to curved skewed panels requires a complete reformulation of the geometric stiffness matrix in oblique curvilinear coordinates, which is algebraically intensive and has deterred many researchers. Singha and Ganapathi (2004) used eight-noded iso-parametric elements with von-Karman nonlinearity to study large-amplitude free vibration of simply supported and clamped composite skew plates, reporting backbone curves for various skew angles and lamination sequences. The study showed that the nonlinear hardening effect increases with skew angle for clamped plates and decreases for simply supported ones, attributable to the change in membrane boundary conditions with skew. Singha and Daripa (2007) extended this analysis to various boundary conditions.

For skewed curved shell panels in the nonlinear range, Civalek (2021) used the discrete singular convolution method for nonlinear vibration of skewed composite cylindrical shells, reporting hardening-type frequency-amplitude relationships for skew angles up to 30°. Trung et al. (2022) presented the first nonlinear bending analysis of skewed elliptic paraboloidal composite shell panels using von-Karman nonlinearity and an eight-noded iso-parametric element in oblique curvilinear coordinates, reporting load-deflection curves for skew angles up to 45° and various boundary conditions. The study found that skew angle has a significant softening effect on the nonlinear stiffness, reducing the load at which nonlinear behavior becomes significant and increasing peak deflections relative to rectangular panels under the same loading. However, the study was limited to unstiffened panels with uniform loading, and did not address the effects of stiffeners or non-uniform boundary conditions.

Duc et al. (2023) studied nonlinear dynamic response of eccentrically stiffened FGM doubly curved skewed panels under thermal and mechanical loading using Donnell's nonlinear theory and smeared stiffener model, representing an important step toward the combined analysis of stiffened skewed curved panels. However, their formulation was limited to shallow panels and did not include the full geometric nonlinearity required for large-amplitude responses. Pham et al. (2024) performed iso-geometric nonlinear static analysis of skewed composite folded plate structures, demonstrating that exact geometric representation is particularly important for skewed configurations because conventional mesh-based methods

introduce additional approximation errors at the skewed boundaries. In summary, the nonlinear analysis of skewed shell panels particularly those with stiffening, complex boundary conditions, and various curvature ratios remains substantially underdeveloped.

2.6 Critical Discussion and Research Gaps

The foregoing review reveals a research landscape that is mature in some areas and significantly incomplete in others. The following critical synthesis organizes the main observations and identifies the specific gaps that motivate the present study.

Shell theories have reached a high level of sophistication. The classical Kirchhoff-Love theory is well understood to be adequate only for very thin homogeneous shells under quasi-static loading well below buckling. FSDT with appropriate shear correction factors is the standard choice for moderately thick shells and for laminated composites in structural engineering applications, providing sufficient accuracy for deflections, stress resultants, and fundamental frequencies at modest computational cost. HSDT, particularly the Reddy third-order theory and the Amabili-Reddy higher-order nonlinear theory, provides improved accuracy for thicker shells and for the through-thickness stress distribution, and should be preferred whenever local failure criteria must be evaluated. The CUF framework represents the most general approach and can generate theories of any desired order, though at higher computational cost. Iso-geometric analysis with NURBS basis functions offers geometric exactness and high continuity, making it attractive for thin shell formulations.

For cylindrical shells, both linear and nonlinear behavior are well understood. A vast body of literature covers static deflections, natural frequencies, forced vibration, post-buckling, and transient responses for a wide range of materials, geometries, and boundary conditions. The finite element method with FSDT and nine-noded iso-parametric elements has proven to be the most reliable and flexible tool for this class of problem. Geometric nonlinearity based on von-Karman assumptions with Newton-Raphson or arc-length solution methods has been successfully applied. More recent higher-order nonlinear theories and iso-geometric methods have demonstrated superior performance for specific classes of problems involving large amplitudes, deep shells, or complex geometries.

For laminated composite shells specifically, the literature shows that material anisotropy, bending-stretching coupling in unsymmetric laminates, and low interlaminar shear stiffness all require careful treatment. FSDT with shear correction factors derived from the specific laminate is the minimum acceptable theory for composites; HSDT is preferred

wherever stress analysis through the thickness is required. For functionally graded shells, GDQ and IGA methods have emerged as strong alternatives to conventional FEM because of their high accuracy with relatively coarse discretizations.

For stiffened shells, the picture is less complete. A reasonable body of work covers linear vibration and buckling of stiffened cylindrical shells using both smeared and discrete stiffener models, and some nonlinear buckling and post-buckling analyses exist. However, systematic parametric studies covering the combined effects of stiffener configuration, lamination sequence, geometric nonlinearity, and complex boundary conditions are less common. For non-cylindrical stiffened shells particularly stiffened conoidal, spherical, and elliptic paraboloidal forms the literature is considerably sparser, and comprehensive design guidelines are not available.

For skewed shell panels, the research gap is most pronounced. The available literature is largely confined to flat skewed plates, with a handful of studies on linear vibration of skewed curved shells. Nonlinear analysis of skewed curved panels is almost entirely absent from the published literature, with only a few very recent papers (Trung et al. 2022, Duc et al. 2023) beginning to address this area for specific configurations. The combination of skewed geometry, stiffening, composite lamination, and geometric nonlinearity in a single investigation has, to the best of the present author's knowledge, not been reported. The absence of such combined analyses is particularly notable given the practical engineering significance of these configurations in composite shell roofing for industrial buildings and in swept wing panel structures.

The specific research gap targeted by the present study can therefore be stated as follows: the nonlinear static and dynamic behavior of stiffened skewed elliptic paraboloidal laminated composite shell panels, under uniformly distributed loading and harmonic excitation, for varying skew angle, curvature ratio, lamination sequence, stiffener configuration, and boundary condition, has not been investigated. This represents a practically important structural configuration, occurring in composite shell roofing for industrial buildings and in swept wing panel structures, for which no quantitative design data currently exists in the published literature. The present work is aimed at filling this gap by providing a rigorous finite element investigation using FSDT-based formulation in oblique curvilinear coordinates, validated against available linear benchmarks and extended systematically into the nonlinear static and dynamic regimes. The results are expected to provide the first comprehensive parametric database for this class of structures and to yield practical design guidance for engineers working with stiffened skewed composite shell systems.

Chapter 3

Scope of the Present Study

3.1 General

The focus of the present investigation is the geometrically nonlinear flexural response of laminated composite cylindrical shell panels reinforced by obliquely oriented stiffeners and examined under five distinct boundary condition combinations, subjected to three different forms of transverse pressure. Each constituent features the anisotropic composite laminate, the singly-curved cylindrical geometry, the skewed stiffener arrangement, and the non-uniform edge restraints independently poses analytical difficulties; taken together, they yield a structural problem of substantial complexity that remains unaddressed in a systematic manner within the published literature. Resolving this combined problem carries clear engineering relevance: cylindrical shell forms are widely favoured in aerospace, civil, and marine applications owing to their high load-carrying efficiency, relative ease of manufacture, and structural elegance.

The nonlinear bending behavior of composite cylindrical shells connects several concurrently active research domains. Geometric nonlinearity the progressive alteration of structural stiffness as finite deformations accumulate becomes consequential whenever transverse displacements are of a magnitude comparable to the panel's reference dimensions. For moderately thin cylindrical panels subjected to transverse pressure, this regime is frequently encountered under service conditions, and formulations that rely on linear kinematic assumptions risk significantly underestimating displacements while overestimating load capacity. While linear bending and free vibration of laminated cylindrical panels have received notable attention in the research community, studies employing geometrically nonlinear frameworks are comparatively limited, and no published investigation has simultaneously considered skewed stiffening and non-uniform edge restraint. The current work is directly motivated by this deficiency.

3.2 Present Study

The oblique orientation of the stiffeners with respect to the shell's principal axes introduces a bending twisting interaction that is entirely absent in conventionally orthogonal stiffening arrangements. When a stiffener is inclined at a skew angle to the panel axes, its flexural rigidity develops components along both the longitudinal and lateral directions,

producing a coupled response in which an applied transverse load generates simultaneous bending and torsion within the stiffener. This interaction modifies the spatial distribution of internal force and moment resultants throughout the shell and alters the geometry of the deformed configuration in a manner that can only be faithfully reproduced by treating each stiffener as a discrete three-dimensional structural member rather than distributing its contribution uniformly across the shell surface. The present study systematically varies the stiffener skew angle φ across a broad range, thereby facilitating a rigorous evaluation of how increasing obliquity influences both the deflection profile and the resultant stress distribution with particular attention to the twisting moment M_{xy}, whose relative magnitude grows progressively with skew angle.

The edge restraint configurations adopted in this study reflect conditions encountered in practical construction. Real shell structures are routinely supported in a non-uniform manner: certain edges may be rigidly integrated into supporting walls or rigid frames while the remaining edges bear against flexible beams or have alternating clamped and simply supported restraints. Accordingly, five boundary condition cases are examined CCCC, SSSS, SCSC, CSCS, and SSCC spanning the fully clamped condition at one extreme, which imposes maximum rotational and translational constraint, through to mixed configurations that disrupt the load-path symmetry associated with uniform edge support. Such asymmetry gives rise to localised stress concentrations and non-symmetric deflection fields that uniform-boundary idealizations cannot predict. Examining these five restraint configurations in conjunction with three load distributions and multiple laminate lay-ups furnishes a thorough understanding of how edge restraint interacts with other structural variables to govern overall flexural behaviour.

To examine the foregoing effects, an iso-parametric finite element model with C^0 continuity has been constructed. The shell surface is discretised using eight-noded serendipity quadrilateral elements, while the stiffeners are modelled as three-noded beam elements sharing nodal degrees of freedom with the adjoining shell elements. The theoretical basis of the formulation is first-order shear deformation theory, which incorporates transverse shear flexibility, a factor of heightened importance in composite laminates where the disparity between in-plane and transverse shear stiffnesses is considerable. Geometrically nonlinear strain terms are introduced through the von Kármán hypothesis. The resultant nonlinear algebraic system is resolved iteratively via the Newton–Raphson algorithm, wherein the tangent stiffness matrix is recomputed at every iteration to reflect the current deformed geometry. Three spatial load distributions are applied uniform, sinusoidal (sin–sin), and

cosinusoidal (cos–cos) enabling direct evaluation of how load non-uniformity influences the overall structural response.

Prior to the parametric investigation, the formulation is verified by comparing computed outputs against established benchmark solutions for configurations where reliable reference data exist. Once the formulation's fidelity is confirmed, a comprehensive parametric study is undertaken. The variables examined include stiffener skew angle, laminate stacking arrangement (cross-ply and angle-ply sequences), composite material system (graphite/epoxy and glass/epoxy), side-to-thickness ratio (a/h), radius-of-curvature ratio ($R_{\gamma\gamma}/b$), and stiffener characteristics encompassing quantity, inclination, cross-sectional depth, and eccentricity. The response quantities of interest are nonlinear central deflection and the full set of force and moment resultants. The parametric results are structured to yield design-relevant conclusions, identifying the laminate and stiffener combinations that deliver superior structural efficiency under each boundary condition and load distribution.

Chapter 4

MATHEMATICAL FORMULATION

4.1 General

This chapter presents the mathematical framework and computational solution strategy employed in the current investigation. An iso-parametric finite element model is established to examine the behaviour of a shallow, singly curved laminated composite cylindrical shell panel (Figure 4.1), incorporating both geometrically linear and nonlinear strain measures. The governing nonlinear equilibrium equations, the shell element description, the nonlinear strain-displacement relationships, and the iterative solution methodology are each elaborated in the sections that follow.

The shell panel is fabricated from graphite-epoxy composite material with a uniform cross-sectional thickness h. Multiple laminae are adhesively bonded through the thickness to form the laminated construction. The fibre orientation angle of each individual lamina is denoted by θ, measured with respect to the global X-axis. The panel is loaded by a transversely applied downward pressure distributed over its surface.

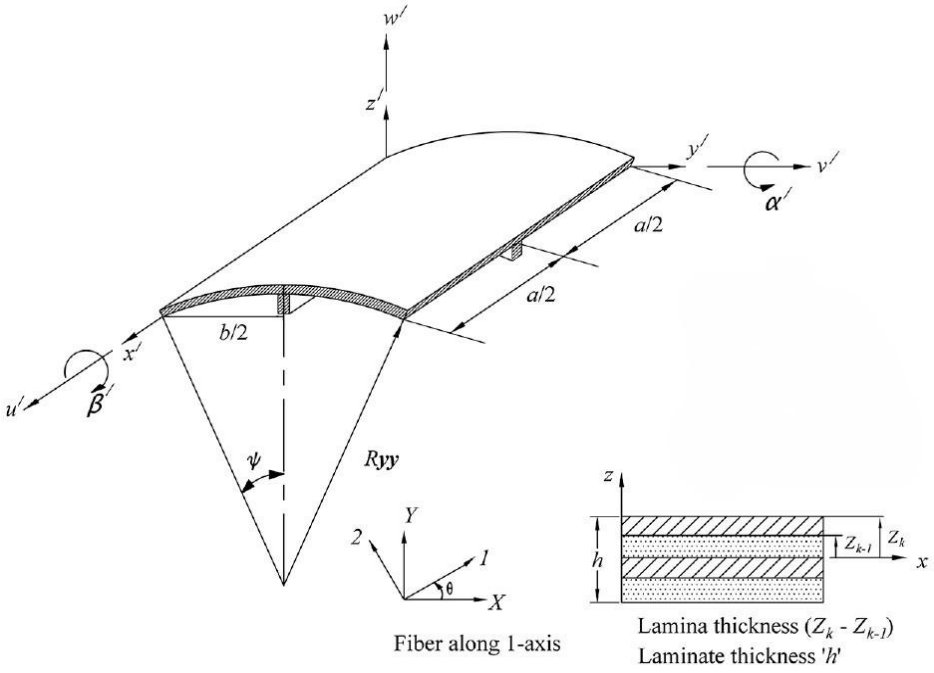

Figure 4.1: Stiffened cylindrical shell panel

4.2 Finite Element Method

In the finite element approach, the cylindrical shell domain is partitioned into a collection of smaller sub-regions, within each of which the governing differential equations are solved numerically. The global structural response is then obtained by assembling the individual equation sets corresponding to each sub-region. Each such sub-region is termed an element, and the systematic subdivision of the problem domain into a finite number of elements constitutes the process known as discretization. Adjacent elements are interconnected at discrete locations designated as nodes.

4.3 Selection of Element

The element type selected for a finite element analysis must be capable of adequately representing the geometry and deformation of the shell both in its original undeformed configuration and throughout the deformation process. In the present work, an eight-noded doubly curved serendipity element with C^0 continuity is employed, characterised by three independent radii of curvature: R_{xx}, R_{yy}, and R_{xy}. For the cylindrical shell geometry, the radius R_{xx} is assigned a numerically large value (10^{30}) so that curvature in that direction is rendered effectively zero.

The curved quadratic iso-parametric element comprises four corner nodes and four mid-side nodes positioned along the element edges. Coordinate transformation between the natural coordinate system (ξ, η) and the Cartesian coordinate system is accomplished through the Jacobian matrix. The displacement field within each element is expressed in terms of the nodal displacements through the interpolation functions.

A geometrically nonlinear iso-parametric C^0 finite element code is developed, utilising eight-noded quadrilateral elements throughout the discretization. The element configuration and the associated shape functions are illustrated in Figure 4.2. The element displacement vector $\{\delta\}$ is expressed as:

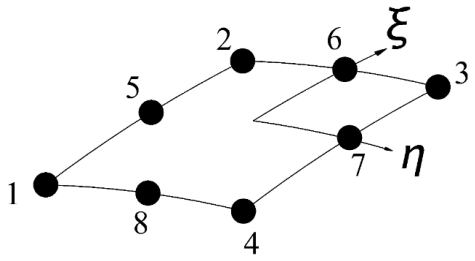

$$N_i=\frac{1}{4}(1+\xi\xi_i)(1+\eta\eta_i)(\xi\xi_i+\eta\eta_i-1) \quad i,j=1,2,3,4$$
$$N_i=\frac{1}{2}(1+\eta\eta_i)(1+\xi^2) \quad i,j=6,8$$
$$N_i=\frac{1}{2}(1+\xi\xi_i)(1+\eta^2) \quad i,j=5,7$$

Figure 4.2: Eight noded element and shape functions.

A nonlinear, iso-parametric C^0 finite element code is proposed which adopts eight noded elements. Figure 4.2 depicts the element and interpolation functions. The element displacements $\{\delta\}$ are given below,

$$\{\delta\} = \sum_{i=1}^{8} [N_i]\{\delta_i\} \qquad \text{where } \{\delta_i\} = \{u_i \quad v_i \quad w_i \quad \alpha_i \quad \beta_i\}^T \qquad (1)$$

$[N_i]$ and $\{\delta_i\}$ are interpolation functions and displacements at the ith node of element.

4.4 Discretization of Shell Surface

The cylindrical shell surface is divided into an appropriate number of finite elements to ensure adequate spatial resolution of the displacement field across the entire domain. The subdivision must be carried out with sufficient refinement to faithfully capture the variation in displacements, strains, and stress resultants throughout the panel. Determining the optimal element density is achieved through a systematic convergence study, wherein the mesh is progressively refined until the computed results stabilize to within an acceptable tolerance; this exercise is presented in the subsequent chapter. While the primary objective of the present work is the investigation of the nonlinear bending response of cylindrical shell panels, the discretization strategy is equally guided by consideration of computational efficiency, ensuring that accurate results are obtained without unnecessary expenditure of computational resources.

4.5 Selection of Shape Functions

Shape functions, also referred to as interpolation functions, are employed to approximate the variation of displacement quantities within each element from the known values at the element nodes. The iso-parametric element formulation is adopted in the present work, whereby the same set of shape functions used to interpolate the displacement field is also applied to map the geometry of the curved shell surface from the natural coordinate space (ξ, η) to the physical Cartesian coordinate space. This iso-parametric mapping ensures geometric consistency between adjacent elements and accurately represents curved boundaries without introducing spurious distortion. The displacement polynomial basis is constructed following Pascal's triangle, which provides a hierarchical and complete polynomial expansion that guarantees spatial isotropy and convergence with mesh refinement.

$$U(\xi,\eta)=A_0 +A_1\xi + A_2\eta + A_3\xi^2 + A_4\xi\eta + A_5\eta^2 + A_6\xi^2\eta + A_7\xi\eta^2 \quad (2)$$

By solving it at eight nodal points we can obtain the shape functions,

$$N_i = \frac{1}{4}(1+\xi\xi_i)(1+\eta\eta_i)(\xi\xi_i+\eta\eta_i-1) \qquad i=1,2,3,4 \quad (3)$$

$$N_i = \frac{1}{2}(1+\xi\xi_i)(1+\eta^2), \qquad i=5,7 \quad (4)$$

$$N_i = \frac{1}{2}(1+\eta\eta_i)(1+\xi^2), \qquad i=6,8 \quad (5)$$

Shape functions for x-stiffener

$$N_i = \xi\xi_i(1+\xi\xi_i) \qquad i=1,3$$
$$N_i = (1-\xi^2) \qquad i=2 \quad (6)$$

Shape function for y-stiffener

$$N_i = \eta\eta_i(1+\eta\eta_i), \qquad i=1,3 \quad (7)$$

$$N_i = (1-\eta^2), \qquad i=2$$

Where N_i denotes the shapes function at i^{th} node having natural coordinates ξ_i and η_i.

The correctness of the shape functions is checked from the relations

$$\sum N_i=1,\ \sum \partial N_i/\partial\xi = 0 \text{ and } \sum \partial N_i/\partial\eta = 0 \quad (8)$$

Interpolation of geometric co-ordinates can also be performed by using the iso-parametric finite element shape functions,

$$x = \sum N_i x_i \text{ and } y = \sum N_i y_i, \qquad i=1 \text{ to } 8 \tag{9}$$

Where x_i and y_i are the geometric co-ordinates of the ith node.

4.6 Selection of Generalized Degrees of Freedom

4.6.1 shell structure

A shell structure is inherently three-dimensional in nature, and a rigorous representation would require three-dimensional elements possessing the corresponding spatial dimensions. However, since the cylindrical shell panels examined in the present study are geometrically thin, adopting full three-dimensional elements would introduce many additional nodes and consequently a disproportionate increase in the total degrees of freedom, rendering the analysis computationally expensive without a commensurate gain in accuracy. To circumvent this inefficiency, a two-dimensional element formulation is adopted, which adequately captures the essential structural behaviour while maintaining computational economy.

Accordingly, five degrees of freedom are assigned to each node of the two-dimensional element: three translational components (*U, V, W*) along the respective coordinate axes and two independent rotational components (θ_x, θ_y) about the in-plane axes. The resulting element retains nodes exclusively at the mid-plane of the shell, consistent with the assumptions of first-order shear deformation theory. Under this formulation, a straight line initially oriented along the thickness direction remains straight following deformation but is not constrained to remain perpendicular to the deformed mid-plane, thereby allowing for the transverse shear deformations that are particularly significant in laminated composite construction. The orientations of the generalised displacement components adopted at each node are illustrated in Figure 4.1.

The following expressions establish the relations between displacement at any point with respect to the co-ordinates ξ and η and the nodal degrees of freedom.

$$u = \sum_{i=1}^{8} N_i u_i \quad v = \sum_{i=1}^{8} N_i v_i \quad w = \sum_{i=1}^{8} N_i w_i \quad \alpha = \sum_{i=1}^{8} N_i \alpha_i$$
$$\beta = \sum_{i=1}^{8} N_i \beta_i \tag{10}$$

The generalized displacement vector $[u]$ of an element is expressed in terms of the shape function $[N]$ and nodal degrees of freedom $\{\delta_i\}$ as:

$$\{\delta\} = \sum_{i=1}^{8} [N_i]\{\delta_i\} \tag{11}$$

$$\text{i.e. } \{u\} = \begin{Bmatrix} u \\ v \\ w \\ \alpha \\ \beta \end{Bmatrix} \begin{bmatrix} [N_i] & & & & \\ & [N_i] & & & \\ & & [N_i] & & \\ & & & [N_i] & \\ & & & & [N_i] \end{bmatrix} \begin{Bmatrix} u_i \\ v_i \\ w_i \\ \alpha_i \\ \beta_i \end{Bmatrix} \tag{12}$$

where, $[N_i] = [N_1 \quad N_2 \quad N_3 \quad \ldots\ldots\ldots\ldots \quad N_7 \quad N_8]$

and, $[u_i] = [u_1 \quad u_2 \quad u_3 \quad \ldots\ldots\ldots\ldots \quad u_7 \quad u_8]$

$[v_i] = [v_1 \quad v_2 \quad v_3 \quad \ldots\ldots\ldots\ldots \quad v_7 \quad v_8]$

$[w_i] = [w_1 \quad w_2 \quad w_3 \quad \ldots\ldots\ldots\ldots \quad w_7 \quad w_8]$

$[\alpha_i] = [\alpha_1 \quad \alpha_2 \quad \alpha_3 \quad \ldots\ldots\ldots\ldots \quad \alpha_7 \quad \alpha_8]$

$[\beta_i] = [\beta_1 \quad \beta_2 \quad \beta_3 \quad \ldots\ldots\ldots\ldots \quad \beta_7 \quad \beta_8]$

4.6.2 stiffeners

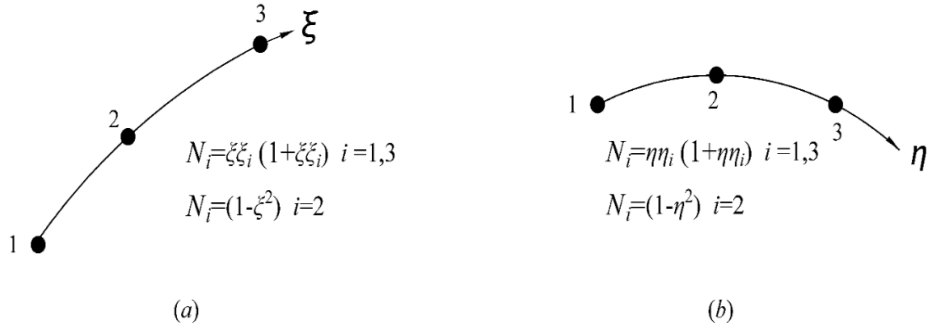

Figure 4.3: Elements for (a) *x*-stiffener and (b) *y*-stiffener.

The stiffeners are single layered composites with longitudinal lamination. Figure 4.3 depicts the three noded elements for stiffener along with interpolation functions.

The displacements and rotations of stiffeners are as follows:

$\{\delta_{sx}\} = \{u_{sx} \quad w_{sx} \quad \alpha_{sx} \quad \beta_{sx}\}^T$ for *x*-stiffener.

$\{\delta_{sy}\} = \{v_{sy} \quad w_{sy} \quad \alpha_{sy} \quad \beta_{sy}\}^T$ for *y*-stiffener.

***x* - stiffener:**

The element displacements $\{\delta_{sx}\}$ are given below,

$$\{\delta_{sx}\} = \sum_{j=1}^{3} [N_{\xi j}]\{\delta_{sxj}\} \qquad \text{where } \{\delta_{sxj}\} = \{u_{sxj} \quad w_{sxj} \quad \alpha_{sxj} \quad \beta_{sxj}\}^T \tag{13}$$

$[N_{\xi j}]$ and $\{\delta_{sxj}\}$ are interpolation functions and displacements at the jth node of the stiffener.

***y* - stiffener:**

The element displacements $\{\delta_{sy}\}$ are given below,

$$\{\delta_{sy}\} = \sum_{j=1}^{3} [N_{\eta j}]\{\delta_{syj}\} \qquad \text{where } \{\delta_{syj}\} = \{v_{syj} \quad w_{syj} \quad \alpha_{syj} \quad \beta_{syj}\}^T \tag{14}$$

$[N_{\eta j}]$ and $\{\delta_{syj}\}$ are interpolation functions and displacements at the jth node of the stiffener element.

4.7 Strain- Displacement Relationship

4.7.1 shell structure

The non-orthogonal (X - Y) and orthogonal (x - y) axes are taken at the mid-depth of panel. The surface of skewed panel is described through the equations given below,

$$x = X + Y\sin\phi,\ y = Y\cos\phi,\ z = Z \text{ where } \phi = \text{skew angle} \tag{15}$$

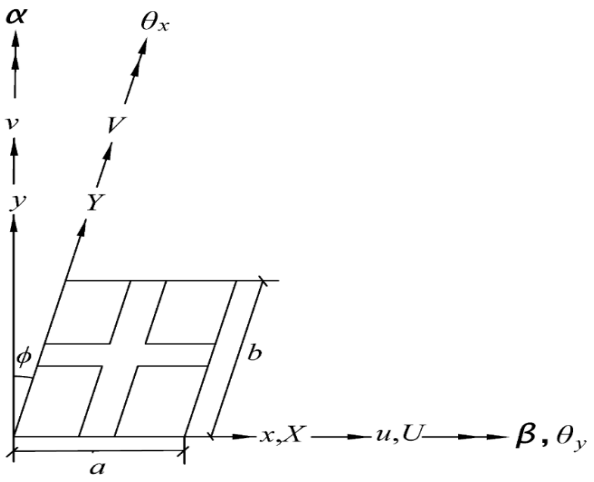

Figure 4.4: Degree of freedom of skewed panel

The displacements (U, V and W) and rotations (θ_x, θ_y) of skewed panel, as depicted in Figure 4.4, are transferred to orthogonal axes using the following equation,

$$\{ d \} = [T]\{\delta\} \tag{16}$$

where $\{d\} = \{U \;\; V \;\; W \;\; \theta_x \;\; \theta_y\}^T$ for $X-Y$ axes.

$\{\delta\} = \{u \;\; v \;\; w \;\; \alpha \;\; \beta\}^T$ for $x-y$ axes.

and $[T] = \begin{bmatrix} sec\phi & 0 & 0 & 0 & 0 \\ -tan\phi & 1 & 0 & 0 & 0 \\ 0 & 0 & 1 & 0 & 0 \\ 0 & 0 & 0 & 1 & -tan\phi \\ 0 & 0 & 0 & 0 & sec\phi \end{bmatrix}$

For any given skew angle (ϕ) $\geq 0^0$, the panels are shallow i.e., rise/span = 0.2.

Hence, for $\phi \geq 0^0$, $r_{xx} = R_{xx}$ and $r_{yy} = R_{yy} \times (\cos\phi)$.

r_{xx}, r_{yy} = Radii of curvatures of non-skewed panel ($\phi = 0^0$).

R_{xx}, R_{yy} = Radii of curvatures of skewed panel ($\phi > 0^0$).

The strain-displacement relations based on improved first order approximation theory for thin shell are established. Details description of the displacements is furnished below.

$$u=u_0 + z\alpha,\ v= v_0+ z\beta,\ w=w_0 \tag{17}$$

Where, u_0, v_0, w_0 = Mid-plane translations along x, y and z axis respectively and z is the distance of fiber from mid-plane along thickness direction.

The generalized strain vector at any arbitrary depth (z) of the panel is given below which follows the guidelines of Reddy (2004).

$$\{\varepsilon\} = \{\varepsilon\}^0 + z\{\kappa\} \tag{18}$$

$$\begin{bmatrix} \varepsilon_x \\ \varepsilon_y \\ \gamma_{xy} \\ \gamma_{xz} \\ \gamma_{yz} \end{bmatrix} = \begin{bmatrix} \varepsilon_x^0 \\ \varepsilon_y^0 \\ \gamma_{xy}^0 \\ \gamma_{xz}^0 \\ \gamma_{yz}^0 \end{bmatrix} + z \begin{bmatrix} k_x \\ k_y \\ k_{xy} \\ k_{xz} \\ k_{yz} \end{bmatrix} \tag{19}$$

where $\{\kappa\} = \left\{\frac{\partial\theta_x}{\partial X} \quad \frac{\partial\theta_y}{\partial Y} \quad \frac{\partial\theta_x}{\partial Y} + \frac{\partial\theta_y}{\partial X} \quad 0 \quad 0\right\}^T$

and $\{\varepsilon\}^0$ is given below,

$$\{\varepsilon\}^0 = \{\varepsilon\}^L + \{\varepsilon\}^{NL} \tag{20}$$

$\{\varepsilon\}^L$, $\{\varepsilon\}^{NL}$ = Linear and nonlinear mid-surface strain vectors, respectively, which are expressed below,

$$\{\varepsilon\}^L = \begin{Bmatrix} \frac{\partial U}{\partial X} - \frac{W}{R_{xx}} \\ \frac{\partial V}{\partial Y} - \frac{W}{R_{yy}} \\ \frac{\partial U}{\partial Y} + \frac{\partial V}{\partial X} - \frac{2W}{R_{xy}} \\ \theta_x + \frac{\partial W}{\partial X} \\ \theta_y + \frac{\partial W}{\partial Y} \end{Bmatrix}, \{\varepsilon\}^{NL} = \begin{Bmatrix} \frac{1}{2}\left(\frac{\partial W}{\partial X} - \frac{U}{R_{xx}}\right)^2 \\ \frac{1}{2}\left(\frac{\partial W}{\partial Y} - \frac{V}{R_{yy}}\right)^2 \\ \left(\frac{\partial W}{\partial X} - \frac{U}{R_{xx}}\right)\left(\frac{\partial W}{\partial Y} - \frac{V}{R_{yy}}\right) \\ 0 \\ 0 \end{Bmatrix} \tag{21}$$

$$\text{and} \quad \begin{bmatrix} k_x \\ k_y \\ k_{xy} \\ k_{xz} \\ k_{yz} \end{bmatrix} = \begin{bmatrix} \frac{\partial \theta_x}{\partial X} \\ \frac{\partial \theta_y}{\partial Y} \\ \frac{\partial \theta_x}{\partial Y} + \frac{\partial \theta_y}{\partial X} \\ 0 \\ 0 \end{bmatrix} \tag{22}$$

The transverse shear strains are taken as constant. Shear correction factors are taken as unity. R_{xy} = radius of cross-curvature. For the hyperbolic paraboloidal panel, $R_{xy} = 10^{40}$ is assigned to have the curvature effectively zero.

The surface equation of any shell form can be represented by the equation $z = f(x, y)$. For shallow shells where, according to Vlasov (1958), the ratio of the rise to the shorter plan dimension is less than 0.2, the surface curvatures can be approximately represented as,

$$\frac{1}{R_x} = \frac{\partial^2 z}{\partial x^2}, \qquad \frac{1}{R_y} = \frac{\partial^2 z}{\partial y^2} \quad \text{and} \quad \frac{1}{R_{xy}} = \frac{\partial^2 z}{\partial x\, \partial y} \tag{23}$$

The strain-displacement equation is furnished below,

$$\{\varepsilon\}^0 = \left([B_L] + \frac{1}{2}[B_{NL}]\right)[T]\{\delta_i\} \tag{24}$$

where $\{\varepsilon\}^0 = \{\varepsilon_X^0 \quad \varepsilon_Y^0 \quad \gamma_{XY}^0 \quad k_X \quad k_Y \quad k_{XY} \quad \gamma_{XZ}^0 \quad \gamma_{YZ}^0\}^T$

$[B]^L$ matrix is the same as given by Chakravorty et al. (1995). $[B]^{NL}$ is the same as given in Bakshi and Chakravorty (2014).

$$[B_{NL}] = [A][G] \tag{25}$$

$$[A] = \begin{bmatrix} \dfrac{\partial w_0}{\partial x} - \dfrac{u_0}{R_{xx}} & 0 \\ 0 & \dfrac{\partial w_0}{\partial y} - \dfrac{v_0}{R_{yy}} \\ \dfrac{\partial w_0}{\partial y} - \dfrac{v_0}{R_{yy}} & \dfrac{\partial w_0}{\partial x} - \dfrac{u_0}{R_{xx}} \end{bmatrix},$$

$$[G] = \begin{bmatrix} -\dfrac{N_i}{R_{xx}} & 0 & \dfrac{\partial N_i}{\partial x} & 0 & 0 \\ 0 & -\dfrac{N_i}{R_{yy}} & \dfrac{\partial N_i}{\partial y} & 0 & 0 \end{bmatrix} \qquad i = 1 \text{ to } 8$$

$$[B_L] = \sum_{i=1}^{8} \begin{bmatrix} \dfrac{\partial N_i}{\partial x} & 0 & 0 & 0 & 0 \\ 0 & \dfrac{\partial N_i}{\partial y} & -\dfrac{1}{R_{yy}} & 0 & 0 \\ \dfrac{\partial N_i}{\partial y} & \dfrac{\partial N_i}{\partial x} & -\dfrac{2}{R_{xy}} & 0 & 0 \\ 0 & 0 & 0 & \dfrac{\partial N_i}{\partial x} & 0 \\ 0 & 0 & 0 & 0 & \dfrac{\partial N}{\partial y} \\ 0 & 0 & 0 & \dfrac{\partial N_i}{\partial y} & \dfrac{\partial N_i}{\partial x} \\ 0 & 0 & \dfrac{\partial N_i}{\partial x} & N_i & 0 \\ 0 & 0 & \dfrac{\partial N_i}{\partial y} & 0 & N_i \end{bmatrix} \tag{26}$$

For $\phi \geq 0^0$, both $[B]^L$ and $[B]^{NL}$ matrices adopt

$r_{xx} = R_{xx}$ and $r_{yy} = -R_{yy}\cos\phi$.

The following can be obtained from Equation (8),

$$\frac{\partial\{\varepsilon\}0}{\partial\{\delta\}} = [T]\left[\overline{B}\right] \qquad \text{and} \qquad [\bar{B}] = [B_L] + [B_{NL}] \tag{27}$$

4.7.2 Strain-displacement relationship for stiffeners

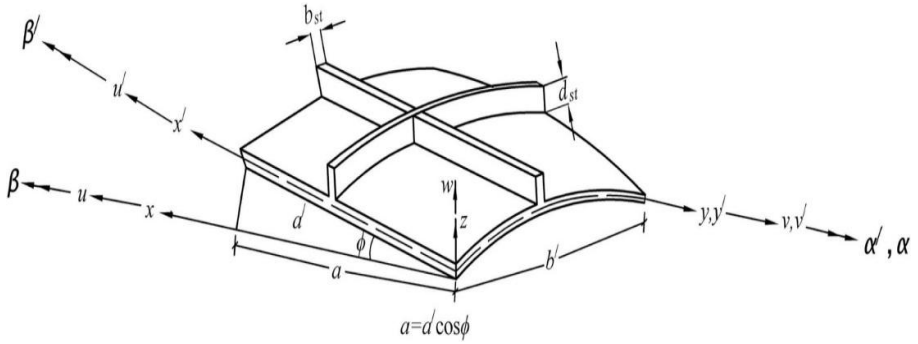

Figure 4.5: Skewed cylindrical panel with biaxial stiffeners

The stiffeners are single layered composites with longitudinal lamination. Figure 4.3 depicts the three noded elements for stiffener along with interpolation functions.

The displacements and rotations of stiffeners are as follows:

$$\{d_{sX}\} = \{U_{sX} \quad W_{sX} \quad \theta_{sX} \quad \theta_{sY}\}^T \qquad \text{for } X\text{ – stiffener.} \tag{28}$$

$$\{d_{sY}\} = \{V_{sY} \quad W_{sY} \quad \theta_{sX} \quad \theta_{sX}\}^T \qquad \text{for } Y\text{ – stiffener.} \tag{29}$$

The $\{d_{sX}\}$ and $\{d_{sY}\}$ are transferred to $\{\delta_{sx}\}$ and $\{\delta_{sy}\}$ using the following equations:

$$\{d_{sX}\} = [T_x]\{\delta_{sx}\} \qquad \text{for } X\text{ – stiffener.} \tag{30}$$

$$\{d_{sY}\} = [T_y]\{\delta_{sy}\} \qquad \text{for } Y\text{ – stiffener} \tag{31}$$

Where, $[T_x] = \begin{bmatrix} 1 & 0 & 0 & 0 \\ 0 & 1 & 0 & 0 \\ 0 & 0 & 1 & 0 \\ 0 & 0 & 0 & 1 \end{bmatrix}$ and $[T_y] = \begin{bmatrix} sec\phi & 0 & 0 & 0 \\ 0 & 1 & 0 & 0 \\ 0 & 0 & sec\phi & 0 \\ 0 & 0 & -tan\phi & 1 \end{bmatrix}$, ϕ = skew angle.

and $\{\delta_{sx}\} = \{u_{sx} \quad w_{sx} \quad \alpha_{sx} \quad \beta_{sx}\}^T$ and $\{\delta_{sy}\} = \{u_{sy} \quad w_{sy} \quad \alpha_{sy} \quad \beta_{sy}\}^T$

X – stiffener:

The element displacements $\{\delta_{sx}\}$ are given below,

$$\{\delta_{sx}\} = \sum_{j=1}^{3} [N_{\xi j}]\{\delta_{sxj}\} \qquad \text{where, } \{\delta_{sxj}\} = \{u_{sxj} \quad w_{sxj} \quad \alpha_{sxj} \quad \beta_{sxj}\}^T \tag{32}$$

$[N_{\xi j}]$ and $\{\delta_{sxj}\}$ are interpolation functions and displacements at the jth node of the stiffener.

The mid-surface strains are as follows:

$$\{\varepsilon_{sX}\} = \begin{Bmatrix} \dfrac{\partial U_{sX}}{\partial X} \\ \dfrac{\partial \theta_{x_{sX}}}{\partial X} \\ \dfrac{\partial \theta_{y_{sX}}}{\partial X} \\ \theta_{x_{sX}} + \dfrac{\partial W_{sY}}{\partial X} \end{Bmatrix} + \begin{Bmatrix} \frac{1}{2}\left(\dfrac{\partial W_{sy}}{\partial X}\right)^2 \\ 0 \\ 0 \\ 0 \end{Bmatrix} = \{\varepsilon_{sX}\}^L + \{\varepsilon_{sX}\}^{NL} \tag{33}$$

The strain-displacement equation is,

$$\{\varepsilon_{sX}\} = \left([B_L]^{sx} + \frac{1}{2}[B_{NL}]^{sx}\right)[T_x]\{\delta_{sxj}\} \tag{34}$$

where $\{\delta_{sxj}\} = \{u_{sxj} \quad w_{sxj} \quad \alpha_{sxj} \quad \beta_{sxj}\}^T$ and j = 1 to 3

Equation (35) leads to the following:

$$\frac{\partial\{\varepsilon_{sX}\}}{\partial\{\delta_{sx}\}} = [T_x][\bar{B}]_x \qquad \text{and } [\bar{B}]_x = [B_L]^{sx} + [B_{NL}]^{sx}$$

The matrices, $[B_{sx}]^L$ and $[B_{sx}]^{NL}$ are given below,

$$[B_{sx}]^L = \sum_{i=1}^{3} \begin{bmatrix} \frac{\partial N_i^{sx}}{\partial x} & \frac{N_i^{sx}}{R_{xx}} & 0 & 0 \\ 0 & 0 & \frac{\partial N_i^{sx}}{\partial x} & 0 \\ 0 & 0 & 0 & \frac{\partial N_i^{sx}}{\partial x} \\ 0 & \frac{\partial N_i^{sx}}{\partial x} & N_i^{sx} & 0 \end{bmatrix}$$

and $[B_{sx}]^{NL} = \frac{1}{2}\left[\frac{\partial w_{sx}}{\partial x} - \frac{u_{sx/}}{R_{xx}}\right] \sum_{i=1}^{3} \begin{bmatrix} \frac{N_i^{sx}}{R_{xx}} & \frac{\partial N_i^{sx}}{\partial x} & 0 & 0 \\ 0 & 0 & 0 & 0 \\ 0 & 0 & 0 & 0 \\ 0 & 0 & 0 & 0 \end{bmatrix}$

For $\phi \geq 0^0$, the above matrices adopt, $r_{xx} = R_{xx}$

Y - stiffener:

The element displacements $\{\delta_{sy}\}$ are given below,

$$\{\delta_{sy}\} = \sum_{j=1}^{3} [N_{\eta j}]\{\delta_{syj}\} \qquad \text{where, } \{\delta_{syj}\} = \{v_{syj} \quad w_{syj} \quad \alpha_{syj} \quad \beta_{syj}\}^T \tag{35}$$

$[N_{\eta j}]$ and $\{\delta_{syj}\}$ are interpolation functions and displacements at the jth node of the stiffener element

The mid-surface strains are as follows:

$$\{\varepsilon_{sY}\} = \begin{Bmatrix} \frac{\partial V_{sY}}{\partial Y} - \frac{w_{sY}}{R_{yy}} \\ \frac{\partial \theta_{y_{sY}}}{\partial Y} \\ \frac{\partial \theta_{x_{sY}}}{\partial Y} \\ \theta_{y_{sY}} + \frac{\partial w_{sY}}{\partial Y} \end{Bmatrix} + \begin{Bmatrix} \frac{1}{2}\left(\frac{\partial w_{sY}}{\partial Y} - \frac{v_{sY}}{R_{yy}}\right)^2 \\ 0 \\ 0 \\ 0 \end{Bmatrix} = \{\varepsilon_{sY}\}^L + \{\varepsilon_{sY}\}^{NL} \tag{36}$$

The strain-displacement equation is,

$$\{\varepsilon_{sY}\} = \left([B_L]^{sy} + \frac{1}{2}[B_{NL}]^{sy}\right)[T_y]\{\delta_{syj}\} \tag{37}$$

where $\{\delta_{syj}\} = \{u_{syj} \quad w_{syj} \quad \alpha_{syj} \quad \beta_{syj}\}^T$ $j = 1$ to 3

Equation (38) leads to the following:

$$\frac{\partial\{\varepsilon_{sY}\}}{\partial\{\delta_{sy}\}} = [T_y][\bar{B}]_y \quad \text{where, } [\bar{B}]_y = [B_L]^{sy} + [B_{NL}]^{sy} \tag{38}$$

$[B_{sy}]^L$ and $[B_{sy}]^{NL}$ are given in Bakshi (2021*a*) considering $r_{yy} = R_{yy}\cos\phi$.

It can be observed from the strain-displacement matrix $[B]$ that interpolation functions are required to derivative with respect to global Cartesian co-ordinates. But the shape functions used to describe the geometry and displacement variation are expressed in natural co-ordinate (ξ, η) system. The relationship between two co-ordinate systems can be computed using chain rule of partial differentiation and it is given below,

$$\begin{bmatrix} \frac{\partial}{\partial\xi} \\ \frac{\partial}{\partial\eta} \end{bmatrix} = \begin{bmatrix} \frac{\partial x}{\partial\xi} & \frac{\partial y}{\partial\xi} \\ \frac{\partial x}{\partial\eta} & \frac{\partial y}{\partial\eta} \end{bmatrix} \begin{bmatrix} \frac{\partial}{\partial x} \\ \frac{\partial}{\partial y} \end{bmatrix} \tag{39}$$

$$\begin{Bmatrix} \frac{\partial}{\partial\xi} \\ \frac{\partial}{\partial\eta} \end{Bmatrix} = [J] \begin{Bmatrix} \frac{\partial}{\partial x} \\ \frac{\partial}{\partial y} \end{Bmatrix} \tag{40}$$

Where $[J]$ is the Jacobian matrix. Hence the derivatives with respect to Cartesian co-ordinate system is,

$$\begin{Bmatrix} \frac{\partial}{\partial x} \\ \frac{\partial}{\partial y} \end{Bmatrix} = [J]^{-1} \begin{Bmatrix} \frac{\partial}{\partial\xi} \\ \frac{\partial}{\partial\eta} \end{Bmatrix} \tag{41}$$

Using equation (42) the Jacobian matrix will be,

$$[J] = \begin{bmatrix} \sum_{i=1}^{8} x_i \frac{\partial N_i}{\partial\xi} & \sum_{i=1}^{8} y_i \frac{\partial N_i}{\partial\xi} \\ \sum_{i=1}^{8} x_i \frac{\partial N_i}{\partial\eta} & \sum_{i=1}^{8} y_i \frac{\partial N_i}{\partial\eta} \end{bmatrix} \tag{42}$$

Now, by using the Jacobian matrix, the elements of strain-displacement matrix are obtained.

4.8 Force-Displacement Relationship

Before evaluating the structural characteristics of a composite material, it is essential to acknowledge that the actual nature of a fibre-reinforced composite lamina is inherently complex, and certain simplifying assumptions are necessary to obtain micromechanical solutions.

The basic assumptions are:

1. Both the fibre and matrix are homogeneous and isotropic.
2. The fibre, matrix, and resulting composite all exhibit linear elastic behaviour.
3. A perfect bond exists between fibre and matrix, preventing any interfacial slipping.
4. Fibres are uniformly spaced, consistent in cross-section, and perfectly aligned.
5. The matrix is void-free.
6. The lamina is initially in a stress-free state.

4.8.1 Elastic Properties of Unidirectional Lamina

4.8.1.1 Stress-strain relationship

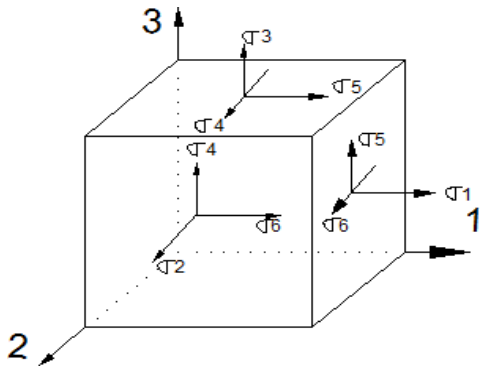

Figure 4.6: Stress components in three-dimensional continuum

$$\begin{Bmatrix}\sigma_1\\ \sigma_2\\ \sigma_3\\ \sigma_4\\ \sigma_5\\ \sigma_6\end{Bmatrix} = \begin{bmatrix}C_{11} & C_{12} & C_{13} & C_{14} & C_{15} & C_{16}\\ C_{21} & C_{22} & C_{23} & C_{24} & C_{25} & C_{26}\\ C_{31} & C_{32} & C_{33} & C_{34} & C_{35} & C_{36}\\ C_{41} & C_{42} & C_{43} & C_{44} & C_{45} & C_{46}\\ C_{51} & C_{52} & C_{53} & C_{54} & C_{55} & C_{56}\\ C_{61} & C_{62} & C_{63} & C_{64} & C_{65} & C_{66}\end{bmatrix}\begin{Bmatrix}\varepsilon_1\\ \varepsilon_2\\ \varepsilon_3\\ \varepsilon_4\\ \varepsilon_5\\ \varepsilon_6\end{Bmatrix}$$

or, $\sigma_i = C_{ij}\varepsilon_j$ (43)

Where, ε_j =strain components corresponding to σ_i and (i,j=1,2,3,4,5,6)

and C_{ij}=constitutive relationship matrix. $W = \frac{\sigma_i \varepsilon_i}{2}$ (44)

Work done per unit volume of the continuum, $W = \frac{C_{ij}\varepsilon_i \varepsilon_j}{2}$ (45)

Substituting σ_i from (44) to (45), we get, $\sigma_i = \frac{\partial W}{\partial \varepsilon_i} = C_{ij}\varepsilon_j$ (46)

Differentiating again with respect to ε_j we get, $\frac{\partial^2 W}{\partial \varepsilon_i \, \partial \varepsilon_j} = C_{ij}$ (47)

Based on the above procedure, if the differentiation is first performed with respect to ε_j and then with respect to ε_i we get,

$$C_{ij} = \frac{\partial^2 W}{\partial \varepsilon_j \, \partial \varepsilon_i} \tag{48}$$

So, we can see from equations (48) and (49) that $C_{ij} = C_{ji}$ and hence it is also established that the constitutive matrix for an anisotropic material is symmetric.

Now from the theory of elasticity compliance matrix can be written as,

$$\begin{Bmatrix} \varepsilon_1 \\ \varepsilon_2 \\ \varepsilon_3 \\ \varepsilon_4 \\ \varepsilon_5 \\ \varepsilon_6 \end{Bmatrix} = \begin{bmatrix} \frac{1}{E_1} & -\frac{\nu_{21}}{E_2} & \frac{\nu_{31}}{E_3} & 0 & 0 & 0 \\ -\frac{\nu_{12}}{E_1} & \frac{1}{E_2} & -\frac{\nu_{32}}{E_3} & 0 & 0 & 0 \\ -\frac{\nu_{13}}{E_1} & -\frac{\nu_{23}}{E_2} & \frac{1}{E_3} & 0 & 0 & 0 \\ 0 & 0 & 0 & \frac{1}{G_{23}} & 0 & 0 \\ 0 & 0 & 0 & 0 & \frac{1}{G_{31}} & 0 \\ 0 & 0 & 0 & 0 & 0 & \frac{1}{G_{12}} \end{bmatrix} \begin{Bmatrix} \sigma_1 \\ \sigma_2 \\ \sigma_3 \\ \sigma_4 \\ \sigma_5 \\ \sigma_6 \end{Bmatrix} \tag{49}$$

By inversing the above compliance matrix, we get the constitutive relationship matrix of the anisotropic material as,

$$\begin{bmatrix}\sigma_1\\ \sigma_2\\ \sigma_3\\ \sigma_4\\ \sigma_5\\ \sigma_6\end{bmatrix}=\begin{bmatrix}C_{11} & C_{12} & C_{13} & 0 & 0 & 0\\ C_{21} & C_{22} & C_{23} & 0 & 0 & 0\\ C_{31} & C_{32} & C_{33} & 0 & 0 & 0\\ 0 & 0 & 0 & C_{44} & 0 & 0\\ 0 & 0 & 0 & 0 & C_{55} & 0\\ 0 & 0 & 0 & 0 & 0 & C_{66}\end{bmatrix}\begin{bmatrix}\varepsilon_1\\ \varepsilon_2\\ \varepsilon_3\\ \varepsilon_4\\ \varepsilon_5\\ \varepsilon_6\end{bmatrix} \quad (50)$$

where, $C_{11}=E_1\frac{1-\nu_{23}\nu_{32}}{\Delta}, C_{12}=E_1\frac{\nu_{21}+\nu_{31}\nu_{23}}{\Delta}=E_2\frac{\nu_{12}+\nu_{32}\nu_{13}}{\Delta}$

$C_{13}=E_1\frac{\nu_{31}+\nu_{21}\nu_{32}}{\Delta}=E_3\frac{\nu_{13}+\nu_{12}\nu_{23}}{\Delta}, C_{22}=E_2\frac{1-\nu_{13}\nu_{31}}{\Delta}, C_{33}=E_2\frac{1-\nu_{12}\nu_{21}}{\Delta},$
$C_{23}=E_2\frac{\nu_{32}+\nu_{12}\nu_{31}}{\Delta}=E_3\frac{\nu_{23}+\nu_{21}\nu_{13}}{\Delta}, C_{44}=G_{23}, C_{55}=G_{31}, C_{66}=G_{12}$
$\Delta=1-\nu_{12}\nu_{21}-\nu_{23}\nu_{32}-\nu_{13}\nu_{31}-2\nu_{12}\nu_{23}\nu_{13}$

4.8.1.2 Reduced Stiffness Matrix of an Individual Lamina

Since individual lamina is extremely thin, the transverse normal stress component may be neglected; however, transverse shear deformation is retained in the present formulation. Accordingly, the condition $\sigma_{33} = 0$ is imposed for each lamina. The in-plane and out-of-plane stress components are then separated, and upon applying this condition, equation (51) reduces to:

$$\begin{Bmatrix}\sigma_1\\ \sigma_2\\ 0\\ \sigma_6\end{Bmatrix}=\begin{bmatrix}C_{11} & C_{12} & C_{13} & 0\\ C_{21} & C_{22} & C_{23} & 0\\ C_{31} & C_{32} & C_{33} & 0\\ 0 & 0 & 0 & C_{66}\end{bmatrix}\begin{Bmatrix}\varepsilon_1\\ \varepsilon_2\\ \varepsilon_3\\ \varepsilon_6\end{Bmatrix} \quad (52)$$

and $\begin{Bmatrix}\sigma_4\\ \sigma_5\end{Bmatrix}=\begin{bmatrix}C_{44} & 0\\ 0 & C_{55}\end{bmatrix}\begin{Bmatrix}\varepsilon_4\\ \varepsilon_5\end{Bmatrix}$ (53)

Solving 52, yields

$$\sigma_1=\left(C_{11}-\frac{C_{13}C_{13}}{C_{33}}\right)\varepsilon_1+\left(C_{12}-\frac{C_{13}C_{23}}{C_{33}}\right)\varepsilon_2 \ =Q_{11}\varepsilon_1+Q_{12}\varepsilon_2$$

$$\sigma_2=\left(C_{12}-\frac{C_{23}C_{13}}{C_{33}}\right)\varepsilon_1+\left(C_{22}-\frac{C_{23}C_{23}}{C_{33}}\right)\varepsilon_2 \\ =Q_{12}\varepsilon_1+Q_{22}\varepsilon_2$$

$$\sigma_{66}=C_{66}\varepsilon_{66}=Q_{66}\varepsilon_6$$

Writing the above equations in a matrix form, we get

$$\begin{Bmatrix}\sigma_1\\ \sigma_2\\ \sigma_6\end{Bmatrix}=\begin{bmatrix}Q_{11} & Q_{12} & 0\\ Q_{12} & Q_{22} & 0\\ 0 & 0 & Q_{66}\end{bmatrix}\begin{Bmatrix}\varepsilon_1\\ \varepsilon_2\\ \varepsilon_6\end{Bmatrix} \quad (54)$$

$$\{\sigma\}_{1,2}=[Q]_{1,2}\{\varepsilon\}_{1,2}\& \quad (55)$$

Where, $Q_{11}=(1-\nu_{12}\nu_{21})^{-1}E_1; Q_{22}=(1-\nu_{12}\nu_{21})^{-1}E_2; Q_{12}=(1-\nu_{12}\nu_{21})^{-1}E_1\nu_{21}$

And $Q_{66}=G_{12}$

The [Q] matrix in equation (55) is termed as the reduced stiffness matrix of an individual lamina in the local co-ordinate system.

4.8.1.3 Transformation Matrix

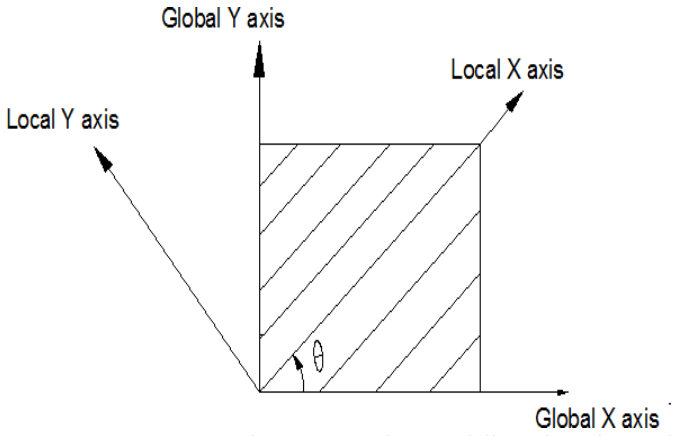

Figure 4.7: Axis Systems in a unidirectional Lamina

Performing transformation of in-plane stress components from local co-ordinate system to global co-ordinate system,

$$\begin{Bmatrix}\sigma_x\\ \sigma_y\\ \tau_{xy}\end{Bmatrix}=\begin{bmatrix}m^2 & n^2 & -2mn\\ n^2 & m^2 & 2mn\\ mn & -mn & m^2-n^2\end{bmatrix}\begin{Bmatrix}\sigma_1\\ \sigma_2\\ \tau_6\end{Bmatrix} \quad (56)$$

$$\{\sigma\}_{x,y}=[M]\{\sigma\}_{1,2} \quad (57)$$

As transverse shear deformation is considered in the present study, thus performing transformation of out-off plane stress components from local co-ordinate system to global co-ordinate system,

$$\begin{Bmatrix}\tau_{yz}\\ \tau_{xz}\end{Bmatrix} = \begin{bmatrix} m & -n \\ n & m \end{bmatrix} \begin{Bmatrix}\tau_4\\ \tau_5\end{Bmatrix} \tag{58}$$

$$\{\sigma\}_{x,y} = [M]'\{\sigma\}_{1,2} \tag{59}$$

and $m = cos\theta\ n = sin\theta$

In Equation (57) $[M]'$ is termed as transformation matrix which is used to transfer in plane stress and strain components from local to global co-ordinate system and in Equation (59) $[M]'$ used to transfer out-off plane stress and strain components from local to global co-ordinate system.

4.8.1.4 Transformation of strain vector from Local to Global Co-Ordinate System

Transformation matrix derived in Equation (59) can also be used to transform in plane strain components from local to global co-ordinate system.

$$\begin{Bmatrix}\varepsilon_x\\ \varepsilon_y\\ \frac{\varepsilon_{xy}}{2}\end{Bmatrix} = \begin{bmatrix} m^2 & n^2 & -2mn \\ n^2 & m^2 & 2mn \\ mn & -mn & m^2-n^2 \end{bmatrix} \begin{Bmatrix}\varepsilon_1\\ \varepsilon_2\\ \frac{\varepsilon_6}{2}\end{Bmatrix} \tag{60}$$

$$\{\varepsilon\}_{x,y} = [M]\{\varepsilon\}_{1,2} \tag{61}$$

Performing transformation of out-off plane stress components from local co-ordinate system to global co-ordinate system,

$$\begin{Bmatrix}\varepsilon_{yz}\\ \varepsilon_{xz}\end{Bmatrix} = \begin{bmatrix} m & -n \\ n & m \end{bmatrix} \begin{Bmatrix}\varepsilon_4\\ \varepsilon_5\end{Bmatrix} \tag{62}$$

$$\{\varepsilon\}_{x,y} = [M]'\{\varepsilon\}_{1,2} \tag{63}$$

4.8.1.5 Transformation of stress-strain matrix from Local to Global Co-Ordinate System

Combining equation (54), (56) and (60) we get in plane stress-strain relationship in global co-ordinate system,

$$\begin{Bmatrix}\sigma_x\\ \sigma_y\\ \tau_{xy}\end{Bmatrix} = \begin{bmatrix} m^2 & n^2 & -2mn \\ n^2 & m^2 & 2mn \\ mn & -mn & m^2-n^2 \end{bmatrix} \begin{bmatrix} Q_{11} & Q_{12} & 0 \\ Q_{12} & Q_{22} & 0 \\ 0 & 0 & Q_{66} \end{bmatrix} \begin{bmatrix} m^2 & n^2 & 2mn \\ n^2 & m^2 & -2mn \\ -mn & mn & m^2-n^2 \end{bmatrix} \tag{64}$$

$$\begin{Bmatrix}\sigma_x\\ \sigma_y\\ \tau_{xy}\end{Bmatrix}=\begin{bmatrix}Q_{xx} & Q_{xy} & Q_{xs}\\ Q_{yx} & Q_{yy} & Q_{ys}\\ Q_{sx} & Q_{xy} & Q_{xs}\end{bmatrix}\begin{Bmatrix}\varepsilon_x\\ \varepsilon_y\\ \varepsilon_{xy}\end{Bmatrix} \quad \because \varepsilon_{xy}=2\gamma_{xy} \tag{65}$$

And combining equation (53), (58) and (62) we get out-off plane stress-strain relationship in global co-ordinate system,

$$\begin{Bmatrix}\tau_{yz}\\ \tau_{xz}\end{Bmatrix}=\begin{bmatrix}m & -n\\ n & m\end{bmatrix}\begin{bmatrix}C_{44} & 0\\ 0 & C_{55}\end{bmatrix}\begin{bmatrix}m & n\\ -n & m\end{bmatrix}\begin{bmatrix}\gamma_{yz}\\ \gamma_{xz}\end{bmatrix} \tag{66}$$

$$\begin{Bmatrix}\tau_{yz}\\ \tau_{xz}\end{Bmatrix}=\begin{bmatrix}m^2G_{23}-n^2G_{31} & mn(G_{23}-G_{31})\\ mn(G_{23}-G_{31}) & n^2G_{23}+m^2G_{31}\end{bmatrix}\begin{Bmatrix}\gamma_{yz}\\ \gamma_{xz}\end{Bmatrix} \tag{67}$$

$$\{\tau\}=(G_{ij})\{\gamma\} \tag{68}$$

$[Q]_{x,y}$ in Equation (65) represents the reduced stiffness of an individual lamina in global co-ordinate system. Elements of $[Q]_{x,y}$ has a specific significance. The elements show the coupling effects of normal and shearing strain on normal stress and in the same way it also represents the coupling of shear strain and normal strain on shear stress. The terms of $[Q]_{x,y}$ are described below,

4.8.2 Stress-Strain Relationship for Laminate

$$Q_{xx}=m^4Q_{11}+n^4Q_{22}+2m^2n^2Q_{12}+4m^2n^2Q_{66}$$
$$Q_{yy}=n^4Q_{11}+m^4Q_{22}+2m^2n^2Q_{12}+4m^2n^2Q_{66}$$
$$Q_{xy}=m^2n^2Q_{11}+m^2n^2Q_{22}+(m^4+n^4)Q_{12}-4m^2n^2Q_{66}$$
$$Q_{xs}=m^3nQ_{11}-mn^3Q_{22}+(mn^3-m^3n)Q_{12}+2(mn^3-m^3n)Q_{66}$$
$$Q_{ys}=mn^3Q_{11}-m^3nQ_{22}+(m^3n-mn^3)Q_{12}+2(m^3n-mn^3)Q_{66}$$
$$Q_{ss}=m^2n^2Q_{11}+m^2n^2Q_{22}-2m^2n^2Q_{12}+(m^2-n^2)Q_{66}$$

A laminate is an assembly of multiple laminae bonded together to function as a single unified structural element. In the present study, the laminate is configured in the form of a shell. The following assumptions are adopted in the analysis of the laminate:

4.8.2.1 Assumptions to Analyze a Laminate

1. Each lamina within the laminate is considered quasi-homogeneous and anisotropic.
2. Displacements remain continuous across the entire thickness of the laminate.
3. The deformations experienced by the laminate are assumed to be small.

4. Both the strain–displacement and stress–strain relationships are taken as linear.
5. Transverse shear deformations are small owing to the thinness of the laminate. A plane section through the laminate thickness remains planar after bending but is not required to remain perpendicular to the deformed mid-plane, thereby accommodating shear deformation effects. A shear correction factor of unity is assumed.
6. Perfect bonding is assumed between adjacent plies, with no inter-ply slipping permitted under loading.

Combining equations (19) and (65), the in-plane stress–strain relationship for the laminate is obtained as:

$$\begin{Bmatrix}\sigma_x\\ \sigma_y\\ \tau_{xy}\end{Bmatrix}=\begin{bmatrix}Q_{xx} & Q_{xy} & Q_{xs}\\ Q_{yx} & Q_{yy} & Q_{ys}\\ Q_{sx} & Q_{sy} & Q_{ss}\end{bmatrix}\begin{Bmatrix}\varepsilon_x\\ \varepsilon_y\\ \gamma_{xy}\end{Bmatrix}=\begin{bmatrix}Q_{xx} & Q_{xy} & Q_{xs}\\ Q_{yx} & Q_{yy} & Q_{ys}\\ Q_{sx} & Q_{sy} & Q_{ss}\end{bmatrix}\left\{\begin{bmatrix}\varepsilon_x^0\\ \varepsilon_y^0\\ \gamma_{xy}^0\end{bmatrix}+z\begin{Bmatrix}k_x\\ k_y\\ k_{xy}\end{Bmatrix}\right\}$$

$$\begin{Bmatrix}\sigma_x\\ \sigma_y\\ \tau_{xy}\end{Bmatrix}==\left\{\begin{bmatrix}Q_{xx} & Q_{xy} & Q_{xs}\\ Q_{yx} & Q_{yy} & Q_{ys}\\ Q_{sx} & Q_{sy} & Q_{ss}\end{bmatrix}\begin{bmatrix}\varepsilon_x^0\\ \varepsilon_y^0\\ \gamma_{xy}^0\end{bmatrix}+z\begin{bmatrix}Q_{xx} & Q_{xy} & Q_{xs}\\ Q_{yx} & Q_{yy} & Q_{ys}\\ Q_{sx} & Q_{sy} & Q_{ss}\end{bmatrix}\begin{bmatrix}k_x\\ k_y\\ k_{xy}\end{bmatrix}\right\} \quad (69)$$

From Equation (67) we get out-off plane stress-strain relationship for a laminate,

$$\begin{Bmatrix}\tau_{yz}\\ \tau_{xz}\end{Bmatrix}=\begin{bmatrix}m^2G_{23}-n^2G_{31} & mn(G_{23}-G_{31})\\ mn(G_{23}-G_{31}) & n^2G_{23}+m^2G_{31}\end{bmatrix}\begin{Bmatrix}\gamma_{yz}^0\\ \gamma_{xz}^0\end{Bmatrix}\because k_{yz}=k_{xz}=0 \quad (70)$$

4.8.3 Equilibrium Equations

Equation (69) and (70) represent in plane and out-off plane stress components of the kth lamina. To get the force and moment resultant of a lamina it is required to integrate stress over its thickness (h).

$$\{F\}=\begin{Bmatrix}N_x\\ N_y\\ N_y\\ M_x\\ M_y\\ M_{xy}\\ Q_x\\ Q_y\end{Bmatrix}=\int_{-\frac{h}{2}}^{\frac{h}{2}}\begin{Bmatrix}\sigma_x dz\\ \sigma_y dz\\ \tau_{xy}dz\\ \sigma_x z dz\\ \sigma_y z dz\\ \tau_{xy}z dz\\ k\tau_{xz}dz\\ k\tau_{yz}dz\end{Bmatrix} \quad (71)$$

Stress varies discontinuously along the fibers and to get the stress resultants of a laminate it is requires adding the stress resultant for each layer numerically. In that way the normal stress resultants of a laminate are,

$$\begin{Bmatrix} N_x \\ N_y \\ N_{xy} \end{Bmatrix} = \sum_{k=1}^{n} \left\{ \begin{bmatrix} Q_{xx} & Q_{xy} & Q_{xs} \\ Q_{yx} & Q_{yy} & Q_{ys} \\ Q_{sx} & Q_{sy} & Q_{ss} \end{bmatrix} \begin{bmatrix} \varepsilon_x^0 \\ \varepsilon_y^0 \\ \gamma_{xy}^0 \end{bmatrix} \int_{z_{k-1}}^{z_k} dz + \begin{bmatrix} Q_{xx} & Q_{xy} & Q_{xs} \\ Q_{yx} & Q_{yy} & Q_{ys} \\ Q_{sx} & Q_{sy} & Q_{ss} \end{bmatrix} \begin{bmatrix} k_x \\ k_y \\ k_{xy} \end{bmatrix} \int_{z_{k-1}}^{z_k} z dz \right\} \tag{72}$$

Bending stress resultants are,

$$\begin{Bmatrix} M_x \\ M_y \\ M_{xy} \end{Bmatrix} = \sum_{k=1}^{n} \left\{ \begin{bmatrix} Q_{xx} & Q_{xy} & Q_{xs} \\ Q_{yx} & Q_{yy} & Q_{ys} \\ Q_{sx} & Q_{sy} & Q_{ss} \end{bmatrix} \begin{bmatrix} \varepsilon_x^0 \\ \varepsilon_y^0 \\ \gamma_{xy}^0 \end{bmatrix} \int_{z_{k-1}}^{z_k} z dz + \begin{bmatrix} Q_{xx} & Q_{xy} & Q_{xs} \\ Q_{yx} & Q_{yy} & Q_{ys} \\ Q_{sx} & Q_{sy} & Q_{ss} \end{bmatrix} \begin{bmatrix} k_x \\ k_y \\ k_{xy} \end{bmatrix} \int_{z_{k-1}}^{z_k} z^2 dz \right\} \tag{73}$$

Transverse shear resultants are,

$$\begin{Bmatrix} Q_x \\ Q_y \end{Bmatrix} = \sum_{k=1}^{n} k \begin{bmatrix} m^2 G_{23} - n^2 G_{31} & mn(G_{23} - G_{31}) \\ mn(G_{23} - G_{31}) & n^2 G_{23} + m^2 G_{31} \end{bmatrix} \begin{Bmatrix} \gamma_{yz}^0 \\ \gamma_{xz}^0 \end{Bmatrix} \int_{z_{k-1}}^{z_k} dz \tag{74}$$

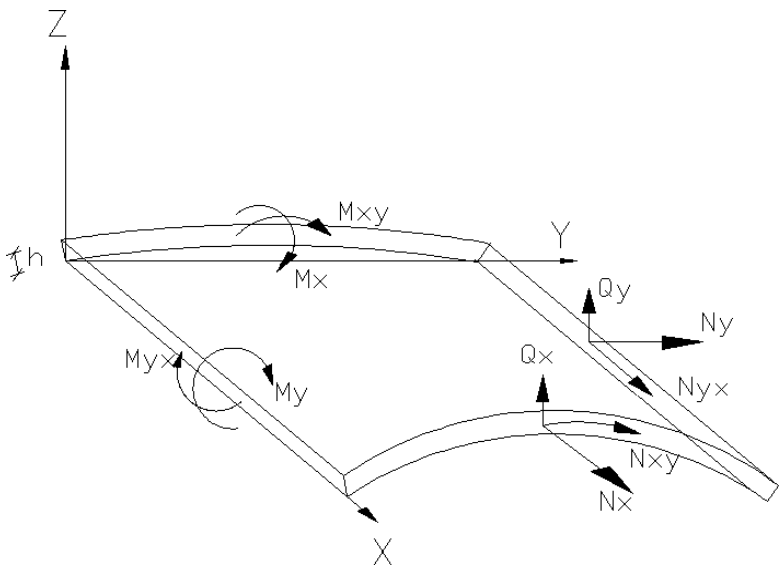

Figure 4.8: Force and Moment Resultants on A Shell Structure

Here, σ_x and σ_γ denote the normal stress components acting along the *X* and *Y* directions respectively, while τ_{xy}, $\tau_{x\gamma}$ and $\tau_{\gamma u}$ represent the shear stress components in the *XY, XZ*, and *YZ* planes respectively. The total thickness of the laminate is represented by *h*. The parameter κ denotes the shear correction factor introduced to account for the non-uniform distribution of transverse shear stress through the thickness; in the present study this factor is taken as unity owing to the relatively small thickness of the laminate. In the present formulation, the following sign convention is adopted: upward deflection, tensile in-plane forces, hogging bending moments, and in-plane shear forces that tend to rotate the shell element in the anti-clockwise direction are all treated as positive

$$\begin{bmatrix} N_x \\ N_y \\ N_{xy} \\ M_x \\ M_y \\ M_x \\ Q_x \\ Q_y \end{bmatrix} = \begin{bmatrix} A_{11} & A_{12} & A_{16} & B_{11} & B_{12} & B_{16} & 0 & 0 \\ A_{12} & A_{22} & A_{26} & B_{12} & B_{22} & B_{26} & 0 & 0 \\ A_{16} & A_{26} & A_{66} & B_{16} & B_{26} & B_{66} & 0 & 0 \\ B_{11} & B_{12} & B_{16} & D_{11} & D_{12} & D_{16} & 0 & 0 \\ B_{12} & B_{22} & B_{26} & D_{12} & D_{22} & D_{26} & 0 & 0 \\ B_{16} & B_{26} & B_{66} & D_{16} & D_{26} & D_{66} & 0 & 0 \\ 0 & 0 & 0 & 0 & 0 & 0 & S_{11} & S_{12} \\ 0 & 0 & 0 & 0 & 0 & 0 & S_{12} & S_{22} \end{bmatrix} \begin{bmatrix} \varepsilon_x^0 \\ \varepsilon_y^0 \\ \gamma_{xy}^0 \\ k_x \\ k_y \\ k_{xy} \\ \gamma_{xz}^0 \\ \gamma_{yz}^0 \end{bmatrix} \tag{75}$$

or, $\{F\} = [D]\{\boldsymbol{\varepsilon}\}$ (76)

$\{F\} = [D](\{\varepsilon\}^L + \{\varepsilon\}^{NL})$

$$\{F\} = [E]\left([B_L] + \frac{1}{2}[B_{NL}]\right)\{\delta_i\} \tag{77}$$

[D] laminate constitutive relationship matrix and is adopted from Chakravorty et al. (1995).

Where, $A_{ij} = \sum_{k=1}^{n} \left(Q_{ij}\right)_k (z_k - z_{k-1})$

$$B_{ij} = \frac{1}{2}\sum_{k=1}^{n} \left(Q_{ij}\right)_k (z_k^2 - z_{k-1}^2)$$

$$D_{ij} = \frac{1}{3}\sum_{k=1}^{n} \left(Q_{ij}\right)_k (z_k^3 - z_{k-1}^3);$$

$$S_{ij} = \sum_{k=1}^{n} \left(G_{ij}\right)_k (z_k - z_{k-1})$$

In the above expressions, z_k and $z_{k-1}\}$ represent the distances measured from the mid-plane of the laminate to the bottom surfaces of the kth and $(k - 1)^{th}$ laminae respectively. The term $\left(Q_{ij}\right)^k$ denotes the in-plane elastic constant matrix of the k-th lamina expressed in the global coordinate system, while G_{ij} refers to the out-of-plane elastic constant matrix of the kth lamina in the global coordinate system. The 8×8 matrix appearing in Equation (75) is designated as the laminate stiffness matrix $[D]$.

The following equation represents the force-deflection relationship of composite shell.

$$\{F\} = [E]\left([B_L] + \frac{1}{2}[B_{NL}]\right)[T]\{\delta_i\} \tag{78}$$

where $\{\delta_i\} = \{u_i \quad v_i \quad w_i \quad \alpha_i \quad \beta_i\}^T$ and i = 1 to 8.

The stress resultants $\{F\}$ and matrix $[E]$ are given in Bakshi and Chakravorty (2014).

For stiffener along X – axis,

$$\{F_{sX}\} = [E_{sX}]\left([B_L]^{sx} + \frac{1}{2}[B_{NL}]^{sx}\right)[T_x]\{\delta_{sxj}\} \tag{79}$$

where $\{F_{sX}\} = \begin{Bmatrix} N_{sx} \\ M_{sx} \\ T_{sx} \\ Q_{sxz} \end{Bmatrix} = \int_{-\frac{d_{sx}}{2}}^{+\frac{d_{sx}}{2}} \int_{-\frac{b_{sx}}{2}}^{+\frac{b_{sx}}{2}} \begin{Bmatrix} \sigma_{sx} \\ \sigma_{sx} z \\ (\tau_{sxy} z - \tau_{sxz} y) \\ k_s \tau_{sxz} \end{Bmatrix} dydz$

b_{sx} and d_{sx} = dimensions X – stiffener. σ_{sx} is longitudinal stress and τ_{sxy} and τ_{sxz} are shear stresses acting on X – stiffener. k_s = Shear correction factor (5/6).

For stiffener along Y –axis:

$$\{F_{sY}\} = [E_{sY}] \left([B_L]^{sy} + \frac{1}{2} [B_{NL}]^{sy} \right) [T_y] \{\delta_{syj}\} \tag{80}$$

where $\{F_{sY}\} = \begin{Bmatrix} N_{sy} \\ M_{sy} \\ T_{sy} \\ Q_{syz} \end{Bmatrix} = \int_{-\frac{d_{sy}}{2}}^{+\frac{d_{sy}}{2}} \int_{-\frac{b_{sy}}{2}}^{+\frac{b_{sy}}{2}} \begin{Bmatrix} \sigma_{sy} \\ \sigma_{sy} z \\ (\tau_{syx} z - \tau_{syz} y) \\ k_s \tau_{syz} \end{Bmatrix} dydz$

b_{sy} and d_{sy} = dimensions of Y – stiffener. σ_{sy} is longitudinal stress and τ_{syx} and τ_{syz} are shear stresses along Y-stiffener. k_s = Shear correction factor (5/6).

$[E_{sX}]$ and $[E_{sY}]$ are given in Bakshi (2021a). The compatibility between shell to stiffener elements follow the steps given in Bakshi (2021a).

4.9 Generalized Inertia Matrix

The generalized inertia matrix per unit area encompasses both translatory and rotary inertia contributions. The mass per unit area and the moment of inertia per unit area serve as measures of resistance to translatory and rotary inertial effects respectively and are expressed as follows. Mass per unit area is denoted by m and is given by

$$m = \rho h$$

Where ρ is mass density of shell.

Moment of inertia per unit area is denoted by I and is given by

$$I = \frac{\rho h^3}{12}$$

Incorporating both the translatory and rotary inertia terms, the generalized inertia matrix $[m]$ takes the following form,

$$[m] = \begin{bmatrix} \rho h & 0 & 0 & 0 & 0 \\ 0 & \rho h & 0 & 0 & 0 \\ 0 & 0 & \rho h & 0 & 0 \\ 0 & 0 & 0 & \frac{\rho h^3}{12} & 0 \\ 0 & 0 & 0 & 0 & \frac{\rho h^3}{12} \end{bmatrix} \tag{81}$$

Inertia matrix for *x*-stiffener:

$$[m_x] = \sum_{i=1}^{3} \begin{bmatrix} \rho . b_{sx}\, d_{sx} & 0 & 0 & 0 \\ 0 & \rho . b_{sx}\, d_{sx} & 0 & 0 \\ 0 & 0 & \frac{\rho . b_{sx}\, {d_{sx}}^2}{12} & 0 \\ 0 & 0 & 0 & \frac{\rho(b_{sx}\, {d_{sx}}^3 + d_{sx}\, {w_{sx}}^3)}{12} \end{bmatrix}$$

Inertia matrix for *y*-stiffener:

$$[m_y] = \sum_{i=1}^{3} \begin{bmatrix} \rho . b_{sy}\, d_{sy} & 0 & 0 & 0 \\ 0 & \rho . b_{sy}\, d_{sy} & 0 & 0 \\ 0 & 0 & \frac{\rho . b_{sy}\, {d_{sy}}^2}{12} & 0 \\ 0 & 0 & 0 & \frac{\rho(b_{sy}\, {d_{sy}}^3 + d_{sy}\, {b_{sy}}^3)}{12} \end{bmatrix}$$

Chapter 5

NUMERICAL RESULTS

5.1 General

This chapter reports the numerical results obtained through geometrically nonlinear finite element analysis of biaxially stiffened skewed laminated composite cylindrical shell panels. The flexural behavior of these panels is examined under three distinct forms of transverse pressure loading uniform, sinusoidal (sin–sin), and cos–cos. The analysis encompasses multiple boundary condition combinations, various lamination sequences, and stiffener skew angles varying from 0° to 35°. All results are presented in terms of non-dimensional central deflections and stress resultants, comprising both force and moment resultants, for two material systems: graphite/epoxy and glass/epoxy composites.

The non-dimensional central deflection is defined as: $\delta = \frac{wE_{22}h^3}{qa^4} \times 10^4$

where w is the central transverse deflection, E_{22} is the transverse elastic modulus, h is the panel thickness, q is the applied pressure intensity, and a is the panel plan dimension. The force resultants N_x and N_y are non-dimensionalised as (N_x or N_y)/$qa \times 10^3$, the in-plane shear resultant as $N_{xy}/qa \times 10^3$, the bending moment resultants M_x and M_y as (M_x or M_y)/$qa^2 \times 10^4$, and the torsional moment resultant as M_{xy}/qab.

5.2 Geometric and Material Properties

The geometric dimensions of the cylindrical shell panels used in the parametric study are presented in Table 5.1. The panels are square in plan with a side-to-thickness ratio of a/h = 100, which corresponds to moderately thin panels. The radii of curvature in both directions are equal, resulting in a spherical-type curvature for the base configuration.

Table 5.1: Geometric dimensions of the cylindrical shell panels

Parameter	Value
Length *(a)*	1000 mm
Width *(b)*	1000 mm
Thickness *(h)*	10 mm
Radii of curvature (R_{xx}, R_{yy})	750 mm

The material properties of the two composite systems graphite/epoxy and glass/epoxy used in all numerical problems are listed in Table 5.2. Graphite/epoxy is a high-stiffness, low-density composite suitable for aerospace and structural applications, whereas glass/epoxy is an isotropic ($E_{11} = E_{22}$) composite with wider civil engineering applicability.

Table 5.2: Material properties of laminated composites (graphite/epoxy and glass/epoxy)

Elastic Constants	Graphite/Epoxy	Glass/Epoxy
E_{11}	142.5 GPa	30.4 GPa
E_{22}	9.790 GPa	30.4 GPa
E_{33}	9.790 GPa	9.95 GPa
G_{12}	4.270 GPa	3.99 GPa
G_{13}	4.270 GPa	11.7 GPa
G_{23}	1.192 GPa	11.7 GPa
v_{12}	0.27	0.247
v_{13}	0.27	0.301
v_{23}	0.25	0.301
ρ	1.0×10^{-6} N-sec²/cm²	2064 kg/m³

5.3 Boundary Conditions

Five boundary conditions are considered in the present study to represent a range of practical support configurations for skewed stiffened cylindrical shell panels:

CCCC: All four edges clamped ($u = v = w = \alpha = \beta = 0$ along all sides).

SSSS: All four edges simply supported ($u = v = w = \alpha = \beta = 0$ at corners; $v = w = \beta = 0$ at $x = 0, a$; $u = w = \alpha = 0$ at $y = 0, b$).

CSCS: Clamped along $x = 0$ and $x = a$; simply supported along $y = 0$ and $y = b$.

SCSC: Simply supported along $x = 0$ and $x = a$; clamped along $y = 0$ and $y = b$.

CCSS: Clamped along $x = 0$ and $x = a$; simply supported along $y = 0$ and $y = b$

SSCC: simply supported along $x = 0$ and $x = a$; Clamped along $y = 0$ and $y = b$

5.4 Non-dimensional Deflections under Uniform Pressure

5.4.1 Cross-ply Laminates

Table 5.4 presents the non-dimensional central deflections of biaxially stiffened cross-ply laminated cylindrical panels subjected to uniform pressure for skew angles ranging from 0° to

35° and five boundary conditions. The laminations considered are 0°/90°, 0°/90°/0°, $(0°/90°)_2$, and $(0°/90°)_S$.

Table 5.3: Non-dimensional deflections ($\delta\times 10^4$) of biaxially stiffened cross-ply cylindrical panels under uniform pressure

lamination	ϕ	CCCC	SSSS	CSCS	SCSC	CCSS	SSCC
$0^0/90^0$	0^0	0.1579	1.2893	1.0694	0.1636	1.2773	1.2772
	5^0	0.1585	1.2894	1.0653	0.1644	1.2562	1.2562
	10^0	0.1604	1.2737	1.0537	0.1665	1.2226	1.2225
	15^0	0.1638	1.2545	1.0542	0.1700	1.1890	1.1889
	20^0	0.1686	1.2662	1.0633	0.1751	1.1865	1.1865
	25^0	0.1752	1.2908	1.0827	0.1821	1.1978	1.1978
	30^0	0.1839	1.3315	1.1149	0.1911	1.2250	1.2250
	35^0	0.1951	1.3912	1.1624	0.2029	1.2706	1.2705
$0^0/90^0/0^0$	0^0	0.2557	0.9514	0.8928	0.1171	0.9905	0.9905
	5^0	0.2568	0.9552	0.8937	0.1177	0.9861	0.9861
	10^0	0.2598	0.9602	0.8959	0.1193	0.9833	0.9833
	15^0	0.2651	0.9676	0.9007	0.1218	0.9834	0.9834
	20^0	0.2728	0.9794	0.9097	0.1254	0.9887	0.9886
	25^0	0.2833	0.9978	0.9251	0.1303	1.0012	1.0013
	30^0	0.2971	1.0254	0.9491	0.1367	1.0237	1.0237
	35^0	0.3148	1.0651	0.9841	0.1451	1.0586	1.0586
$(0^0/90^0)_2$	0^0	0.1540	1.0256	0.8637	0.1576	1.0248	1.0248
	5^0	0.1546	1.0295	0.8642	0.1582	1.0181	1.0181
	10^0	0.1565	1.0324	0.8655	0.1601	1.0110	1.0110
	15^0	0.1598	1.0371	0.8694	0.1634	1.0068	1.0068
	20^0	0.1645	1.0472	0.8783	0.1682	1.0089	1.0089
	25^0	0.1710	1.0662	0.8944	0.1748	1.0202	1.0202
	30^0	0.1795	1.0969	0.9199	0.1834	1.0434	1.0434
	35^0	0.1905	1.1421	0.9571	0.1946	1.0809	1.0809
$(0^0/90^0)_S$	0^0	0.1492	0.9501	0.8779	0.1482	0.9753	0.9753
	5^0	0.1499	0.9527	0.8786	0.1489	0.9715	0.9715
	10^0	0.1517	0.9557	0.8801	0.1507	0.9686	0.9685
	15^0	0.1548	0.9608	0.8840	0.1539	0.9681	0.9681
	20^0	0.1594	0.9704	0.8920	0.1584	0.9726	0.9726
	25^0	0.1656	0.9869	0.9065	0.1646	0.9845	0.9845
	30^0	0.1738	1.0131	0.9295	0.1727	1.0064	1.0064
	35^0	0.1844	1.0518	0.9638	0.1832	1.0407	1.0407

From Table 5.3, it is observed that under CCCC boundary conditions, deflection consistently increases with skew angle for all cross-ply laminations, reflecting the reduction in overall stiffness as the panel geometry becomes more skewed. The $(0°/90°)_S$ symmetric laminate exhibits the lowest deflections among cross-ply configurations under the fully clamped condition, indicating the beneficial role of symmetry in providing coupled bending-stretching

stiffness. Under SSSS boundary conditions, an initial slight decrease in deflection is observed for certain laminations at lower skew angles, but deflections rise significantly at higher skew angles (≥ 25°) due to the growing influence of skew-induced anisotropy. The SCSC configuration consistently yields the lowest deflections overall, demonstrating that clamping along the curved edges provides a highly effective restraint against transverse bending.

The CCSS and SSCC configurations show nearly identical deflections due to the symmetric nature of the panel geometry, confirming that the formulation correctly captures the symmetry of the boundary conditions. Among all laminations, the 0°/90°/0° three-layer cross-ply laminate under SCSC conditions yields deflections in the range of 0.1171–0.1451, which are the lowest recorded for cross-ply panels under uniform pressure, highlighting the benefit of both the orthotropic fibre orientation and the edge clamping.

5.4.2 Angle-ply Laminates

Table 5.4 presents the corresponding results for angle-ply laminates under uniform pressure. The laminations investigated are 45°/−45°, 45°/−45°/45°, $(45°/-45°)_2$, and $(45°/-45°)_S$.

Table 5.4: Non-dimensional deflections ($\delta \times 10^4$) of biaxially stiffened angle-ply cylindrical panels under uniform pressure

lamination	ϕ	CCCC	SSSS	CSCS	SCSC	CCSS	SSCC
$45^0/-45^0$	0^0	0.2780	0.7393	0.6297	0.3746	0.7685	0.7685
	5^0	0.2792	0.7167	0.6228	0.3821	0.7423	0.7423
	10^0	0.2825	0.6843	0.6108	0.3911	0.7039	0.7039
	15^0	0.2883	0.6749	0.6016	0.4019	0.6722	0.6722
	20^0	0.2967	0.6944	0.5999	0.4149	0.6516	0.6515
	25^0	0.3081	0.7215	0.6073	0.4307	0.6430	0.6430
	30^0	0.3231	0.7577	0.6285	0.4504	0.6460	0.6460
	35^0	0.3424	0.8043	0.6585	0.4750	0.6604	0.6603
$45^0/-45^0/45^0$	0^0	0.2707	0.6087	0.5267	0.3743	0.6205	0.6206
	5^0	0.2718	0.5906	0.5227	0.3647	0.5997	0.5997
	10^0	0.2751	0.5634	0.5191	0.3573	0.5703	0.5703
	15^0	0.2806	0.5420	0.5183	0.3524	0.5438	0.5438
	20^0	0.2888	0.5403	0.5217	0.3506	0.5377	0.5377
	25^0	0.2998	0.5478	0.5316	0.3555	0.5403	0.5403
	30^0	0.3143	0.5715	0.5489	0.3701	0.5519	0.5519
	35^0	0.3330	0.6063	0.5742	0.3888	0.5727	0.5727
$(45^0/-45^0)_2$	0^0	0.2634	0.5835	0.5145	0.3469	0.5974	0.5974
	5^0	0.2645	0.5659	0.5090	0.3533	0.5766	0.5766
	10^0	0.2677	0.5475	0.4987	0.3611	0.5465	0.5465
	15^0	0.2732	0.5492	0.4935	0.3707	0.5203	0.5203
	20^0	0.2811	0.5650	0.4976	0.3824	0.5048	0.5047
	25^0	0.2920	0.5884	0.5080	0.3967	0.5029	0.5029
	30^0	0.3062	0.6193	0.5256	0.4147	0.5126	0.5126
	35^0	0.3246	0.6587	0.5510	0.4373	0.5378	0.5378
$(45^0/-45^0)_S$	0^0	0.2626	0.5580	0.5015	0.3482	0.5677	0.5677
	5^0	0.2637	0.5477	0.4969	0.3455	0.5481	0.5481
	10^0	0.2669	0.5413	0.4919	0.3538	0.5201	0.5201
	15^0	0.2724	0.5416	0.4906	0.3636	0.4984	0.4984
	20^0	0.2803	0.5545	0.4943	0.3753	0.4937	0.4938
	25^0	0.2912	0.5751	0.5045	0.3897	0.4971	0.4971
	30^0	0.3054	0.6038	0.5217	0.4075	0.5085	0.5085
	35^0	0.3239	0.6413	0.5466	0.4297	0.5281	0.5281

Under uniform pressure, angle-ply laminates exhibit a distinctive non-monotonic behaviour under SSSS boundary conditions: deflections decrease from 0° to approximately 15°–20° before rising with further increase in skew angle. This dip arises from the beneficial redistribution of loads along the dominant fibre directions at moderate skew angles. The $(45°/-45°)_S$ symmetric laminate achieves the lowest deflections among angle-ply panels under

SSSS conditions, particularly at 0° where δ= 0.5580, representing approximately a 24.5% reduction compared to the basic 45°/−45° laminate.

Under CCCC conditions, angle-ply deflections increase monotonically with skew angle, similar to cross-ply panels. However, the overall magnitudes are higher compared to cross-ply configurations, indicating that angle-ply laminates are better suited to simply supported configurations where the membrane action associated with their off-axis fibre orientation can be fully utilized. The SCSC condition again provides the most effective restraint, with deflections ranging from 0.3469 to 0.4750 for the 45°/−45° laminate.

5.5 Non-dimensional Deflections under Sinusoidal (Sin-Sin) Pressure

Sinusoidal pressure loading of the form $q = q_0 \sin(\pi x/a) \sin(\pi y/b)$ distributes the load intensity in a manner that vanishes at all four edges and peaks at the panel centre. This loading condition is significantly less severe than uniform pressure and is used to study how the spatial distribution of load affects the structural response of stiffened cylindrical panels.

The non-dimensional deflections for cross-ply and angle-ply panels under sin-sin pressure are presented in Tables 6.5 and 6.6, respectively. A comparison of these values with those under uniform pressure (Tables 5.3 and 5.4) reveals that sin-sin loading consistently produces lower deflections across all configurations typically 25% to 65% lower, depending on the lamination and boundary condition. This confirms the expectation that a load concentrated near the centre with zero edge values produces substantially less panel bending than a uniform load of the same intensity.

For cross-ply laminates under sin-sin pressure, deflections increase monotonically with skew angle for all boundary conditions. The CCCC condition produces the lowest deflections, while SSSS yields the highest for cross-ply panels. The symmetric laminate $(0°/90°)_S$ performs competitively under all conditions. Under angle-ply laminates with SSSS support, a slight dip in deflection is again observed near $\phi = 5°$ to 10°, consistent with the behaviour under uniform pressure but less pronounced.

5.6 Non-dimensional Deflections under Cos-Cos Pressure

Cosinusoidal pressure loading of the form $q = q_0 \cos(\pi x/a) \cos(\pi y/b)$ is characterised by its maximum at the panel centre and negative values (suction) near the edges. This loading condition represents an intermediate severity between sinusoidal and uniform pressure distributions. The non-dimensional deflections for cross-ply and angle-ply panels under cos-cos pressure are reported in Tables 6.7 and 6.8.

The results show that cos-cos loading produces deflections that are intermediate between sin-sin and uniform pressure values, confirming the anticipated ordering: sin-sin < cos-cos < uniform, for all configurations and skew angles. This result aligns with the observation from the PPT presentation that uniform load is the most critical loading condition, cos-cos is intermediate, and sin-sin produces the lowest deflections. This ranking is consistent across all laminations, boundary conditions, and skew angles investigated.

Under cos-cos pressure, the effect of skew angles is more prominent for angle-ply laminates than for cross-ply laminates. The CCCC boundary condition consistently provides the most rigid response, while SSSS with angle-ply laminates benefits from the improved load redistribution offered by the off-axis fibre orientation.

5.7 Stress Resultants

The force and moment resultants are important indicators of the internal stress state in composite panels and provide insight into the dominant load-carrying mechanism. Tables 6.9, 6.10 and 6.11 report representative non-dimensional stress resultants in-plane forces N_x, N_y, N_{xy}, and bending moments M_x, M_y, M_{xy} for selected configurations under uniform, sin-sin, and cos-cos pressures, respectively.

Several significant trends are evident from the stress resultant results:

Effect of skew angle on in-plane forces: The membrane force N_x under CCCC $(0°/90°)_S$ increases from 0.5123 at ϕ=0° to 0.7048 at ϕ=35°, reflecting the progressive redistribution of in-plane forces as the panel geometry becomes more rhombic. N_x shows a substantial compressive increase with skew angle, indicating growing meridional compression.

Dominance of twisting moments at high skew angles: For angle-ply panels under SSSS conditions, the twisting moment M_{xy} becomes dominant at high skew angles ($\phi \geq 25°$), as reported for SSSS (45°/-45°/45°) where M_{xy} reaches 189.73 at ϕ=35°. This confirms that skew geometry significantly activates coupling between bending and twisting.

High bending moments in CCSS angle-ply panels: The CCSS $(45°/-45°)_S$ configuration exhibits the largest bending moments M_x across all skew angles under uniform pressure, peaking at M_x =229.85 at ϕ= 35°, while simultaneously showing large in-plane shear forces N_{xy}. This suggests that mixed boundary conditions combined with angle-ply lamination lead to high localised bending near the constrained edges.

SCSC cross-ply panels low bending response: The SCSC (0°/90°/0°) configuration shows consistently low M_x values (in the range of 2.1120 to 3.1151), indicating that clamping along

the curved edges effectively reduces bending at the mid-surface, redistributing loads through in-plane membrane action.

Under sin-sin and cos-cos pressures, the stress resultant magnitudes are lower than for uniform pressure, consistent with the deflection trends. However, the qualitative patterns dominance of M_{xy} at high skew angles for angle-ply panels, low M_x for SCSC cross-ply panels are preserved, suggesting that the fundamental structural mechanisms are loading-type independent.

5.8 Selection of Optimal Configurations

Based on the systematic investigation of deflections and stress resultants across all loading types, boundary conditions, and lamination sequences, the following observations are made regarding the optimal configurations:

Best overall deflection performance: SCSC boundary condition with (0°/90°/0°) cross-ply lamination consistently produces the lowest non-dimensional deflections under all three loading types across all skew angles.

Best angle-ply configuration: $(45°/-45°)_S$ symmetric laminate under SSSS or CSCS boundary conditions offers the best performance among angle-ply laminates, with the lowest deflections particularly at zero skew angle.

Load type sensitivity: Panels under uniform pressure are the most critical design scenario and should be used as the basis for design. The sinusoidal loading provides an optimistic (lower bound) estimate of structural response.

Skew angle effect: Deflections generally increase with skew angles. The rate of increase is more rapid beyond ϕ=25°, particularly for angle-ply laminates under CCCC conditions. Designers should treat skew angles above 25° with caution in practical applications.

5.9 Summary

This chapter presented comprehensive numerical results for the geometrically nonlinear bending analysis of biaxially stiffened skewed composite cylindrical shell panels. The key findings can be summarised as follows:

(i) The proposed finite element code was validated against benchmark solutions with differences of less than 0.2%, confirming their accuracy for stiffened composite cylindrical shell panels.

(ii) Deflections increase monotonically with skew angles under CCCC conditions for both cross-ply and angle-ply laminates, while angle-ply panels under SSSS exhibit a favourable dip near ϕ= 15° to 20°.

(iii) The ranking of load severity is confirmed as: uniform > cos-cos > sin-sin, consistent across all boundary conditions and laminations.

(iv) SCSC boundary condition with cross-ply lamination provides the best deflection performance, while CCSS angle-ply panels exhibit the highest bending moments, particularly at high skew angles.

(v) Twisting moments become dominant for angle-ply panels at high skew angles, underscoring the need for geometric nonlinear analysis in the design of skewed stiffened composite shell panels.

CHAPTER 6

RESULTS AND DISCUSSIONS

6.1 General

This chapter reports the outcomes and discussion of numerical analyses conducted on biaxially stiffened skewed laminated composite cylindrical shell panels. A geometrically nonlinear finite element model incorporating C^0 continuity, based on first-order shear deformation theory (FSDT) with von Kármán nonlinear strain terms, is utilized throughout the investigation. The shell panels are discretised using eight-noded iso-parametric elements, while the stiffeners are modelled with three-noded beam elements. Three transverse pressure distributions are applied: uniform ($q = q_0$), sinusoidal ($q = q_0 \sin(\pi x/a) \sin(\pi y/b)$), and cosinusoidal ($q = q_0 \cos(\pi x/a) \cos(\pi y/b)$). Five edge restraint configurations are considered CCCC, SSSS, CSCS, SCSC, and CCSS and the stiffener skew angle φ is incremented from 0° to 35° in intervals of 5°. Both cross-ply and angle-ply lamination sequences are examined for graphite/epoxy and glass/epoxy material systems.

The non-dimensional central deflection is expressed as: $\delta = \frac{wE_{22}h^3}{qa^4} \times 10^4$

where w denotes the central transverse deflection, E is Young's modulus, h is the panel thickness, a is the plan dimension, and q_0 is the reference load intensity. The elastic material properties of both composite systems employed in the analysis are tabulated.

6.2 Results and Discussions

The non-dimensional deflections and critical stress resultants (N_x, N_y, N_{xy}, M_x, M_y, M_{xy}) of biaxially stiffened cylindrical panels are reported in Tables 5.3-6.11 for all three load types. Results are presented separately for cross-ply and angle-ply laminates and discussed with respect to the effects of boundary condition, skew angle, lamination sequence, and load distribution.

6.2.1 Non-Dimensional Deflections under Uniform Pressure

Tables 5.3, and 5.4 present the non-dimensional deflections of biaxially stiffened cross-ply and angle-ply cylindrical panels, respectively, under uniform pressure for skew angles from 0° to 35° and all six boundary conditions.

From Table 5.3 it is observed that for all cross-ply laminates under uniform pressure, the CCCC and SCSC boundary conditions consistently produce the lowest non-dimensional deflections, while SSSS yields the highest values. For the 0°/90°/0° laminate under CCCC, the deflection

increases monotonically from 0.2557 at ϕ=0° to 0.3148 at ϕ =35°, an increase of 23.1%. Under SSSS with the same laminate, deflections rise from 0.9514 to 1.0651 an increase of 12% confirming that all boundary conditions become more flexible as the skew angle increases under uniform loading.

For angle-ply laminates under uniform pressure (Table 5.3), a markedly different trend is observed at the SSSS boundary condition. The 45°/−45°/45° laminate under SSSS shows a reduction in deflection from 0.6087 at ϕ=0° to a minimum of 0.5403 at ϕ=20°, before rising again to 0.6063 at ϕ=35°. This non-monotonic, favourable dip near ϕ=15°–20° is a hallmark of angle-ply panels, where the enhanced twisting stiffness at intermediate skew angles temporarily counteracts the geometric softening induced by the skewed boundary. No such dip is observed for CCCC panels, where deflections increase monotonically for all laminations. Comparing Tables 5.4 and 5.5 angle-ply laminates provide substantially lower deflections than cross-ply laminates under SSSS for example, the $(45°/-45°)_S$ laminate gives δ = 0.5580 at ϕ= 0° compared to 0.9501 for the $(0°/90°)_S$ laminate, a reduction of 41.3%. This confirms the superior bending stiffness of angle-ply configurations under simply supported conditions.

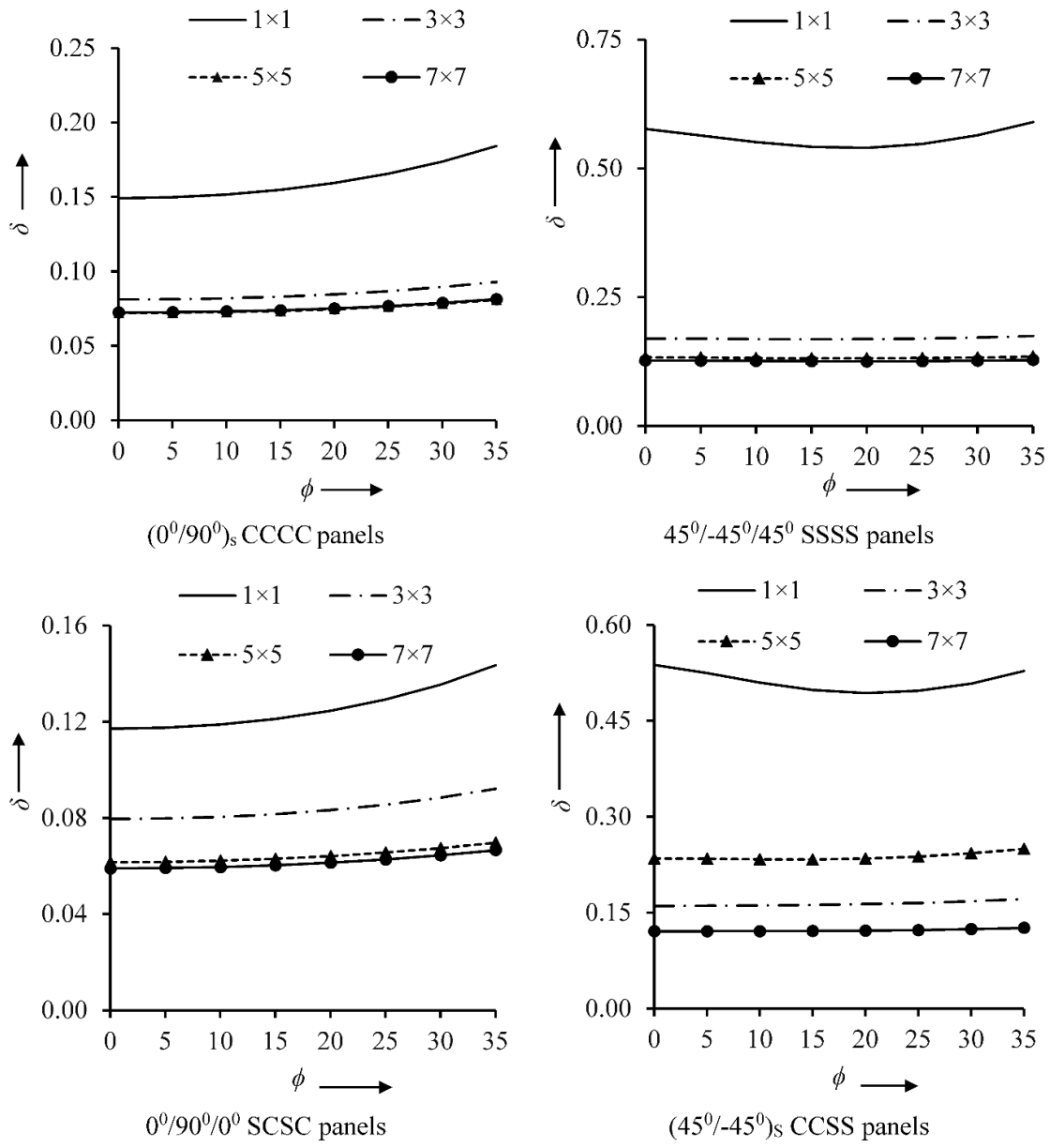

Figure 6.9: Load-deflection curve of cylindrical panel under uniform pressure

6.2.2 Non-Dimensional Deflections under Sinusoidal Pressure

Tables 6.5 and 6.6 present the deflections under sinusoidal (sin-sin) loading for cross-ply and angle-ply laminates. The sinusoidal distribution concentrates the load at the panel centre and produces significantly lower deflections than uniform loading across all configurations.

Table 6.5: Non-dimensional deflections (δ) of biaxially stiffened cross-ply cylindrical panels under sin-sin pressure.

lamination	ϕ	CCCC	SSSS	CSCS	SCSC	CCSS	SSCC
$0^0/90^0$	0^0	0.1970	0.3576	0.3427	0.2225	0.3568	0.3568
	5^0	0.1977	0.3597	0.3438	0.2233	0.3573	0.3573
	10^0	0.1997	0.3647	0.3470	0.2255	0.3606	0.3606
	15^0	0.2032	0.3725	0.3525	0.2291	0.3666	0.3666
	20^0	0.2082	0.3830	0.3608	0.2342	0.3753	0.3753
	25^0	0.2150	0.3962	0.3721	0.2410	0.3868	0.3868
	30^0	0.2240	0.4125	0.3872	0.2495	0.4017	0.4017
	35^0	0.2354	0.4341	0.4069	0.2601	0.4207	0.4207
$0^0/90^0/0^0$	0^0	0.1685	0.3603	0.3469	0.1867	0.3580	0.3580
	5^0	0.1690	0.3619	0.3480	0.1873	0.3582	0.3582
	10^0	0.1703	0.3660	0.3510	0.1890	0.3609	0.3609
	15^0	0.1726	0.3723	0.3561	0.1918	0.3660	0.3660
	20^0	0.1758	0.3812	0.3635	0.1959	0.3738	0.3738
	25^0	0.1802	0.3929	0.3734	0.2013	0.3844	0.3844
	30^0	0.1858	0.4078	0.3864	0.2083	0.3984	0.3984
	35^0	0.1928	0.4266	0.4031	0.2170	0.4163	0.4163
$(0^0/90^0)_2$	0^0	0.1766	0.3393	0.3158	0.2079	0.3361	0.3361
	5^0	0.1770	0.3411	0.3168	0.2085	0.3366	0.3366
	10^0	0.1783	0.3454	0.3198	0.2103	0.3395	0.3395
	15^0	0.1805	0.3522	0.3247	0.2133	0.3447	0.3447
	20^0	0.1837	0.3614	0.3317	0.2177	0.3524	0.3524
	25^0	0.1879	0.3733	0.3409	0.2233	0.3629	0.3629
	30^0	0.1932	0.3879	0.3528	0.2306	0.3764	0.3764
	35^0	0.2000	0.4059	0.3676	0.2396	0.3935	0.3935
$(0^0/90^0)_S$	0^0	0.1795	0.3527	0.3311	0.2005	0.3539	0.3539
	5^0	0.1800	0.3543	0.3322	0.2011	0.3544	0.3544
	10^0	0.1814	0.3585	0.3350	0.2029	0.3572	0.3572
	15^0	0.1838	0.3653	0.3399	0.2060	0.3624	0.3624
	20^0	0.1873	0.3747	0.3468	0.2104	0.3703	0.3703
	25^0	0.1919	0.3869	0.3562	0.2162	0.3811	0.3811
	30^0	0.1978	0.4020	0.3685	0.2237	0.3951	0.3951
	35^0	0.2051	0.4207	0.3842	0.2330	0.4129	0.4129

$\delta = wEh^3/q_0a^4$. Sinusoidal load $q = q_0\sin(\pi x/a)\sin(\pi y/b)$. Biaxial stiffeners. Graphite/epoxy composite.

Table 6.6: Non-dimensional deflections (δ) of biaxially stiffened angle-ply cylindrical panels under sin-sin pressure.

lamination	ϕ	CCCC	SSSS	CSCS	SCSC	CCSS	SSCC
$45^0/-45^0$	0^0	0.1997	0.2466	0.2308	0.2161	0.2313	0.2313
	5^0	0.2004	0.2472	0.2309	0.2190	0.2303	0.2303
	10^0	0.2025	0.2487	0.2322	0.2238	0.2305	0.2305
	15^0	0.2061	0.2528	0.2350	0.2304	0.2325	0.2325
	20^0	0.2113	0.2607	0.2400	0.2390	0.2383	0.2383
	25^0	0.2183	0.2721	0.2474	0.2497	0.2499	0.2499
	30^0	0.2276	0.2871	0.2576	0.2629	0.2641	0.2641
	35^0	0.2394	0.3060	0.2710	0.2789	0.2816	0.2816
$45^0/-45^0/45^0$	0^0	0.1788	0.2191	0.2115	0.1997	0.2255	0.2255
	5^0	0.1794	0.2177	0.2122	0.1965	0.2230	0.2230
	10^0	0.1812	0.2190	0.2146	0.1953	0.2230	0.2230
	15^0	0.1843	0.2231	0.2186	0.1960	0.2253	0.2253
	20^0	0.1887	0.2299	0.2243	0.2009	0.2299	0.2299
	25^0	0.1948	0.2396	0.2318	0.2082	0.2370	0.2370
	30^0	0.2028	0.2522	0.2414	0.2176	0.2467	0.2467
	35^0	0.2129	0.2680	0.2535	0.2295	0.2595	0.2595
$(45^0/-45^0)_2$	0^0	0.1778	0.2093	0.2004	0.1914	0.2013	0.2013
	5^0	0.1784	0.2108	0.2009	0.1937	0.2014	0.2014
	10^0	0.1801	0.2144	0.2028	0.1980	0.2040	0.2040
	15^0	0.1831	0.2205	0.2062	0.2040	0.2086	0.2086
	20^0	0.1875	0.2292	0.2111	0.2118	0.2152	0.2152
	25^0	0.1934	0.2405	0.2178	0.2215	0.2245	0.2245
	30^0	0.2011	0.2545	0.2267	0.2332	0.2382	0.2382
	35^0	0.2110	0.2717	0.2383	0.2475	0.2547	0.2547
$(45^0/-45^0)_S$	0^0	0.1754	0.2021	0.1982	0.1891	0.2051	0.2051
	5^0	0.1759	0.2028	0.1989	0.1891	0.2046	0.2046
	10^0	0.1777	0.2059	0.2011	0.1931	0.2064	0.2064
	15^0	0.1807	0.2119	0.2047	0.1989	0.2103	0.2103
	20^0	0.1850	0.2212	0.2102	0.2157	0.2162	0.2162
	25^0	0.1909	0.2329	0.2174	0.2157	0.2243	0.2243
	30^0	0.1986	0.2472	0.2266	0.2271	0.2349	0.2349
	35^0	0.2084	0.2645	0.2382	0.2409	0.2498	0.2498

$\delta = wEh^3/q_0a^4$. Sinusoidal load $q = q_0 \sin(\pi x/a) \sin(\pi y/b)$. Biaxial stiffeners. Graphite/epoxy composite.

Under sin-sin pressure, the deflection of the 0°/90° laminate under SSSS at ϕ= 0° reduces to 0.3576, compared to 1.2893 under uniform pressure, a reduction of approximately 72.3%. This dramatic decrease confirms that the spatial distribution of load is a dominant factor in the

bending response of stiffened cylindrical panels. Under sinusoidal loading, cross-ply deflections increase monotonically with skew angles for all boundary conditions. The (0°/90°/0°) laminate under CCCC increases from 0.1685 at ϕ=0° to 0.1928 at ϕ= 5° (a 14.4% increase), while under SSSS it rises from 0.3603 to 0.4266 (18.4%). For angle-ply panels under sin-sin loading the non-monotonic dip observed under uniform pressure largely disappears, and deflections increase steadily with skew angle for all boundary conditions.

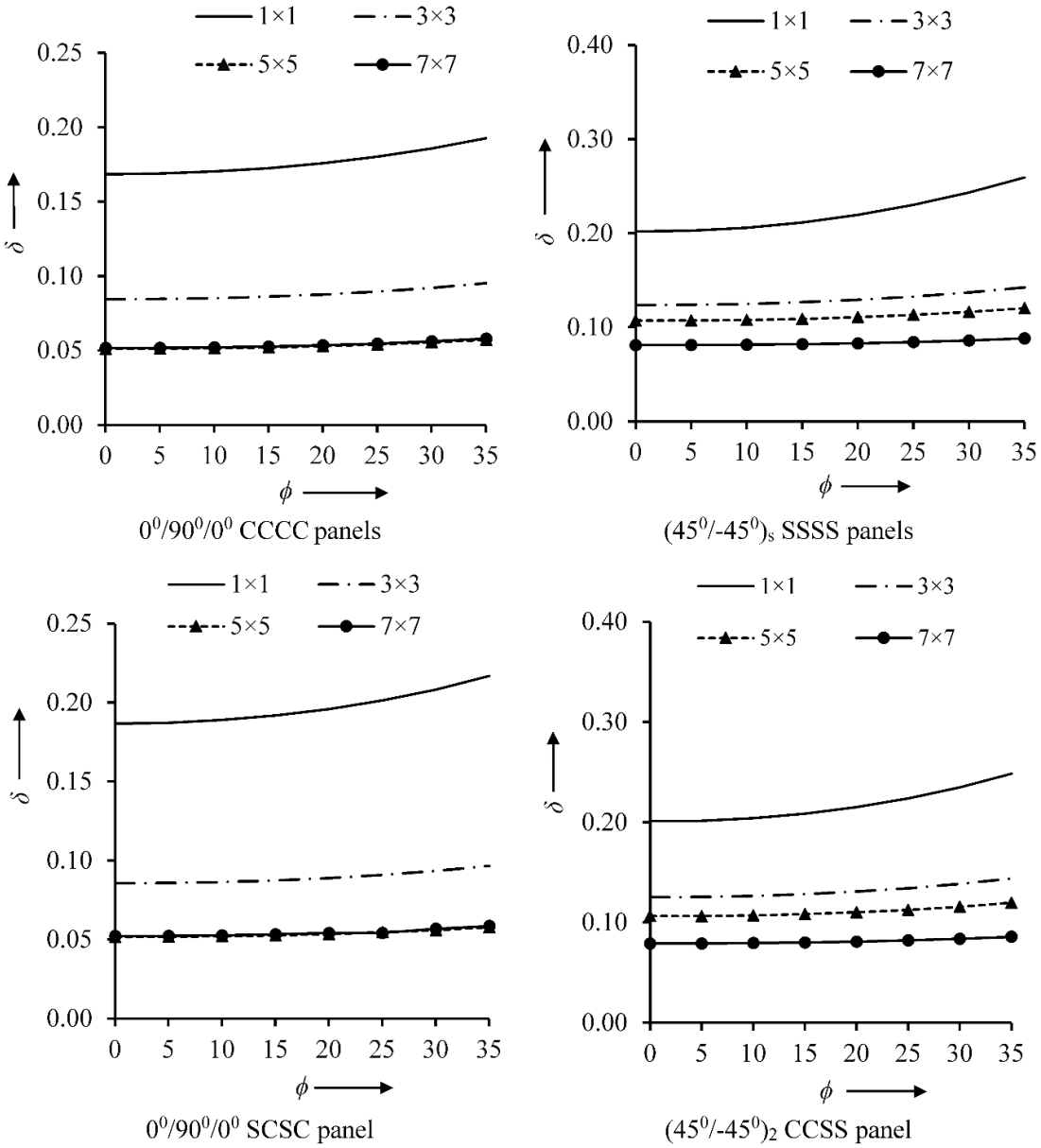

Figure 6.10: Load-deflection curve of cylindrical panel under sin-sin pressure

6.2.3 Non-Dimensional Deflections under Cosine Pressure

Tables 6.7 and 6.8 report deflections under cosine (cos-cos) loading. Cosine loading activates a broader area of the panel than sinusoidal loading and produces intermediate deflection values lower than uniform but higher than sin-sin loading.

Table 6.7: Non-dimensional deflections (δ) of biaxially stiffened cross-ply cylindrical panels under cos-cos pressure.

lamination	ϕ	CCCC	SSSS	CSCS	SCSC	CCSS	SSCC
$0^0/90^0$	0^0	0.3301	1.0812	0.8668	0.3707	0.8699	0.8699
	5^0	0.3314	1.0769	0.8625	0.3724	0.8659	0.8659
	10^0	0.3352	1.0603	0.8527	0.3774	0.8544	0.8544
	15^0	0.3418	1.0420	0.8540	0.3861	0.8539	0.8539
	20^0	0.3514	1.0494	0.8618	0.3987	0.8620	0.8620
	25^0	0.3645	1.0719	0.8786	0.4157	0.8794	0.8794
	30^0	0.3816	1.1091	0.9065	0.4378	0.9081	0.9081
	35^0	0.4036	1.1632	0.9475	0.4661	0.9499	0.9499
$0^0/90^0/0^0$	0^0	0.3061	0.8599	0.7751	0.3329	0.7434	0.7434
	5^0	0.3072	0.8631	0.7758	0.3346	0.7444	0.7444
	10^0	0.3108	0.8683	0.7780	0.3395	0.7468	0.7468
	15^0	0.3169	0.8763	0.7828	0.3477	0.7517	0.7517
	20^0	0.3258	0.8889	0.7916	0.3596	0.7605	0.7605
	25^0	0.3378	0.9080	0.8062	0.3756	0.7750	0.7750
	30^0	0.3536	0.9357	0.8286	0.3962	0.7969	0.7969
	35^0	0.3739	0.9749	0.8609	0.4223	0.8286	0.8286
$(0^0/90^0)_2$	0^0	0.3016	0.8970	0.7053	0.3555	0.7047	0.7047
	5^0	0.3027	0.9005	0.7056	0.3571	0.7051	0.7051
	10^0	0.3063	0.9036	0.7066	0.3620	0.7061	0.7061
	15^0	0.3123	0.9089	0.7099	0.3703	0.7093	0.7093
	20^0	0.3210	0.9196	0.7175	0.3823	0.7170	0.7170
	25^0	0.3329	0.9386	0.7315	0.3984	0.7311	0.7311
	30^0	0.3484	0.9684	0.7536	0.4194	0.7535	0.7535
	35^0	0.3685	1.0116	0.7858	0.4462	0.7861	0.7861
$(0^0/90^0)_S$	0^0	0.3127	0.8448	0.7392	0.3495	0.7180	0.7180
	5^0	0.3139	0.8474	0.7398	0.3511	0.7188	0.7188
	10^0	0.3175	0.8511	0.7415	0.3560	0.7207	0.7207
	15^0	0.3237	0.8574	0.7455	0.3641	0.7247	0.7247
	20^0	0.3328	0.8681	0.7533	0.3760	0.7325	0.7325
	25^0	0.3451	0.8853	0.7668	0.3919	0.7459	0.7459
	30^0	0.3612	0.9114	0.7878	0.4125	0.7667	0.7667
	35^0	0.3820	0.9490	0.8186	0.4388	0.7971	0.7971

$\delta = wEh^3/q_0a^4$. Cosine load $q = q_0\cos(\pi x/a)\cos(\pi y/b)$. Biaxial stiffeners. Graphite/epoxy composite.

Table 6.8: Non-dimensional deflections (δ) of biaxially stiffened angle-ply cylindrical panels under cos-cos pressure**.**

lamination	ϕ	CCCC	SSSS	CSCS	SCSC	CCSS	SSCC
$45^0/-45^0$	0^0	0.2287	0.5016	0.4143	0.2891	0.4172	0.4172
	5^0	0.2296	0.5040	0.4117	0.2945	0.4135	0.4135
	10^0	0.2323	0.4975	0.4065	0.3022	0.4068	0.4068
	15^0	0.2368	0.4938	0.4034	0.3123	0.4023	0.4023
	20^0	0.2435	0.4986	0.4052	0.3250	0.4029	0.4029
	25^0	0.2526	0.5126	0.4126	0.3406	0.4095	0.4095
	30^0	0.2644	0.5356	0.4262	0.3597	0.4221	0.4221
	35^0	0.2797	0.5675	0.4462	0.3831	0.4414	0.4414
$45^0/-45^0/45^0$	0^0	0.1948	0.3592	0.3030	0.2222	0.3055	0.3055
	5^0	0.1956	0.3594	0.3024	0.2241	0.3040	0.3040
	10^0	0.1978	0.3547	0.2999	0.2283	0.3006	0.3006
	15^0	0.2017	0.3498	0.2976	0.2348	0.2974	0.2974
	20^0	0.2072	0.3496	0.2981	0.2438	0.2970	0.2970
	25^0	0.2148	0.3564	0.3026	0.2560	0.3010	0.3010
	30^0	0.2247	0.3704	0.3118	0.2710	0.3096	0.3096
	35^0	0.2375	0.3914	0.3261	0.2893	0.3233	0.3233
$(45^0/-45^0)_2$	0^0	0.1882	0.3794	0.3159	0.2284	0.3196	0.3196
	5^0	0.1889	0.3807	0.3111	0.2326	0.3166	0.3166
	10^0	0.1911	0.3764	0.3077	0.2391	0.3107	0.3107
	15^0	0.1949	0.3742	0.3080	0.2479	0.3063	0.3063
	20^0	0.2004	0.3781	0.3128	0.2592	0.3058	0.3058
	25^0	0.2078	0.3890	0.3222	0.2731	0.3099	0.3099
	30^0	0.2175	0.4065	0.3222	0.2901	0.3188	0.3188
	35^0	0.2301	0.4311	0.3366	0.3107	0.3327	0.3327
$(45^0/-45^0)_S$	0^0	0.1858	0.3638	0.2993	0.2185	0.3009	0.3009
	5^0	0.1865	0.3649	0.2984	0.2228	0.2990	0.2990
	10^0	0.1887	0.3606	0.2953	0.2293	0.2950	0.2950
	15^0	0.1924	0.3569	0.2928	0.2382	0.2915	0.2915
	20^0	0.1978	0.3588	0.2934	0.2494	0.2913	0.2913
	25^0	0.2052	0.3678	0.2982	0.2632	0.2956	0.2956
	30^0	0.2148	0.3838	0.3075	0.2799	0.3044	0.3044
	35^0	0.2272	0.4068	0.3218	0.3003	0.3183	0.3183

$\bar{w} = wEh^3/q_0a^4$. Cosine load $q = q_0\cos(\pi x/a)\cos(\pi y/b)$. Biaxial stiffeners. Graphite/epoxy composite.

The (0°/90°) laminate under SSSS gives a cos-cos deflection of 1.0812 at ϕ=0°, intermediate between 1.2893 (uniform) and 0.3576 (sin-sin). This hierarchy uniform > cos-cos > sin-sin holds consistently across all laminations and boundary conditions, confirming that a design based on uniform loading is conservative for the other load types. Under cosine loading, cross-ply SSSS panels show a slight dip near ϕ=10°–15°; for example, the (0°/90°) laminate decreases from 1.0812 at ϕ=0° to a minimum of 1.0420 at ϕ=15° before rising to 1.1632 at φ = 35°. For angle-ply panels under cosine loading, the (45°/−45°/45°) laminate under SSSS similarly exhibits a dip at ϕ=15°–20°, reaching 0.3496, before increasing to 0.3914 at ϕ=35°. These intermediate dips are attributed to the coupling between the cosine load distribution and skew-induced bending-twisting interaction in angle-ply panels.

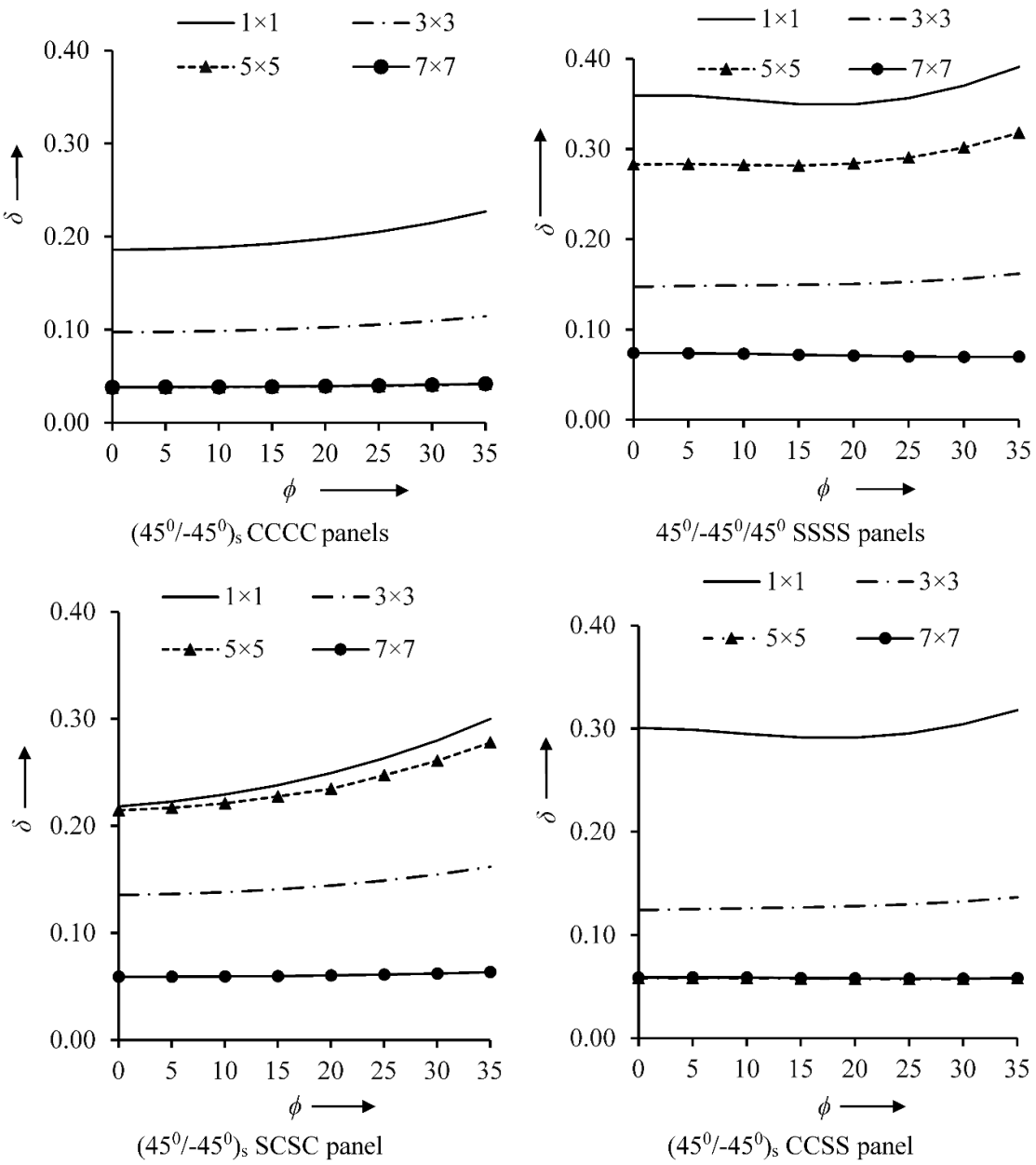

Figure 6.11: Load-deflection curve of cylindrical panel under cos-cos pressure

6.2.4 Effect of Skew Angle on Deflection

Across all three load types (Tables 5.3–6.8), the CCCC boundary condition consistently yields the minimum deflections, and SSSS yields the maximum. The intermediate CSCS and SCSC conditions generally approach CCCC performance levels. For cross-ply laminates, deflections increase monotonically with skew angles under all load types. For angle-ply laminates under uniform and cosine loads at SSSS, a favorable reduction in deflection is observed near ϕ= 15°–20°, beyond which deflections rise again. This behavior is physically explained by the

interaction of skew-induced bending-twisting coupling and the angle-ply stacking sequence: at intermediate skew angles, the twisting stiffness of angle-ply laminates temporarily compensates for the geometric softening, creating a local peak in structural rigidity. The minimum deflection across all configurations is achieved by the CCCC $(0°/90°)_S$ laminate at ϕ= 0° under sin-sin loading (δ = 0.1754), while the maximum is found for SSSS (0°/90°) at ϕ = 35° under uniform pressure (δ= 1.3912).

6.2.5 Stress Resultants under Uniform Pressure

Table 6.9 presents the critical non-dimensional stress resultants in-plane forces N_x, N_y, N_{xy}, bending moments M_x, M_y, and twisting moment M_{xy} for representative boundary condition and lamination combinations under uniform pressure. The critical values correspond to the numerically maximum absolute values occurring at any location in the panel.

Table 6.9: Non-dimensional stress resultants of biaxially stiffened cylindrical panels under uniform pressure.

ϕ	Stress resultants	N_x	N_y	N_{xy}	M_x	M_y	M_{xy}
0^0	CCCC $(0^0/90^0)_S$	0.5123	-38.580	3.4606	58.836	63.019	2.2336
	SSSS $(45^0/-45^0/45^0)$	-36.725	0.5228	-72.788	140.28	-99.426	135.02
	SCSC $(0^0/90^0/0^0)$	0.3689	-45.198	-2.3215	2.1120	8.7870	0.4271
	CCSS $(45^0/-45^0)_S$	6.9961	5.7432	75.121	210.90	124.13	-116.01
5^0	CCCC $(0^0/90^0)_S$	0.5157	-38.726	3.4589	59.148	63.035	2.1555
	SSSS $(45^0/-45^0/45^0)$	7.4837	-47.536	75.000	135.75	74.754	137.03
	SCSC $(0^0/90^0/0^0)$	0.4426	-46.08	-2.3877	-2.1240	8.8275	0.4323
	CCSS $(45^0/-45^0)_S$	8.5382	5.5991	78.983	209.33	123.46	-113.47
10^0	CCCC $(0^0/90^0)_S$	0.5255	-39.168	3.4832	59.937	63.078	-2.419
	SSSS $(45^0/-45^0/45^0)$	-38.770	6.0418	77.827	-136.08	72.813	130.79
	SCSC $(0^0/90^0/0^0)$	0.4914	-47.38	-2.5487	-2.2387	8.8653	0.4392
	CCSS $(45^0/-45^0)_S$	-35.407	7.312	82.845	207.02	122.39	103.58
15^0	CCCC $(0^0/90^0)_S$	0.5421	-39.923	-3.6237	61.234	63.146	2.1115
	SSSS $(45^0/-45^0/45^0)$	-39.765	9.5938	80.814	-144.60	74.290	121.12
	SCSC $(0^0/90^0/0^0)$	0.6439	-48.632	-2.7216	-2.3677	8.9012	0.4476
	CCSS $(45^0/-45^0)_S$	-36.016	-46.549	86.97	205.71	121.85	-92.185
20^0	CCCC $(0^0/90^0)_S$	0.5665	-41.022	-3.7366	-3.7366	63.091	63.243
	SSSS $(45^0/-45^0/45^0)$	-40.794	-52.085	84.28	-154.60	81.264	122.67
	SCSC $(0^0/90^0/0^0)$	0.7438	-50.047	-2.8722	-2.5142	8.9418	0.4577
	CCSS $(45^0/-45^0)_S$	-36.918	-47.262	91.607	206.91	122.69	115.65
25^0	CCCC $(0^0/90^0)_S$	0.6000	-42.512	-3.8847	65.589	63.371	-2.9090
	SSSS $(45^0/-45^0/45^0)$	-44.872	-56.338	88.257	-166.23	-128.13	145.21
	SCSC $(0^0/90^0/0^0)$	0.7869	-52.300	-3.009	-2.6833	8.9873	0.4698
	CCSS $(45^0/-45^0)_S$	38.318	-50.138	96.738	211.23	125.30	131.51
30^0	CCCC $(0^0/90^0)_S$	0.6449	-44.46	-4.0745	68.846	63.533	-3.1846
	SSSS $(45^0/-45^0/45^0)$	-50.449	-61.526	92.634	-179.65	-137.04	167.24
	SCSC $(0^0/90^0/0^0)$	0.7881	-55.673	-3.1510	-2.8808	9.0419	0.4846
	CCSS $(45^0/-45^0)_S$	44.948	-54.470	-66.532	218.82	129.79	148.08
35^0	CCCC $(0^0/90^0)_S$	0.7048	-46.965	-4.3150	73.036	63.733	-3.503
	SSSS $(45^0/-45^0/45^0)$	-56.727	-67.787	97.327	204.83	152.57	189.73
	SCSC $(0^0/90^0/0^0)$	0.7632	-59.757	-3.3168	-3.1151	9.1092	0.5027
	CCSS $(45^0/-45^0)_S$	50.956	-59.739	-70.344	229.85	136.28	165.73

Critical (maximum absolute) non-dimensional stress resultants. Uniform load $q = q_0$.

Graphite/epoxy composite.

From Table 6.19, the bending moment M_x is highest for the SSSS (45°/−45°/45°) configuration, reaching 204.83 at ϕ=35°. The CCCC $(0°/90°)_S$ panel consistently shows the lowest M_x growing from 58.836 at ϕ=0° to 73.036 at ϕ= 35°- a 24.2% increase. The in-plane shear resultant N_{xy} and torsional moment M_{xy} grow significantly with skew angle for angle-ply panels

under SSSS, illustrating the increasing importance of torsional effects at higher skew angles. For example, M_{xy} for the SSSS (45°/−45°/45°) panel reaches 189.73 at ϕ= 35°, comparable to M_x = 204.83, indicating that torsional failure modes must be considered alongside bending failure at large skew angles. CCSS $(45°/-45°)_S$ panels show the highest bending moments overall, with M_x reaching 229.85 at ϕ=35°.

6.2.6 Stress Resultants under Sinusoidal Pressure

Table 6.10 reports critical stress resultants under sin-sin loading. The concentrated central loading distribution reduces N_{xy} and M_{xy} values compared to uniform loading for most configurations, while M_x and M_y remain significant.

Table 6.10: Non-dimensional stress resultants of biaxially stiffened cylindrical panels under sin-sin pressure.

ϕ	Stress resultants	N_x	N_y	N_{xy}	M_x	M_y	M_{xy}
0^0	CCCC ($0^0/90^0/0^0$)	0.3474	-41.809	3.1821	32.718	58.494	2.0912
	SSSS ($45^0/-45^0$) S	0.2034	-28.09	-26.759	53.595	40.074	25.829
	SCSC ($0^0/90^0/0^0$)	-3.3755	-35.199	-3.7482	20.325	65.604	-2.5805
	CCSS ($45^0/-45^0$)$_2$	-19.454	-28.737	31.463	51.747	38.209	-29.826
5^0	CCCC ($0^0/90^0/0^0$)	0.35	-41.997	3.178	32.867	58.509	2.0938
	SSSS ($45^0/-45^0$) S	3.0637	-28.223	26.851	53.697	40.167	25.94
	SCSC ($0^0/90^0/0^0$)	-3.3702	-35.508	3.7694	20.416	65.596	2.5945
	CCSS ($45^0/-45^0$)$_2$	-19.712	-28.709	33.363	50.432	36.95	-30.161
10^0	CCCC ($0^0/90^0/0^0$)	0.357	-42.509	-3.2625	33.28	58.549	2.1027
	SSSS ($45^0/-45^0$) S	6.3111	3.631	28.702	54.795	41.013	-27.048
	SCSC ($0^0/90^0/0^0$)	-3.3546	-36.421	3.8219	20.694	65.505	2.6181
	CCSS ($45^0/-45^0$)$_2$	-20.013	-28.962	35.394	49.8	36.188	-30.711
15^0	CCCC ($0^0/90^0/0^0$)	0.3687	-43.361	-3.3409	33.975	58.618	2.1182
	SSSS ($45^0/-45^0$) S	9.5889	5.5092	30.69	56.86	42.597	-28.761
	SCSC ($0^0/90^0/0^0$)	-3.3292	-37.904	3.9075	21.17	65.326	2.6512
	CCSS ($45^0/-45^0$)$_2$	-20.387	-29.529	37.63	50.095	35.917	-32.309
20^0	CCCC ($0^0/90^0/0^0$)	0.386	-44.587	-3.4481	34.98	58.713	-2.2336
	SSSS ($45^0/-45^0$) S	-22.009	-29.081	32.76	59.889	44.921	-30.801
	SCSC ($0^0/90^0/0^0$)	-3.2958	-39.921	4.0294	21.864	65.057	2.6941
	CCSS ($45^0/-45^0$)$_2$	-20.88	-30.592	40.032	53.525	36.124	-34.514
25^0	CCCC ($0^0/90^0/0^0$)	0.4096	-46.239	-3.5882	36.340	58.839	-2.3515
	SSSS ($45^0/-45^0$) S	-22.688	9.1683	34.851	63.924	48.016	-33.279
	SCSC ($0^0/90^0/0^0$)	-3.2568	-42.461	4.1930	22.806	64.691	-2.7492
	CCSS ($45^0/-45^0$)$_2$	-21.570	-31.996	42.514	57.167	36.818	-37.172
30^0	CCCC ($0^0/90^0/0^0$)	0.4412	-48.418	-3.767	38.12	59.000	-2.489
	SSSS ($45^0/-45^0$) S	-23.712	-32.837	36.91	69.075	51.967	-36.325
	SCSC ($0^0/90^0/0^0$)	-3.2152	-45.55	4.4062	24.041	-62.261	-2.9363
	CCSS ($45^0/-45^0$)$_2$	-22.806	-33.802	45.006	60.874	39.095	-40.406
35^0	CCCC ($0^0/90^0/0^0$)	0.4832	-51.235	-3.9931	40.414	59.198	-2.6512
	SSSS ($45^0/-45^0$) S	-25.220	-35.583	38.908	75.531	56.919	-40.098
	SCSC ($0^0/90^0/0^0$)	-3.1814	-49.267	4.6798	25.633	63.650	-3.1869
	CCSS ($45^0/-45^0$)$_2$	25.498	-36.099	47.477	64.583	41.416	-44.377

Critical (maximum absolute) non-dimensional stress resultants. Sinusoidal load $q = q_0 \sin(\pi x/a) \sin(\pi y/b)$. Graphite/epoxy composite.

Under sin-sin pressure, the CCCC (0°/90°/0°) panel shows stable and comparatively low stress resultants. The bending moment M_x increases from 32.718 at ϕ=0° to 40.414 at ϕ=35° a 23.5% rise. For CCSS (45°/−45°) $_2$ panels, the torsional resultant M_{xy} grows significantly from −29.826 at ϕ=0° to −44.377 at ϕ=35° (a 48.7% increase), confirming the dominant role of torsional effects in angle-ply panels under skewed geometries. The SCSC (0°/90°/0°) configuration

exhibits sign reversals in N_x with skew angle, reflecting shifts in the in-plane force distribution as the panel geometry changes.

6.2.7 Stress Resultants under Cosine Pressure

Table 6.11 presents critical stress resultants under cosine loading. The cosine distribution activates the panel more broadly than the sinusoidal case, resulting in generally higher M_x and M_y values.

Table 6.11: Non-dimensional stress resultants of biaxially stiffened cylindrical panels under cos-cos pressure.

ϕ	Stress resultants	N_x	N_y	N_{xy}	M_x	M_y	M_{xy}
0^0	CCCC $(0^0/90^0/0^0)$	-16.761	21.225	-17.986	117.16	69.444	61.404
	SSSS $(45^0/-45^0)_S$	28.36	32.876	-48.123	118.73	93.941	105.43
	SCSC $(0^0/90^0/0^0)$	16.643	26.733	-24.472	90.007	72.106	53.36
	CCSS $(45^0/-45^0)_2$	27.95	31.28	-38.05	169.05	99.64	98.01
5^0	CCCC $(0^0/90^0/0^0)$	-16.837	21.357	-18.074	118.08	69.994	61.851
	SSSS $(45^0/-45^0)_S$	28.687	31.459	-46.436	122.11	96.496	107.64
	SCSC $(0^0/90^0/0^0)$	17.284	27.012	-25.228	92.28	77.766	58.543
	CCSS $(45^0/-45^0)_2$	28.052	30.145	-38.992	167.32	98.839	96.523
10^0	CCCC $(0^0/90^0/0^0)$	-17.067	21.689	-18.282	119.9	71.074	62.753
	SSSS $(45^0/-45^0)_S$	28.488	30.586	-44.978	126.77	99.868	104.67
	SCSC $(0^0/90^0/0^0)$	18.187	27.756	-26.8	95.459	83.619	67.656
	CCSS $(45^0/-45^0)_2$	27.59	29.472	-39.687	165.27	97.838	88.516
15^0	CCCC $(0^0/90^0/0^0)$	-17.84	22.231	-18.619	122.68	72.726	66.647
	SSSS $(45^0/-45^0)_S$	28.105	30.467	-44.023	133.1	104.35	99.061
	SCSC $(0^0/90^0/0^0)$	19.331	28.972	-28.153	104.41	89.687	77.212
	CCSS $(45^0/-45^0)_2$	27.058	29.477	-40.422	164.16	97.321	82.51
20^0	CCCC $(0^0/90^0/0^0)$	-18.983	23.005	-19.096	126.54	75.005	71.07
	SSSS $(45^0/-45^0)_S$	-28.271	-32.632	-43.926	141.14	109.97	104.35
	SCSC $(0^0/90^0/0^0)$	20.711	30.674	25.222	113.8	96.003	87.309
	CCSS $(45^0/-45^0)_2$	26.844	30.217	-41.465	165.04	98.096	86.492
25^0	CCCC $(0^0/90^0/0^0)$	-20.332	24.043	-19.735	131.62	78.524	76.963
	SSSS $(45^0/-45^0)_S$	-29.686	-35.554	-44.959	150.78	116.66	113.73
	SCSC $(0^0/90^0/0^0)$	22.338	32.888	-30.07	123.72	102.63	98.078
	CCSS $(45^0/-45^0)_2$	27.052	31.644	-42.888	168.37	-92.664	98.931
30^0	CCCC $(0^0/90^0/0^0)$	-21.934	25.484	-20.562	138.14	82.885	84.857
	SSSS $(45^0/-45^0)_S$	-31.567	-39.13	-47.322	162.06	124.42	124.67
	SCSC $(0^0/90^0/0^0)$	24.247	35.664	-30.628	134.33	109.66	109.71
	CCSS $(45^0/-45^0)_2$	27.651	33.717	-44.671	174.3	109.66	112.65
35^0	CCCC $(0^0/90^0/0^0)$	-23.852	27.402	21.623	146.45	87.986	93.655
	SSSS $(45^0/-45^0)_S$	-33.887	-43.459	-51.212	175.17	133.36	147.19
	SCSC $(0^0/90^0/0^0)$	27.224	39.087	-30.953	145.86	117.25	122.47
	CCSS $(45^0/-45^0)_2$	28.603	-36.642	-46.794	183.05	116.74	127.14

Critical (maximum absolute) non-dimensional stress resultants. Cosine load $q = q_o\cos(\pi x/a)\cos(\pi y/b)$. Graphite/epoxy composite.

Under cosine loading, M_x values are considerably higher than under sin-sin loading for the same configurations. For CCCC (0°/90°/0°), M_x increases from 117.16 at ϕ=0° to 146.45 at ϕ =35°-a 25% increase. The SSSS $(45°/-45°)_S$ panel shows M_x values rising from 118.73 to 175.17 over the same range, a 47.5% increase, highlighting the vulnerability of simply supported angle-ply panels at large skew angles under cosine loading. The most critical stress

state in the entire study is identified as the CCSS (45°/−45°) $_2$ configuration at ϕ=35° under cosine pressure, which produces M_x=183.05. Engineers designing skewed composite cylindrical panels must therefore pay particular attention to this configuration when assessing bending strength.

6.2.8 Effect of Load Distribution on Structural Response

A comparison of the results across Tables 6.8, 6.9, and 6.10 reveals that the severity hierarchy uniform > cosine > sinusoidal holds for both deflections and most stress resultants. However, an important distinction exists where cosine loading governs the bending moments M_x and M_y more severely than uniform loading for many configurations, even though uniform loading produces the highest deflections. This means a panel adequately designed for deflection under uniform loading may still be critical in bending under cosine loading. The twisting resultant M_{xy} and in-plane shear N_{xy} are most severe under uniform loading for angle-ply panels at large skew angles. Therefore, a comprehensive design of skewed stiffened panels must consider all three load types, as each governs a different aspect of structural response. The following sub-sections present the effect of load distribution for each of the four boundary conditions considered.

(i) CCCC (Clamped on All Four Edges) Boundary Condition

The CCCC boundary condition significantly reduces the peak deflections compared to the SSSS case for all three load types. Under uniform pressure, deflections are suppressed by the clamped edges, and the maximum displacement occurs near the panel centre with a steep gradient toward the boundaries. Sinusoidal loading produces a similar but slightly reduced central deflection, while cosine loading results in a distinctly different profile: the deflection is near zero at the centre and exhibits small positive and negative oscillations, particularly for coarse mesh refinements, confirming that the clamped condition effectively neutralises the cosine load's influence at the centre. The severity hierarchy for deflection remains as uniform > sinusoidal > cosine.

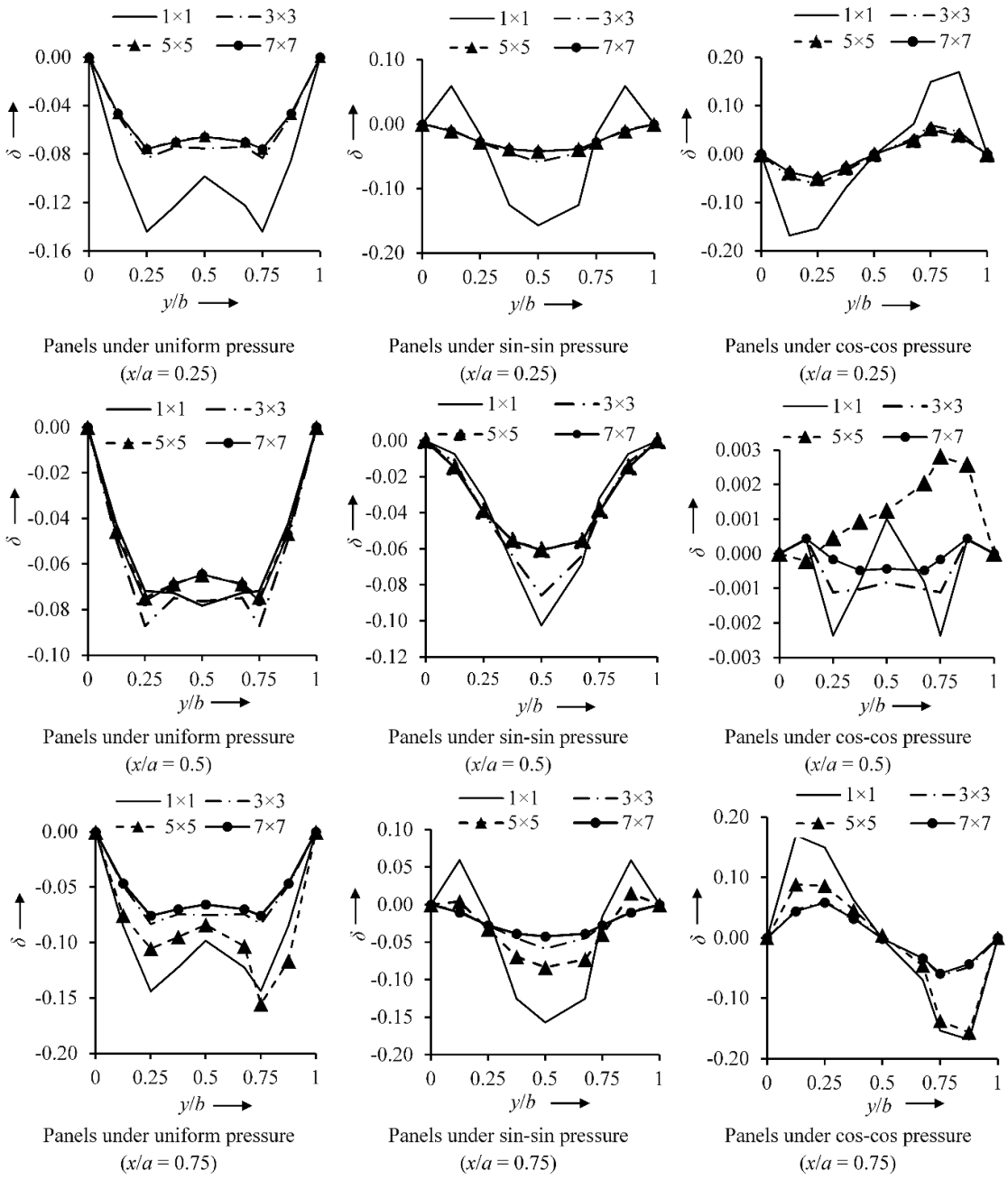

Figure 6.12: Cylindrical panel(ϕ=0^0) with CCCC boundary condition

The bending moments under CCCC conditions are substantially elevated near the clamped boundaries, where the negative moment peaks are most critical. Cosine loading governs the negative bending moments M_x and M_y at the clamped edges for many configurations, exceeding the values produced by uniform loading. This is attributed to the steep deflection of gradients imposed by the clamped restraints interacting with the edge-concentrated cosine load. The

twisting moment M_{xy} is most severe under uniform loading for angle-ply panels, with the skew angle amplifying the coupling effects. In-plane shear N_{xy} follows a similar trend.

For the CCCC boundary condition, special attention must be given to the bending moment demand at the clamped edges under cosine loading. Although overall deflections are smallest for this case, the local moment concentrations near the boundaries may govern the design of the edge stiffeners and the panel thickness.

(ii) SSSS (Simply Supported on All Four Edges) Boundary Condition

Under this boundary condition, uniform pressure produces the largest central deflections, as the absence of edge restraint allows maximum transverse displacement across the entire panel. The deflection profile is broadly distributed and symmetric about the panel centre. Sinusoidal loading produces moderate deflections with a smooth, bell-shaped distribution, while cosine loading results in comparatively smaller deflections due to the load being concentrated near the panel edges where the boundary support is most effective. The severity hierarchy for deflection is thus: uniform > sinusoidal > cosine.

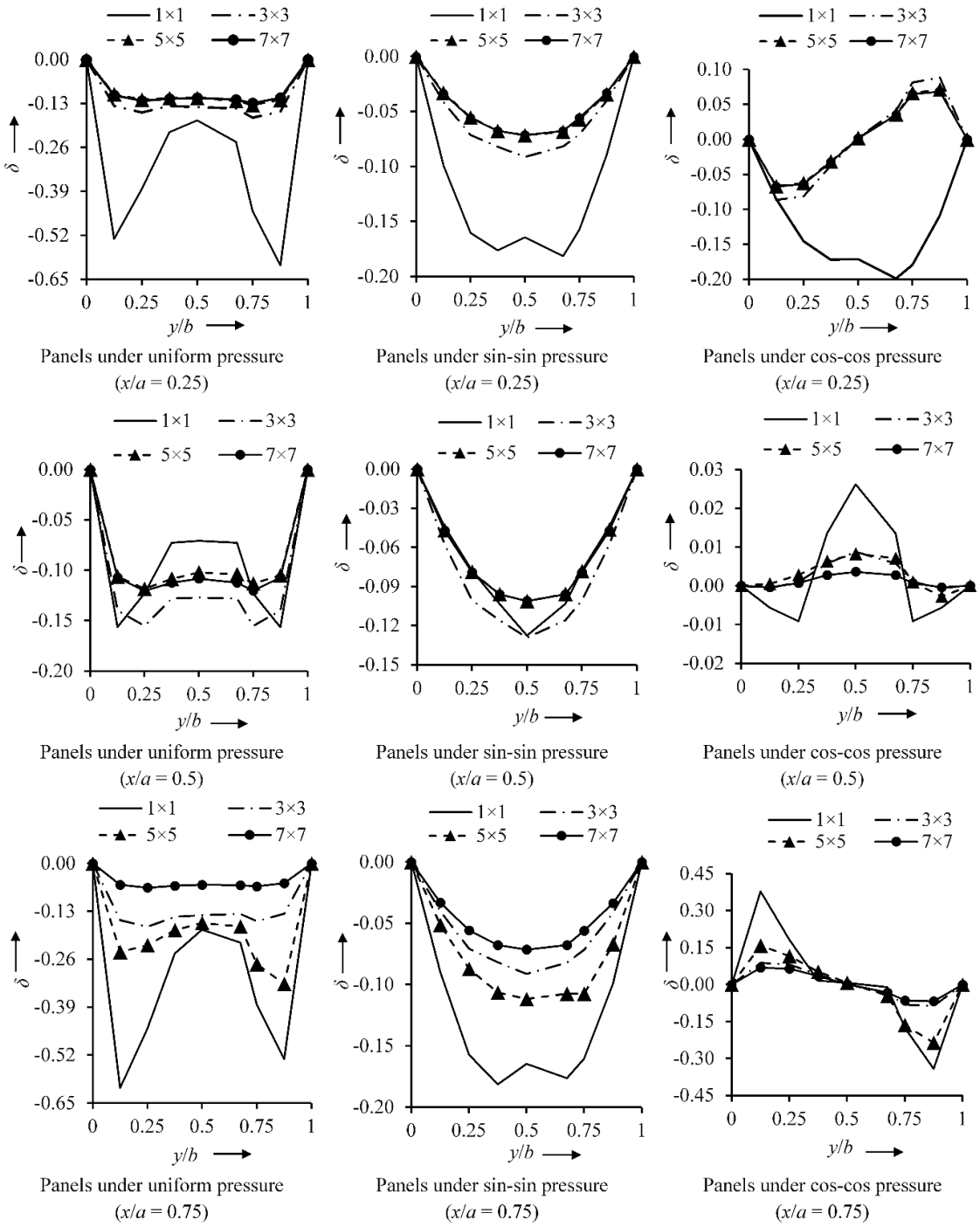

Figure 6.13: Cylindrical panel(ϕ=0^0) with SSSS boundary condition

Regarding bending moments M_x and M_y, cosine loading governs over uniform loading for most panel configurations under SSSS conditions, particularly at intermediate skew angles. This is because the cosine load distribution intensifies the curvature near the edges, which is unsupported in the rotational sense under simply supported conditions, thereby amplifying

bending. The twisting moment M_{xy} and in-plane shear resultant N_{xy} are most critical under uniform loading for angle-ply panels, especially as the skew angle increases beyond 30°, where the coupling between bending and twisting becomes significant.

For the SSSS boundary condition, the design of the panel must not rely solely on uniform load deflection checks. Cosine loading must be independently assessed for bending moment capacity, as it can govern the flexural design even when deflections remain within limits under uniform pressure.

(iii) SCSC (Simply Supported on Loaded Edges, Clamped on Unloaded Edges) Boundary Condition

The SCSC boundary condition introduces directional asymmetry in the deflection response. Under uniform pressure, the simply supported loaded edges permit larger deflections along the x-direction, while the clamped unloaded edges restrict lateral spread, resulting in an elongated deflection trough aligned with the span direction. Sinusoidal loading produces a comparable but slightly smaller deflection profile, with good mesh convergence achieved at 5×5 and 7×7 refinements. Cosine loading produces non-trivial deflections near the simply supported edges and near-zero values at mid-span, reflecting the load's concentration at the edges that are free to rotate. The severity hierarchy for deflection is: uniform > sinusoidal > cosine.

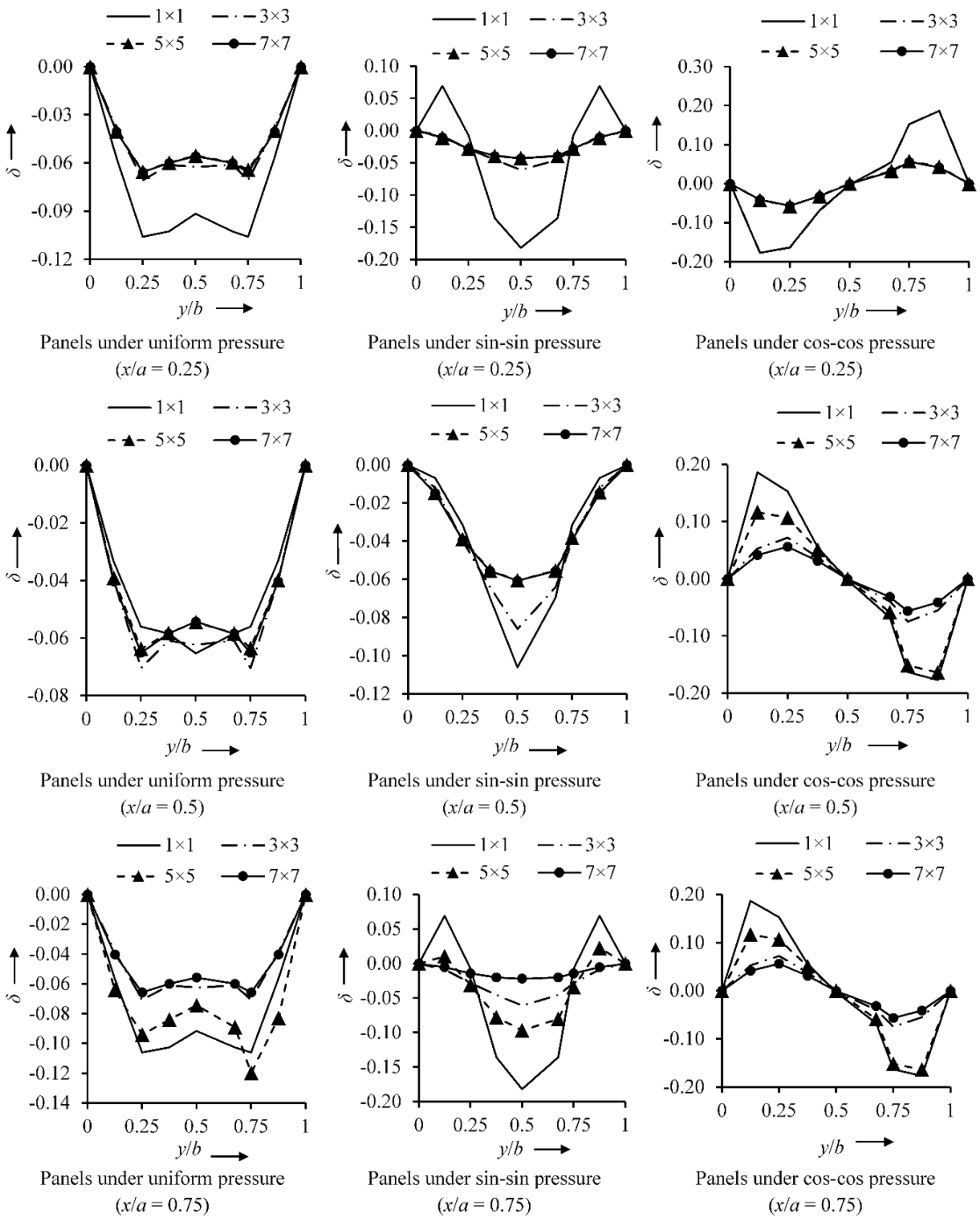

Figure 6.14: Cylindrical panel(ϕ=0^0) with SCSC boundary condition

The bending moment distribution under SCSC conditions is characterized by large positive moments M_x near the mid-span of the simply supported edges and large negative moments along the clamped unloaded edges. Cosine loading governs the positive bending moments along the span for intermediate and large skew angles, exceeding the values under uniform

pressure. This is a direct consequence of the cosine load aligning with the simply supported edge, where rotational freedom amplifies the bending curvature. The twisting resultant M_{xy} and in-plane shear N_{xy} are most severe under uniform loading for skew angles beyond 30°.

For the SCSC boundary condition, the governing load case changes depending on the structural quantity under consideration. While deflection and twisting response are dominated by uniform loading, the bending moment along the span is critical under cosine loading. A complete design assessment must therefore incorporate all three load distributions.

(iv) CCSS (Clamped on Two Adjacent Edges, Simply Supported on the Remaining Two) Boundary Condition

The CCSS boundary condition produces the most non-uniform deflection field of all the cases considered. Under uniform pressure, the panel deflects significantly near the simply supported corner, with peak deflections occurring closer to $x/a = 0.75$ rather than at mid-span, owing to the asymmetric stiffness distribution. Sinusoidal loading shifts the deflection peak back toward the panel centre but with a notable asymmetry inherited from the boundary condition. Cosine loading, while producing the smallest overall deflections, generates non-negligible values near the simply supported edges and exhibits oscillatory behaviour for coarser meshes, confirming the sensitivity of this load type to boundary asymmetry. The severity hierarchy for deflection follows: uniform > sinusoidal > cosine, though the peak locations differ from those in the symmetric boundary conditions.

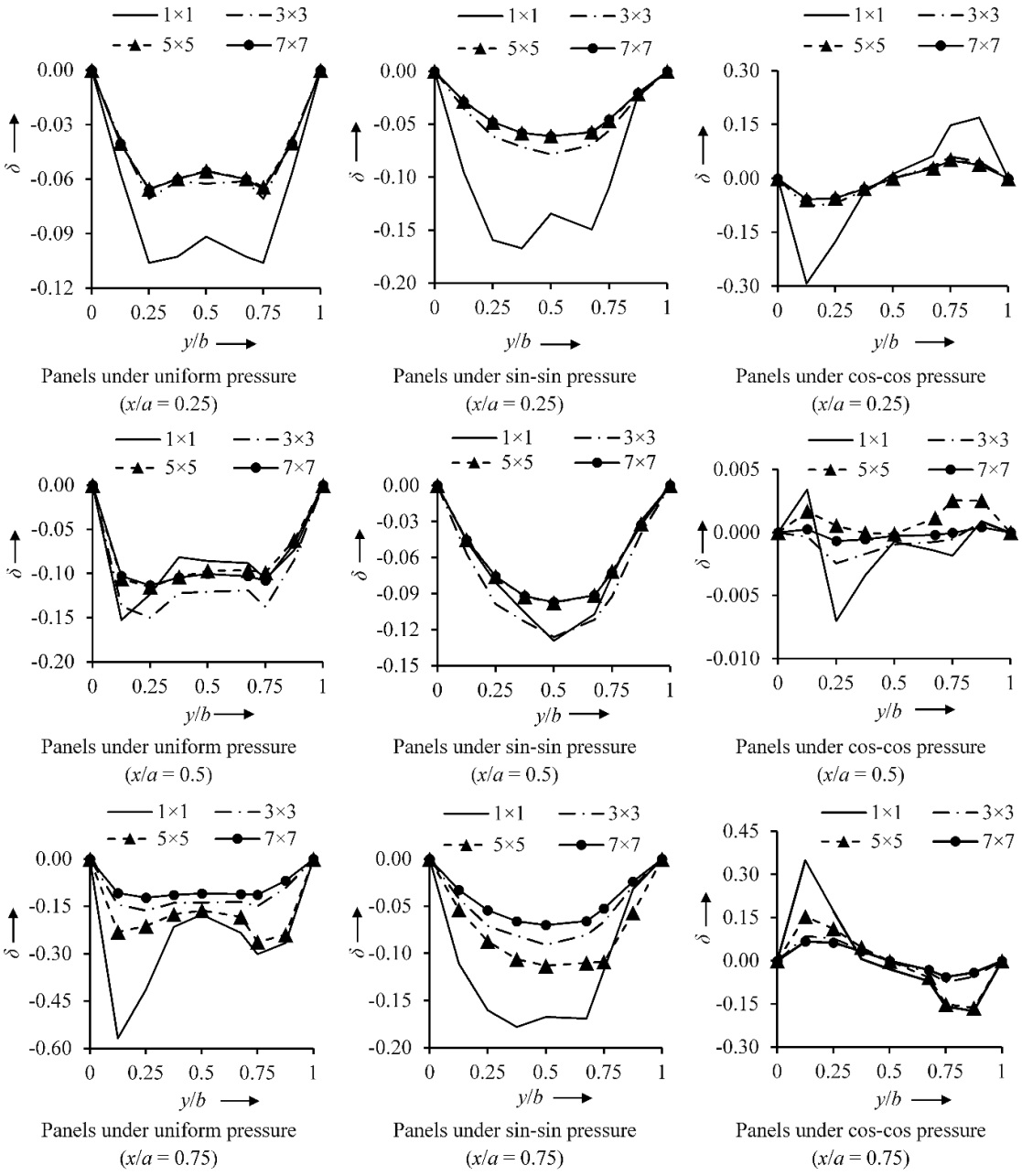

Figure 6.15: Cylindrical panel(ϕ=0^0) with CCSS boundary condition

The bending moments under CCSS conditions are asymmetrically distributed, with the largest negative moments occurring at the clamped edges and positive moments near the simply supported region. Cosine loading governs the bending moments M_x and M_y in the simply supported region for most panel configurations, particularly at intermediate skew angles, while uniform loading remains critical at the clamped edges. The twisting resultant M_{xy} is most severe

under uniform loading for angle-ply panels at large skew angles, consistent with observations for the other boundary conditions. In-plane shear N_{xy} follows the same trend.

The CCSS boundary condition presents the most complex design scenario, as the load case governing each structural response quantity varies with the location on the panel. Deflections near the clamped zone are governed by uniform loading, whereas bending moments in the simply supported region are critical under cosine loading. A comprehensive design of panels with this boundary condition must evaluate all three load types at multiple critical locations.

In summary, the effect of load distribution on structural response is boundary-condition-dependent. While the deflection severity hierarchy (uniform > sinusoidal > cosine) is broadly maintained across all four boundary conditions, the bending moment hierarchy can reverse depending on the degree and type of edge restraint. Panels with fully or partially simply supported edges are more susceptible to cosine loading in bending, whereas fully clamped panels experience the cosine load's influence primarily at the restrained boundaries. The twisting and shear resultants are consistently most critical under uniform loading for angle-ply configurations. These observations collectively emphasise that a robust design of skewed stiffened panels requires consideration of all three load types regardless of the boundary condition.

6.2.9 Effect of Lamination Sequence

Across all load types and boundary conditions, angle-ply laminates particularly $(45°/-45°)_S$ provide significantly lower deflections than cross-ply laminates under SSSS conditions, owing to the enhanced shear coupling that improves effective bending stiffness along diagonal directions. Conversely, cross-ply laminates such as 0°/90°/0° and $(0°/90°)_S$ perform better under CCCC conditions, where fibre-aligned stiffness contributes directly to clamped-edge resistance. The symmetric laminates $(0°/90°)_S$ and $(45°/-45°)_S$ generally outperform their asymmetric counterparts in reducing deflections due to balanced bending-extension coupling. For stress resultants, CCCC cross-ply panels produce the lowest bending moments, making them the safest configurations from a strength perspective. Angle-ply panels under SSSS or CCSS conditions exhibit the highest bending and torsional resultants and must be designed with greater care at elevated skew angles.

CHAPTER 7

CONCLUSIONS

7.1 General

This chapter outlines the principal conclusions drawn from the present study on the geometrically nonlinear flexural behaviour of skewed stiffened laminated composite cylindrical shell panels. The investigation employed a geometrically nonlinear iso-parametric C^0 finite element formulation founded on first-order shear deformation theory (FSDT), utilising eight-noded quadrilateral shell elements and three-noded eccentric composite stiffener elements. The flexural response was examined for four edge restraint configurations CCC, SSSS, SCSC, and CCSS, for cross-ply and angle-ply laminations of graphite/epoxy composite, stiffener skew angles varying from 0° to 35° in increments of 5°, and three transverse load distributions: uniform, sinusoidal (sin–sin), and cosinusoidal (cos–cos) pressure. The reliability of the proposed formulation was established through benchmark comparisons prior to conducting the full parametric study.

7.2 Conclusions

The relative flexural performance of skewed biaxially stiffened composite cylindrical shell panels is evaluated for four boundary conditions: CCCC (all edges clamped), SSSS (all edges simply supported), SCSC (straight edges clamped, curved edges simply supported), and CCSS (two adjacent edges clamped, two adjacent edges simply supported). Cross-ply and angle-ply laminations of graphite/epoxy composite are considered throughout. An iso-parametric C^0 nonlinear finite element code is employed for the performance assessment. The principal findings are summarised in the following sub-sections.

7.2.1 Validation of the Formulation

The accuracy of the proposed nonlinear finite element code is verified through benchmark problems prior to the parametric investigations.

1. Non-dimensional central deflections of simply supported composite spherical panels computed by the present code agree with the closed-form solutions of Reddy [1989] to within 0.2% across all lamination schemes, confirming the correctness of the nonlinear bending formulation.
2. Load–deflection curves of clamped isotropic plates at skew angles of 15° and 45° demonstrate close agreement with the numerical results of Buraghain and Patodi [1978], thereby validating the skewed panel formulation.
3. Nonlinear deflections of centrally stiffened composite panels under uniform loading match well with those reported by Liao, C.L. and Lee, Z.Y. [1993] up to the first limit point, confirming the accurate incorporation of composite stiffeners within the formulation.

7.2.2 Effect of Boundary Conditions

Among the four boundary conditions examined, the following observations are noted:

1. The CCCC configuration consistently yields the lowest non-dimensional deflections across all lamination sequences, skew angles, and loading types, as complete edge clamping provides maximum resistance to transverse deformation.
2. The SSSS configuration produces the largest deflections for cross-ply laminates under both uniform and cos–cos loading, reflecting the reduced edge restraint and consequent greater panel flexibility.
3. The SCSC configuration yields considerably lower deflections than SSSS for cross-ply laminates. Notably, the three-layer (0°/90°/0°) cross-ply laminate records markedly reduced deflections under SCSC compared to all other boundary conditions except CCCC, confirming that restraining the straight longitudinal edges is structurally more beneficial for cylindrical panels than restraining the curved edges.
4. The CCSS configuration produces deflections intermediate between CCCC and SSSS; however, this configuration generates the highest bending moment M_x and twisting moment M_{xy} among all four boundary conditions, particularly for angle-ply laminates, rendering it the most critical case from a stress resultant design perspective.
5. The flexural performance of cylindrical shell panels is strongly dependent on edge restraint. For cross-ply laminates under all loading types, the boundary conditions rank consistently in order of increasing deflection as: CCCC < SCSC < CCSS < SSSS.

7.2.3 Effect of Skew Angle

1. For cross-ply laminates, non-dimensional deflections increase monotonically with skew angle under all three load distributions and all four boundary conditions, with maximum deflections consistently occurring at ϕ=35°.
2. For angle-ply laminates under uniform pressure in the SSSS configuration, a localised reduction in deflection is observed in the vicinity of ϕ=15°–20°, beyond which deflections increase at higher skew angles. This non-monotonic trend is attributed to bending–twisting coupling activated at moderate skew angles in angle-ply composites.
3. Under sin–sin pressure, deflections increase smoothly and monotonically with skew angle for both cross-ply and angle-ply laminates across all boundary conditions, making this the most predictable loading case for design application.
4. At larger skew angles ($\phi \geq 25°$), twisting moments $M_{x\gamma}$ increase substantially across all configurations, with the most pronounced growth occurring for the CCSS boundary condition combined with angle-ply laminates, underscoring the necessity of accounting for torsional effects in the design of skewed panels.

7.2.4 Effect of Load Distribution

1. Uniform pressure produces the highest deflections and represents the most critical loading scenario for all panel configurations and boundary conditions.
2. Sinusoidal (sin-sin) pressure, concentrated at the panel centre, produces the lowest deflections across all boundary conditions and laminations. It is the most favourable transverse loading condition for the configurations studied.
3. Cosinusoidal (cos-cos) pressure responses are intermediate between uniform and sin-sin loading for all boundary conditions and laminations. The rank order of deflection magnitude uniform > cos-cos > sin-sin is maintained consistently for all configurations.
4. Under uniform pressure, the CCSS/$(45°/-45°)_S$ panel produces the highest M_x = 229.85 at ϕ = 35°. Under cosine pressure, the CCSS/$(45°/-45°)_2$ configuration governs with M_x = 183.05 which, while lower in absolute magnitude, represents the critical case for bending design under that load type. This configuration is the most critical from a bending strength perspective.
5. The SSSS boundary condition with the 45°/−45°/45° laminate generates the highest in-plane shear force N_{xy} and twisting moment M_{xy} under uniform pressure at large skew angles. The torsional resultants increase monotonically with skew angle and must be explicitly considered in design.

6. The transverse membrane force N_y is compressive in most SCSC and CCCC cross-ply panel cases. This compressive membrane action arises from the cylindrical curvature and contributes to the overall stiffness of the panel, partially offsetting bending deflections.
7. Under sin-sin pressure, the CCSS $(45°/-45°)_2$ angle-ply panel records the highest in-plane shear N_{xy} and twisting moment M_{xy}, both increasing monotonically from $\phi = 0°$ to 35°. This highlights the risk associated with partial edge restraint for angle-ply panels under distributed loading.
8. The force and moment resultants clearly demonstrate that deflection alone is not a sufficient benchmark for assessing the bending performance of skewed cylindrical shell panels. Critical stress resultants equally govern the structural behaviour. It is therefore strongly recommended that deflections and critical force and moment resultants be studied together for realistic performance predictions of skewed stiffened composite cylindrical shell panels.

7.2.5 Effect of Material System

Graphite/epoxy panels consistently exhibit lower non-dimensional deflections than glass/epoxy panels across all boundary conditions, lamination sequences, and skew angles, owing to the significantly higher longitudinal and transverse elastic moduli of graphite fibres. The performance advantage of graphite/epoxy over glass/epoxy is more pronounced under CCCC conditions where the full material stiffness is mobilised, and less pronounced under SSSS where panel flexibility is dominated by the absence of edge rotational restraint rather than material stiffness.

Chapter 8

Scope for Future Work

Based on the findings of the present study and its scope limitations, the following directions are identified for future research:

- The present formulation may be extended to free vibration, buckling, and dynamic stability analysis of skewed stiffened cylindrical shell panels under combined loading conditions.
- The study considered a central biaxial stiffener; future work may explore multiple stiffeners with varying eccentricities, depth ratios (d_{st}/h), and orientations to arrive at optimized stiffener configurations for minimum deflection or minimum weight design.
- The analysis may be extended to other doubly curved shell geometries such as elliptic paraboloids, hyperbolic paraboloids, and conical shells under similar parametric investigations.
- Additional boundary conditions such as CSCS, CFCF, and FCFC may be incorporated to provide a more complete picture of edge restraint effects on bending behavior.
- The influence of geometric imperfections, delamination, fibre misalignment, and material nonlinearity on the bending response of skewed stiffened panels warrants further investigation.
- Optimization frameworks incorporating metaheuristic algorithms or machine learning approaches may be applied to identify optimal lamination sequences and stiffener layouts for the cylindrical shell panel configurations studied here.

Chapter 9

REFERENCES

[1] Donnell, L. H. (1934). A new theory for the buckling of thin cylinders under axial compression and bending. *Transactions of the American Society of Mechanical Engineers*, *56*(8), 795-806. http s://doi.org/10.1115/1.4019867

[2] Vlasov, V. Z. (1947). Membrane theory of thin shells formed by second order surfaces. *Prikl. Mat. Mekh., Akademiya Nauk., SSSR, XI*, *4*

[3] Ambartsumyan, S. A. (1953). Calculation of laminated anisotropic shells. *Izvestiia Akademiia Nauk Armenskoi SSR, Ser. Fiz. Mat. Est. Tekh. Nauk*, *6*(3), 15.

[4] Reissner, E. (1955). On transverse vibrations of thin, shallow elastic shells. *Quarterly of Applied Mathematics*, *13*(2), 169-176.https://doi.org/10.1090/qam/69715

[5] Greene, B.E., Strome, D.R. and Weikel, R.C., (1961). Application of the stiffness method of analysis of shell structures', Proceedings Aviation Conference of ASME, Los Angeles, CA.

[6] Ambartsumyan, S. A. (1964). Theory of anisotropic shells. NASA Report, TT F–118

[7] Hadid, H. A. (1964). An analytical and experimental investigation into the bending theory of elastic conoidal shells (Doctoral dissertation, University of Southampton).

[8] Greene, B. E., Jones, R. E., & Strome, D. R. (1968, December). Dynamic analysis of shells using doubly curved finite elements. In Proc. 2nd Conf. Matrix Methods Struct. Mech. (pp. 185-212).

[9] Ergatoudis, I. R. O. N. S., Irons, B. M., & Zienkiewicz, O. C. (1968). Curved, isoparametric,"quadrilateral" elements for finite element analysis. Int. J. Solids Struct., *4*(1), 31-42.https://doi.org/10.1016/0020-7683(68)90050-7

[10] Gallagher, R.H.,(1969). Analysis of plate and shell structures – applications of finite element method in engineering', Vanderbilt University, ASCE Publication.

[11] Ahmad, S., Irons, B. M., & Zienkiewicz, O. C. (1970). Analysis of thick and thin shell structures by curved finite elements. Int. J. Numer. Methods Eng., *2*(3), 419-451. https://doi.org/10.1002/nme.1620020310

[12] Bandyopadhyay, J.N., (1978). 'Analytical study of the shell characteristics of hyperbolic paraboloid and paraboloid of revolution shell structures', Ph.D. Dissertation, Department of Civil Engineering, I.I.T., Kharagpur.

[13] Bert, C.W. and Reddy, V.S., (1982). 'Cylindrical shells of bimodulus material', Journal of Engineering Mechanics Division, ASCE, Vol. 108, No. EM5, pp. 675–688. https://doi.org/10.1061/(ASCE)0733-9399(1982)108:5(675)

[14] Bert, C.W. and Kumar, M., (1982). 'Vibration of cylindrical shells of bimodulus composite materials', Journal of Sound and Vibration, Vol. 81, No. 1, pp. 107–121. https://doi.org/10.1016/0022-460X(82)90174-7

[15] Soldatos, K.P. and Tzivanidis, G.J., (1982a). 'Buckling and Vibration of Cross-Ply Laminated Circular Cylindrical Panels', Journal of Applied Mathematics and Physics, Vol. 33, pp. 230–239. https://doi.org/10.1007/BF00944973

[16] Soldatos, K.P. and Tzivanidis, G.J., (1982b). 'Buckling and Vibration of Cross-Ply Laminated Noncircular Cylindrical Panels', Journal of Sound and Vibration, Vol. 82, No. 3, pp. 425–434. https://doi.org/10.1016/0022-460X(82)90015-8

[17] Soldatos, K.P., (1983). 'Free vibrations of antisymmetric angle-ply laminated circular cylindrical shell panels', Quarterly Journal of Mechanics and Applied Mathematics, Vol. 36, No. 2, pp. 207–221. https://doi.org/10.1093/qjmam/36.2.207

[18] Reddy, J.N., (1984). 'Exact solutions of moderately thick laminated shells', Journal of Engineering Mechanics, Vol. 110, No. 5, pp. 794–809. https://doi.org/10.1061/(ASCE)0733-9399(1984)110:5(794)

[19] Reddy, J.N. and Liu, C.F.,(1985). 'A Higher Order Shear Deformation Theory of Laminated Elastic Shells', International Journal of Engineering Science, Vol. 23, No. 3, pp. 319–330. https://doi.org/10.1016/0020-7225(85)90051-5

[20] Reddy, J.N. and Chandrashekhara, K.,(1985). 'Geometrically Nonlinear Transient Analysis of Laminated Doubly Curved Shells', International Journal of Non-Linear Mechanics, Vol. 20, No. 2, pp. 79–90. https://doi.org/10.1016/0020-7462(85)90002-2

[21] Saigal, S., Kapania, R.K. and Yang, T.Y.,(1986). 'Geometrically Nonlinear Finite Element Analysis of Imperfect Laminated Shells', Journal of Composite Materials, Vol. 20, No. 2, pp. 197–214. https://doi.org/10.1177/002199838602000206

[22] Chandrashekhara, K., (1989). 'Free Vibrations of Anisotropic Laminated Doubly Curved Shells', Computers and Structures, Vol. 33, No. 2, pp. 435–440. https://doi.org/10.1016/0045-7949(89)90018-2

[23] Ghosh, B. and Bandyopadhyay, J.N., (1989). 'Bending Analysis of Conoidal Shells Using Curved Quadratic Isoparametric Element', Computers and Structures, Vol. 33, No. 3, pp. 717–728. https://doi.org/10.1016/0045-7949(89)90248-X

[24] Liao, C.L. and Reddy, J.N., (1990). 'Analysis of anisotropic, stiffened composite laminates using a continuum-based shell element', Computers and Structures, Vol. 34, pp. 805–815. https://doi.org/10.1016/0045-7949(90)90351-2

[25] Ghosh, B. and Bandyopadhyay, J.N., (1990). 'Analysis of paraboloid of revolution type shell structures using isoparametric doubly curved shell elements', Computers and Structures, Vol. 36, No. 5, pp. 791–800. https://doi.org/10.1016/0045-7949(90)90149-V

[26] Tsai, C.T. and Palazotto, A.N., (1991). 'On the Finite Element Analysis of Nonlinear Vibration for Cylindrical Shells with High Order Shear Deformation Theory',

International Journal of Nonlinear Mechanics, Vol. 26, No. 3–4, pp. 379–388. https://doi.org/10.1016/0020-7462(91)90013-X

[27] Schimmels, S.A. and Palazotto, A.N., (1994). Nonlinear geometric and material behavior of shell structures with large strains', Journal of Engineering Mechanics, Vol. 120, pp. 320–345. https://doi.org/10.1061/(ASCE)0733-9399(1994)120:2(320)

[28] Kant, T. and Kommineni, J.R., (1992). 'Geometrically Nonlinear Analysis of Doubly Curved Laminated and Sandwich Fiber Reinforced Composite Shells with A Higher Order Theory and C0 Finite Elements', Journal of Reinforced Plastics and Composites, Vol. 11, No. 9, pp. 1048–1076. https://doi.org/10.1177/073168449201100901

[29] Dey, A., Bandyopadhyay, J.N. and Sinha, P.K., (1992). 'Finite Element Analysis of Laminated Composite Conoidal Shell Structures', Computers and Structures, Vol. 43, No. 3, pp. 469–476. https://doi.org/10.1016/0045-7949(92)90282-6

[30] Kant, T. and Kommineni, J.R., (1994a). 'Large Amplitude Free Vibration Analysis of Cross Ply Composite and Sandwich Laminates with A Refined Theory and C0 Finite Elements', Computers and Structures, Vol. 50, No. 1, pp. 123–134. https://doi.org/10.1016/0045-7949(94)90444-8

[31] Kant, T. and Kommineni, J.R., (1994b). 'Geometrically Nonlinear Transient Analysis of Laminated Composite and Sandwich Shells With A Refined Theory and C0 Finite Elements', Computers and Structures, Vol. 52, No. 6, pp. 1243–1259. https://doi.org/10.1016/0045-7949(94)90183-X

[32] Goswami, S. and Mukhopadhyay, M., (1994). 'Finite element analysis of laminated composite stiffened shell', Journal of Reinforced Plastics and Composites, Vol. 13, pp. 574–616. https://doi.org/10.1177/073168449401300701

[33] Chandrashekhar, K. and Bhimaraddi, A., (1994). 'Thermal stress analysis of laminated doubly curved shells using a shear flexible finite element', Computers and Structures, Vol. 52, pp. 1023–1030. https://doi.org/10.1016/0045-7949(94)90086-8

[34] Dey, A., Bandyopadhyay, J.N. and Sinha, P.K., (1994). 'Behaviour of Paraboloid of Revolution Shell Using Cross-Ply and Antisymmetric Angle-Ply Laminates', Computers and Structures, Vol. 52, No. 6, pp. 1301–1308. https://doi.org/10.1016/0045-7949(94)90190-2

[35] Ghosh, B. and Bandyopadhyay, J.N., (1994). 'Bending Analysis of Conoidal Shells with Cut-Outs', Computers and Structures, Vol. 53, No. 1, pp. 9–18. https://doi.org/10.1016/0045-7949(94)90127-9

[36] Mizusawa, T. and Kito, H., (1995). 'Vibration of Antisymmetric Angle-Ply Laminated Cylindrical Panels by the Spline Strip Method', Computers and Structures, Vol. 56, No. 4, pp. 589–604. https://doi.org/10.1016/0045-7949(94)00555-M

[37] Chakravorty, D. and Bandyopadhyay, J.N., (1995). 'On the Free Vibration of Shallow Shells', Journal of Sound and Vibration, Vol. 185, No. 4, pp. 673–684. https://doi.org/10.1006/jsvi.1995.0408

[38] Goswami, S. and Mukhopadhyay, M., (1995). 'Geometrically nonlinear analysis of laminated composite stiffened shells', Journal of Reinforced Plastics and Composites, Vol. 14, pp. 1317–1336. https://doi.org/10.1177/073168449501401205

[39] Chakravorty, D., Bandyopadhyay, J.N. and Sinha, P.K., (1995). 'Free Vibration Analysis of Point-Supported Laminated Composite Doubly Curved Shells – A Finite Element Approach', Computers and Structures, Vol. 54, No. 2, pp. 191–198. https://doi.org/10.1016/0045-7949(94)00329-2

[40] Chakravorty, D., Bandyopadhyay, J.N. and Sinha, P.K., (1995b). 'Finite Element Free Vibration Analysis of Conoidal Shells', Computers and Structures, Vol. 56, No. 6, pp. 975–978. https://doi.org/10.1016/0045-7949(94)00573-S

[41] Bardell, N.S., Dunsdon, J.M. and Langley, R.S., (1997). 'Free and Forced Vibration Analysis of Thin, Laminated, Cylindrically Curved Panels', Computers and Structures, Vol. 38, No. 1–4, pp. 453–462. https://doi.org/10.1016/0045-7949(95)00181-6

[42] Gunay, E., (1999). 'Finite Element Analysis of Laminated Stiffened Cylindrical Shallow Shell', Applied Composite Materials, Vol. 6, No. 6, pp. 381–395. https://doi.org/10.1023/A:1008998119062

[43] Chang, T.P. and Chang, H.C., (2000). 'Nonlinear Vibration Analysis of Geometrically Nonlinear Shell Structures', Mechanics Research Communications, Vol. 27, No. 2, pp. 173–180. https://doi.org/10.1016/S0093-6413(00)00075-X

[44] Ferreira, A.J.M. and Barbosa, J.T., (2000). 'Buckling Behaviour of Composite Shells', Composite Structures, Vol. 50, No. 1, pp. 93–98. https://doi.org/10.1016/S0263-8223(00)00090-8

[45] Ram, K.S.S. and Babu, T.S., (2001). 'Study of bending of laminated composite shells. Part I: Shells without a cutout', Composite Structures, Vol. 51, pp. 103–116. https://doi.org/10.1016/S0263-8223(00)00129-X

[46] Rougui, M., Moussaoui, F. and Benamar, R., (2007). 'Geometrically Nonlinear Free and Forced Vibrations of Simply Supported Circular Cylindrical Shells: A Semi-Analytical Approach', International Journal of Nonlinear Mechanics, Vol. 42, No. 9, pp. 1102–1115. https://doi.org/10.1016/j.ijnonlinmec.2007.06.004

[47] Ganapathi, M., Patel, B.P. and Pawargi, D.S., (2002). 'Dynamic Analysis of Laminated Cross-Ply Composite Non-Circular Thick Cylindrical Shells Using Higher-Order Theory', International Journal of Solids and Structures, Vol. 39, No. 24, pp. 5945–5962. https://doi.org/10.1016/S0020-7683(02)00495-X

[48] Turkmen, H.S., (2002). 'Structural Response of Laminated Composite Shells Subjected to Blast Loading: Comparison of Experimental and Theoretical Methods', Journal of Sound and Vibration, Vol. 249, No. 4, pp. 663–678. https://doi.org/10.1006/jsvi.2001.3829

[49] Nayak, A.N. and Bandyopadhyay, J.N., (2002). 'Free Vibration Analysis and Design Aids of Stiffened Conoidal Shells', Journal of Engineering Mechanics, Vol. 128, No. 4, pp. 419–427. https://doi.org/10.1061/(ASCE)0733-9399(2002)128:4(419)

[50] Amabili, M. and Païdoussis, M.P., (2003). 'Review of Studies on Geometrically Nonlinear Vibrations and Dynamics of Circular Cylindrical Shells and Panels, With and Without Fluid–Structure Interaction', Applied Mechanics Reviews, Vol. 56, No. 4, pp. 349–381. https://doi.org/10.1115/1.1565347

[51] Ganapathi, M., Patel, B.P., Patel, H.G. and Pawargi, D.S., (2003). 'Vibration Analysis of Laminated Cross-Ply Oval Cylindrical Shells', Journal of Sound and Vibration, Vol. 262, No. 1, pp. 65–86. https://doi.org/10.1016/S0022-460X(02)01070-6

[52] Djoudi, M.S. and Bahai, H., (2003). 'A Shallow Shell Finite Element for the Linear and Nonlinear Analysis of Cylindrical Shells', Engineering Structures, Vol. 25, No. 6, pp. 769–778. https://doi.org/10.1016/S0141-0296(03)00002-4

[53] Chaudhuri, R.A., (2008). 'A Nonlinear Zigzag Theory for Finite Element Analysis of Highly Shear-Deformable Laminated Anisotropic Shells', Composite Structures, Vol. 85, No. 4, pp. 350–359. https://doi.org/10.1016/j.compstruct.2007.11.002

[54] Ganapathi, M., Patel, B.P., Gupta, S.S. et al., (2004). 'Free-Vibration Characteristics of Laminated Angle-Ply Non-Circular Cylindrical Shells', Defense Science Journal, Vol. 54, No. 4, pp. 429–442. https://doi.org/10.14429/dsj.54.2073

[55] Sahoo, S. and Chakravorty, D., (2004). 'Finite Element Bending Behaviour of Composite Hyperbolic Paraboloidal Shells With Various Edge Conditions', Journal of Strain Analysis for Engineering Design, Vol. 39, No. 5, pp. 1–15. https://doi.org/10.1243/0309324041896465

[56] Amabili, M., (2004). 'Non-linear vibrations of doubly curved shallow shells', International Journal of Non-Linear Mechanics, Vol. 40, pp. 683–710. https://doi.org/10.1016/j.ijnonlinmec.2004.08.007

[57] Lee, S.J., Reddy, J.N. and Abadi, F.S., (2006). 'Nonlinear Finite Element Analysis of Laminated Composite Shells with Actuating Layers', Finite Elements in Analysis and Design, Vol. 43, No. 1, pp. 1–21. https://doi.org/10.1016/j.finel.2006.06.008

[58] Nayak, A.N. and Bandyopadhyay, J.N., (2006). 'Dynamic Response Analysis of Stiffened Conoidal Shells', Journal of Sound and Vibration, Vol. 291, No. 3–5, pp. 1288–1297. https://doi.org/10.1016/j.jsv.2005.07.024

[59] Nanda, N. and Bandyopadhyay, J.N., (2007). 'Nonlinear Free Vibration Analysis of Laminated Composite Cylindrical Shells with Cutouts', Journal of Reinforced Plastics and Composites, Vol. 26, No. 14, pp. 1413–1427. https://doi.org/10.1177/0731684407079465

[60] Kundu, C.K. and Sinha, P.K., (2007). 'Post Buckling Analysis of Laminated Composite Shells', Composite Structures, Vol. 78, No. 3, pp. 316–324. https://doi.org/10.1016/j.compstruct.2005.10.005

[61] Kundu, C.K., Maiti, D.K. and Sinha, P.K., (2007). 'Nonlinear finite element analysis of laminated composite doubly curved shells in hygrothermal environment', Journal of Reinforced Plastics and Composites, Vol. 26, pp. 1461–1478. https://doi.org/10.1177/0731684407079751

[62] Sahoo, S. and Chakravorty, D., (2007). 'Static Bending of Point Supported Composite Hypar Shell Roofs', Journal of Structural Engineering, Vol. 34, No. 2, pp. 1–8.

[63] Das, H.S. and Chakravorty, D., (2007). 'Design Aids and Selection Guidelines for Composite Conoidal Shell Roofs – A Finite Element Application', Journal of Reinforced Plastics and Composites, Vol. 26, No. 17, pp. 1793–1819. https://doi.org/10.1177/0731684407079751

[64] Nanda, N. and Bandyopadhyay, J.N., (2008). 'Nonlinear Transient Response of Laminated Composite Shells', Journal of Engineering Mechanics, Vol. 134, No. 11, pp. 983–990. https://doi.org/10.1061/(ASCE)0733-9399(2008)134:11(983)

[65] Han, S.C., Tabiei, A. and Park, W.T., (2008). 'Geometrically Nonlinear Analysis of Laminated Composite Thin Shells Using a Modified First Order Shear Deformable Element Based Lagrangian Shell Element', Composite Structures, Vol. 82, No. 3, pp. 465–474. https://doi.org/10.1016/j.compstruct.2007.01.027

[66] Pradyumna, S. and Bandyopadhyay, J.N., (2008). 'Static and Free Vibration Analyses of Laminated Shells Using A Higher Order Theory', Journal of Reinforced Plastics and Composites, Vol. 27, No. 2, pp. 167–186. https://doi.org/10.1177/0731684407081385

[67] Dogan, A. and Arslan, H.M., (2009). 'Effects of Curvature on Free Vibration Characteristics of Laminated Composite Cylindrical Shallow Shells', Scientific Research and Essay, Vol. 4, No. 4, pp. 226–238.

[68] Nanda, N. and Bandyopadhyay, J.N., (2009). 'Geometrically Nonlinear Transient Analysis of Laminated Composite Shells Using the Finite Element Method', Journal of Sound and Vibration, Vol. 325, No. 1–2, pp. 174–185. https://doi.org/10.1016/j.jsv.2009.03.002

[69] Acharyya, A.K., Chakravorty, D. and Karmakar, A., (2009). 'Bending Characteristics of Delaminated Composite Cylindrical Shells', Journal of Reinforced Plastics and Composites, Vol. 28, No. 8, pp. 965–978. https://doi.org/10.1177/0731684407084250

[70] Amabili, M. and Reddy, J.N., (2010). 'A New Nonlinear Higher Order Shear Deformation Theory for Large-Amplitude Vibrations of Laminated Doubly Curved Shells', International Journal of Nonlinear Mechanics, Vol. 45, No. 4, pp. 409–418. https://doi.org/10.1016/j.ijnonlinmec.2009.12.013

[71] Acharyya, A.K., Chakravorty, D. and Karmakar, A., (2010). 'Natural Frequencies and Mode Shapes of Composite Cylindrical Delaminated Shells by Finite Element', Journal of Reinforced Plastics and Composites, Vol. 29, No. 2, pp. 226–237. https://doi.org/10.1177/0731684408091006

[72] Amabili, M., (2010). 'Nonlinear Vibrations of Laminated Circular Cylindrical Shells: Comparison of Different Shell Theories', Composite Structures, Vol. 94, No. 1, pp. 207–220. https://doi.org/10.1016/j.compstruct.2011.07.001

[73] Nanda, N. and Pradyumna, S., (2011). 'Nonlinear Dynamic Response of Laminated Shells with Imperfections in Hygrothermal Environments', Journal of Composite Materials, Vol. 45, No. 20, pp. 2103–2112. https://doi.org/10.1177/0021998311401061

[74] Adali, S. and Cagdas, I.U., (2011). 'Failure Analysis of Curved Composite Panels Based on First-Ply and Buckling Failures', Procedia Engineering, Vol. 10, pp. 1591–1596. https://doi.org/10.1016/j.proeng.2011.04.266

[75] Neogi, S.D., Karmakar, A. and Chakravorty, D., (2011). 'Impact Response of Simply Supported Skewed Hypar Shell Roofs by Finite Element', Journal of Reinforced Plastics and Composites, Vol. 30, No. 21, pp. 1795–1805. https://doi.org/10.1177/0731684411422338

[76] Kumari, S. and Chakravorty, D., (2011). 'Bending of Delaminated Composite Conoidal Shells Under Uniformly Distributed Load', Journal of Engineering Mechanics, Vol. 137, No. 10, pp. 660–668. https://doi.org/10.1061/(ASCE)EM.1943-7889.0000263

[77] Pradyumna, S. and Bandyopadhyay, J.N., (2011). 'Dynamic Instability Behavior of Laminated Hypar and Conoid Shells Using A Higher-Order Shear Deformation Theory', Thin-Walled Structures, Vol. 49, No. 1, pp. 77–84. https://doi.org/10.1016/j.tws.2010.08.008

[78] Avramov, K.V., (2012). 'Nonlinear Modes of Vibrations for Simply Supported Cylindrical Shell with Geometrical Nonlinearity', Acta Mechanica, Vol. 223, No. 2, pp. 279–292. https://doi.org/10.1007/s00707-011-0556-1

[79] Bich, D.H. and Nguyen, N.X., (2012). 'Nonlinear Vibration of Functionally Graded Circular Cylindrical Shells Based on Improved Donnell Equations', Journal of Sound and Vibration, Vol. 331, No. 25, pp. 5488–5501. https://doi.org/10.1016/j.jsv.2012.07.024

[80] Amabile, M., (2013). 'A New Nonlinear Higher Order Shear Deformation Theory with Thickness Variation for Large-Amplitude Vibrations of Laminated Doubly Curved Shells', Journal of Sound and Vibration, Vol. 332, No. 19, pp. 4620–4640. https://doi.org/10.1016/j.jsv.2013.03.024

[81] Alijani, F. and Amabili, M., (2013). 'Nonlinear Vibrations of Thick Laminated Circular Cylindrical Panels', Composite Structures, Vol. 96, pp. 643–660. https://doi.org/10.1016/j.compstruct.2012.09.016

[82] Amabili, M., (2014). 'A Nonlinear Higher-Order Thickness Variation and Shear Deformation Theory for Large-Amplitude Vibrations of Laminated Doubly Curved Shells', International Journal of Nonlinear Mechanics, Vol. 58, pp. 57–75. https://doi.org/10.1016/j.ijnonlinmec.2013.08.006

[83] Alijani, F. and Amabili, M., (2014). 'Nonlinear Vibrations of Shells: A Literature Review from 2003 to 2013', International Journal of Nonlinear Mechanics, Vol. 58, pp. 233–257. https://doi.org/10.1016/j.ijnonlinmec.2013.09.012

[84] Bakshi, K. and Chakravorty, D., (2014). 'Geometrically Linear and Nonlinear First-Ply Failure Loads of Composite Cylindrical Shells', Journal of Engineering Mechanics, Vol. 140, 04014094. https://doi.org/10.1061/(ASCE)EM.1943-7889.0000808

[85] Gupta, A.K., Patel, B.P. and Nath, Y., (2015). 'Progressive Damage of Laminated Cylindrical/Conical Panels Under Meridional Compression', European Journal of Mechanics A/Solids, Vol. 53, pp. 329–341. https://doi.org/10.1016/j.euromechsol.2015.04.009

[86] Mahapatra, T.R., Panda, S.K. and Kar, V.R., (2015). 'Geometrically nonlinear flexural analysis of hygro-thermo-elastic laminated composite doubly curved shell panel', International Journal of Mechanics and Materials Design, Vol. 12, pp. 153–171. https://doi.org/10.1007/s10999-015-9299-9

[87] Mahapatra, T.R., Panda, S.K. and Kar, V.R., (2016). 'Nonlinear hygro-thermo-elastic vibration analysis of doubly curved composite shell panel using finite element micromechanical model', Mechanics of Advanced Materials and Structures, Vol. 23, pp. 1343–1359. https://doi.org/10.1080/15376494.2015.1085606

[88] Chaubey, A.K., Kumar, A. and Mishra, S.S., (2018). 'Dynamic analysis of laminated composite rhombic elliptic paraboloid due to mass variation', Journal of Aerospace Engineering, Vol. 31, 04018059. https://doi.org/10.1061/(ASCE)AS.1943-5525.0000881

[89] Sayyad, A.S. and Ghugal, Y.M., (2019). 'Static and free vibration analysis of laminated composite and sandwich spherical shells using a generalized higher-order shell theory', Composite Structures, Vol. 219, pp. 129–146. https://doi.org/10.1016/j.compstruct.2019.03.054

[90] Huang, S. and Qiao, P., (2020). 'A new semi-analytical method for nonlinear stability analysis of stiffened laminated composite doubly-curved shallow shells', Composite Structures, Vol. 251, 112526. https://doi.org/10.1016/j.compstruct.2020.112526

[91] Bakshi, K., (2021). 'Numerical study on nonlinear bending performance of transversely loaded composite singly curved stiffened surfaces', Journal of Strain Analysis for Engineering Design, Vol. 56, pp. 430–442. https://doi.org/10.1177/0309324720977415

[92] Gupta, A. and Pradyumna, S., (2021). 'Geometrically nonlinear bending analysis of variable stiffness composite laminated shell panels with a higher-order theory', Composite Structures, Vol. 276, 114527. https://doi.org/10.1016/j.compstruct.2021.114527

[93] Draiche, K., Tounsi, A. and Ibrahim, K.D., (2024). 'An improved mathematical model for static and dynamic analysis of functionally graded doubly-curved shells', Archive

of Applied Mechanics, Vol. 94, pp. 1589–1611. https://doi.org/10.1007/s00419-024-02595-5

[94] Benounas, S., Belarbi, M.O., Van Vinh, P. et al., (2024). 'Finite element model for free vibration analysis of functionally graded doubly curved shallow shells by using an improved first-order shear deformation theory', Structures, Vol. 64, 106594. https://doi.org/10.1016/j.istruc.2024.106594

[95] Long, L., Yaylaci, M. and Lezgy-Nazargah, M., (2025). 'A new shear deformation theory for composite multilayered shells of revolution with retainment of Koiter's recommendation: Static and free vibration analyses', Structures, Vol. 73, 108421. https://doi.org/10.1016/j.istruc.2025.108421